Gesundheit / Health
Band / Volume 67
ISBN 978-3-89336-928-7

JÜLICH
FORSCHUNGSZENTRUM

67

Member of the Helmholtz Association

Expression and purification of human Presenilin 2

Ge Yang

Gesundheit
Health

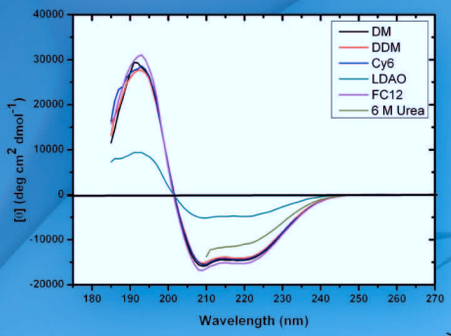

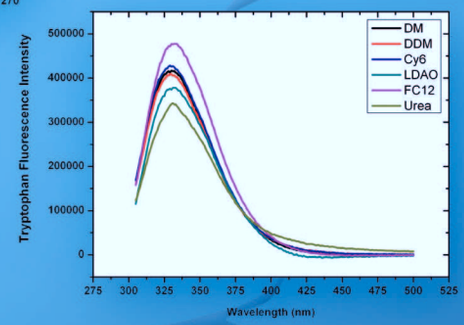

Expression, purification and biophysical characterization of human Presenilin 2

Ge Yang

JÜLICH
FORSCHUNGSZENTRUM

Schriften des Forschungszentrums Jülich
Reihe Gesundheit / Health Band / Volume 67

Forschungszentrum Jülich GmbH
Institute of Complex Systems
Strukturbiochemie (ICS-6)

Expression, purification and biophysical characterization of human Presenilin 2

Ge Yang

Schriften des Forschungszentrums Jülich
Reihe Gesundheit / Health — Band / Volume 67

ISSN 1866-1785 — ISBN 978-3-89336-928-7

Bibliographic information published by the Deutsche Nationalbibliothek.
The Deutsche Nationalbibliothek lists this publication in the Deutsche
Nationalbibliografie; detailed bibliographic data are available in the
Internet at http://dnb.d-nb.de.

Publisher and Distributor: Forschungszentrum Jülich GmbH
Zentralbibliothek
52425 Jülich
Tel: +49 2461 61-5368
Fax: +49 2461 61-6103
Email: zb-publikation@fz-juelich.de
www.fz-juelich.de/zb

Cover Design: Grafische Medien, Forschungszentrum Jülich GmbH

Printer: Grafische Medien, Forschungszentrum Jülich GmbH

Schriften des Forschungszentrums Jülich
Reihe Gesundheit / Health, Band / Volume 67

D 61 (Diss. Düsseldorf, Univ., 2012)

ISSN 1866-1785
ISBN 978-3-89336-928-7

The complete volume is freely available on the Internet on the Jülicher Open Access Server (JUWEL)
at www.fz-juelich.de/zb/juwel

Table of Contents

List of Figures

List of Tables

1 Introduction

1.1 Histopathology of Alzheimer's disease

Alzheimer's disease (AD), together with heart disease, cancer, and stroke, is considered to be one of the four leading causes of death in developed nations. It is predicted that by 2050, 1 in 85 persons will be living with AD all over the world (1).

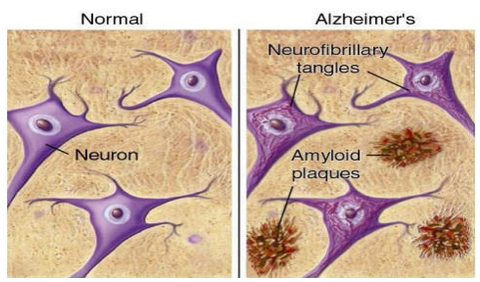

Figure 1.1: Schematic illustration of histopathology of AD brain tissue.
Normal brain tissue (left) and AD brain tissue (right) are shown (5).

AD is named after a German scientist Dr. Alois Alzheimer. He is the first person who systemically studied the AD disease. He reported the three commonly observed hallmarks in the brain tissue of AD patients: amyloid plaques, neurofibrillary tangles and connection loss between neurons. Amyloid plaques are insoluble plaques composing of mainly aggregated amyloid peptide and mis-folded proteins as well as cell debris. They are deposited between the nerve cells (2). Neurofibrillary tangles are commonly found inside the nerve cells. They consist of improperly folded and hyper-phosphorylated tau proteins (3, 4). In AD brain, the physiological structure of microtubule formed by tau protein functioning to transport nutrients within the nerve cells collapses. Therefore neurons are under stress condition due to lack of nutrients and over time gradually lose their ability to function and eventually shrink and lose connections between each other. When the connections lose, the nerve cells could not communicate with each other. As a consequence, the general functions of the brain of AD patient decreases significantly as compared with the normal

aged brain **(Figure 1.1)**. Hence, developing of AD progressively influences daily living through memory and cognitive loss and is therefore considered to be is an irreversible, progressive neurodegenerative brain disease.

Due to the above histopathological changes, the following typical symptoms are commonly observed for AD patients. They may suddenly lose their minds and confused by themselves. They easily lose temper and are sometimes aggressive. Their emotion fluctuates a lot. Initially have trouble with language, as the disease develops, they may exhibit language ability and long-term memory loss. They will withdraw from society due to inability for communication and easily to be frightened. Finally normal body functions are lost (6).

1.2 Genetics of Alzheimer's disease

Depending on the onset age, AD is classified into early onset familial AD (FAD) and late onset sporadic AD. Early onset FAD refers to the AD cases with an onset age of below 65. Only about 0.1 % of the total AD cases are attributed to FAD (7).

Genetic investigation of FAD discovered firstly that the *APP* gene is closely related with AD. Mutations on this gene were found to be able to alter the APP processing (8). The *APP* gene locates on chromosome 21. It encodes a type I transmembrane protein, the amyloid precursor protein (APP) with 770 amino acids. The APP protein sequence contains the amyloid peptide. Researcher figures out that many mis-sense mutations on APP protein responsible for FAD are located near to the gamar-secretase cleavage sites indicating the effect of alteration of APP protein cleavage on the cause of FAD.

Further studies on AD found that two homologous genes presenilin 1 (*PSEN1*) and presenilin 2 (*PSEN2*) are responsible for most of FAD cases (9, 10). *PSEN1* and *PSEN2* gens resides on chromosome 14 and 1 respectively. They encodes presenilin1 (PS1) and presenilin2 (PS2) proteins separately both of which are trans-membrane proteins. More than 150 identified mutations in these genes are reported to be related with FAD. Many of these mutations are found to cluster either within the transmembrane domain or along a sequence stretch in the

intracellular loop indicating their roles in modulating the substrate processing (11). Collectively, mutations from these three genes above (*APP, PSEN1* and *PSEN2*) are responsible for about 30 to 50 % of FAD cases, and about only 0.5 % of total AD cases (12).

It is found that late onset sporadic AD is responsible for the majority of AD cases. Unlike FAD, sporadic AD is not genetically inherited. Studies on sporadic AD reveal that some genetic mutations may act as risk factors which will increase the possibility for developing AD. Apolipoprotein E (*APOE*) ε4 is one of the well-studied major risk factors (13). *APOE* is a cytoplasmic apolipoprotein that acts on lipids transportation and metabolism. It is encoded by a gene on chromosome 19. There are 3 common alleles (ε2, ε3, and ε4) among which ε4 is found to be a major risk factor for AD in different ethnic groups and across different ages ranging from 40 to 90 (14). ApoE2 and ApoE3 function on the clearance of soluble and fibrillar forms of beta-amyloid (Aβ) via promoting its proteolysis. However, ApoE4 exhibits an impaired ability for Aβ clearance explaining the reason why it is the major risk factor for AD (14, 15).

1.3 Biochemistry of Alzheimer's Diseasea

Due to the deposition of the improperly folded proteins in brain tissue of AD patients, AD is also considered to be a protein mis-folding disease. Amyloid plaques commonly found in the brain tissue of AD patients contain Aβ peptides fragments ranging from 39 to 43 amino acids in length. Aβ is generated from proteolysis of APP protein via several intra-membrane cleavages events. APP is a type I transmembrane protein with a large extracellular domain and a small intracellular domain. APP contains the Aβ sequence. It undergoes proteolysis through two different pathways: the non-amyloidogenic pathway and the amyloidogenic pathway.

In the non-amyloidogenic pathway, which is the major physiological pathway, the large extracellular domain of APP is cleaved by α-secretase within the Aβ sequence releasing the soluble fragment of APP (sAPPα). α-Secretase is a type I membrane protein and a metalloprotease. It locates either on the cell surface or

in the cell membrane (16). The remaining membrane embedded fragment of APP (C83) after α-secretase cleavage then becomes the substrate for γ-secretase. The processing of C83 by γ-secretase then generates the p3 peptide and the APP intracellular domain (AICD). This pathway therefore avoids the production of aggregation prone form of Aβ peptide.

In the amyloidogenic pathway, Aβ is produced by sequential cleavage of APP by β-secretase and γ-secretase (**Figure 1.2**). β-secretase, also known as BACE (β-site of amyloid precursor protein cleaving enzyme) or Memapsin 2, is a membrane associated aspartic protease whose active site contains two aspartate residues locating in the extracellular domain of the protein (17). Cleavage of APP by β-secretase results in the soluble fragment (sAPPβ) and membrane embedded fragment (C99). Sequential cleavage of C99 by γ-secretase then releases the Aβ peptide and the AICD (18).

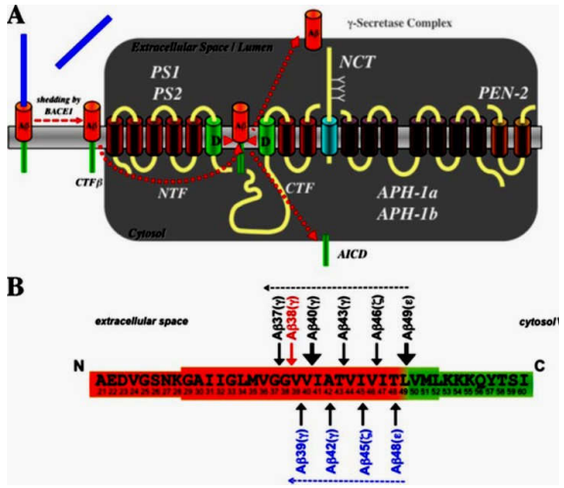

Figure 1.2: Illustration of amyloidogenic pathway of APP processing.
A. Sequential cleavage of APP by β-secretase and γ-secretase.
B. Multiple cleavage sites of γ-secretase on C99. Large black arrows indicate the major cleavage sites (enlarged); Dashed arrows indicate the cleavage direction. Orange color represents the transmembrane part of APP while its intracellular domain is in green (18).

1.4 Component of Gamma Secretase

In vivo (19, 20) and *in vitro* (21) reconstitution studies revealed that γ-secretase is composed of four subunits: Presenilin (PS1 or PS2), anterior pharynx defective

1 (APH1-a or APH1-b), nicastrin (NCT), and presenilin enhancer 2 (PEN2), each of which is indispensable for physiological activity of γ-Secretase (22). Heterogeneous co-expresseion of the four subunit in yeast indicated that γ-secretase may exist in a 1:1:1:1 stoichiometry (23).

Presenilins are 467 (PS1) or 448 (PS2) amino acids membrane proteins. PS1 and PS2 shares about 63 % sequence similarity. Evidence for presenilins containing the catalytic subunit of γ-secretase was obtained by mutation study on either of two conserved trans-membrane aspartate residues. Upon mutation, it is observed experimentally that Aβ production was substantially reduced and β-APP was significantly accumulated (24). Further evidence was found by photo-affinity labelling of presenilins by potent γ-secretase inhibitors. These inhibitors were designed to function as transition state analogue directing to the active sites of an aspartyl protease. The results showed that NTF-CTF and NTF-NTF dimer were labelled. However, the failure in labelling of the uncleaved form of PS1 suggested that intact PS1 may be an aspartyl protease zymogen. Its activation may require the presence of other γ-secretase subunit (25).

NCT is a 709 amino acid type I transmembrane glycoprotein. Kaether *et al* reported that PS is complexed with NCT through the secretory pathway to the cell surface during which presenilin bound NCT becomes glycosylated (26). Furtherly, Herreman *et al* found that glycosylation of nicastrin is not required for γ-secretase activity and NCT trafficking due to the observation that inhibition of nicastrin glycosylation by mannosidase I inhibitors did not affect the cleavage of substrates by γ-secretase and the immature nicastrin-presenilin complex still appeared at the cell surface (27). NCT within the γ–secretase is considered to function as the substrate receptor as evidenced by the observation that NCT co-immunoprecipitated the substrates of γ–secretase (28).

APH-1 are 265(APH-1a) or 257 (APH-1b) amino acids trans-membrane proteins. They are predicted to contain seven trans-membrane segments. By using co-immunoprecipitation and nickel affinity pull-down methods, Lee *et al* found that APH-1 associates with nicastrin and the heterodimers of the presenilin

N-terminal and C-terminal fragments (29). Within the γ–secretase complex, APH-1 functions as a presenilin stabilizer since inactivation of endogenous APH-1 leads to the decrease of presenilin levels, the accumulation of γ-Secretase substrate and the reduction of the relevant products (30).

PEN-2 is a 101 amino acids trans-membrane protein which spans the membrane two times with its N- and C-termini facing the lumen of the endoplasmic reticulum (ER) (31). By RNA interference study it was found that NCT and APH-1 stabilize the presenilin holo-protein in the complex, whereas PEN-2 initiates the auto-cleavage of presenilin and confers γ-secretase cleavage activity to the protease complex (32). PEN-2 is the last subunit which incorporates into γ-secretase. It not only functions as the activator of presenilin endo-proteolysis but also functions in the maturation of NCT as evidenced by the observation that its incorporation allows the trafficking of γ-secretase complex from ER to Golgi where NCT will be fully glycosylated (33).

However, *in vitro* reconstitution of bacterially expressed, recombinant presenilin into liposomes revealed that presenilin holo-protein itself is an zymogen and PEN-2 alone is sufficient enough to promote the endo-proteolysis of presenilin generating the active form of γ-secretase which is independent of other subunits (34). This finding by *Ahn K, et al* answered the long-standing question about the presenilin activation and the identity of presenilinase. The role of the other γ-secretase subunit identified via *in vivo* studies on the assembling, trafficking as well as maturation of γ-secretase into fully stable and active membrane protease complex therefore requires further investigations (35).

1.5 Structure analysis of presenilins

A topology of six trans-membrane segments of PS1 with the both N and C termini pointing to the cytoplasm was reported by Harris (36). In their study, different chimeric proteins were cloned by fusing a reporter protein to the C-terminal of each of the 10 potential trans-membrane segments identified by prediction. The reporter protein contains three artificial glycosylation sites. When the fusion protein is expressed *in vivo*, the reporter will be glycosylated. When the reporter

is located in the lumen of the ER or in the extracellular space, it will be protected from proteases cleavage from the cytoplasm. By this method PS1-NTF was found to span the membrane 6 times, while no trans-membrane fragment was observed for PS1-CTF although within which there are 3 TMs were predicted (36).

A seven trans-membrane segment model with the N-termini pointing to the extracellular space and the C-termini facing cytoplasm was proposed by Dewji *et al* (37). In their experiment, they use antibodies which were generated against particular sequences in the PS1 or PS2 protein. These specific antibodies allowed the detection of the epitopes of the PS proteins only when they were exposed at the cell surface. It was concluded that PS-NTF crosses membrane 6 times, while PS-CTF spans the membrane only one time (37). An opposite topology is proposed by Nakai *et al* (38). In their work, the C-terminal hydrophilic region of *E. coli* leader peptidase was fused to the C-terminal end of different PS1 deletion mutants as a reporter protein. Based on their *in vitro* and *in vivo* experiments, they reported similarly that N-terminal fragments contained six TM helixes and C-terminal contained only one TM helix. However, N-termini was found to face the cytoplasm and C-termini was found to point to the exoplasm just the opposite as found by Dewji NN *et al* (38).

Li *et al*. reported a topology of eight trans-membrane segments for PS with both the N and C termini facing the cytoplasm. In their study, β-galactosidase is fused to the C-terminus of different segments of PS. Due to the fact that β-galactosidase is active only within the cytoplasm of cells but not in the exoplasm, one can deduce the topology of the membrane protein by dectecting the β-galactosidase activity of different fused proteins. Again similar result was reported for PS-NTF with six TM helixes. However, for PS-CTF they argued that it spans membrane twice (39).

A study by Spasic D*, et al* investigating the trafficking and topology of PS1 using glycosylation consensus sequences inserted at different positions in PS1 revealed a nine trans-membrane segment topology. PS1 and PS2 knock-out cells

lines were used to eliminate the influence of endogenous PS due to its possible oligomerization with the fusion proteins. It was concluded according to their results that PS1-NTF crossed the membrane 6 times while PS1-CTF passed the membrane for 3 times with the N-termini facing the cytoplasm and the C-termini facing the exoplasm (40).

Collectively, all the structural information mentioned above agreed that the presenilin N-terminal domain passes the membrane six times and differ from each other with the C-terminal domain. Structural investigation of the PS1 C-terminal domain by NMR study revealed that the C-terminal domain contains three trans-membrane segments. However, the protein was produced by *in vitro* translation as a precipitate and solubilized with 100 mM SDS, therefore the structure validation might be compromised because of the well-known denaturing effect of SDS (41). What's more, the topologies concluded from fusion studies also depend to great extent on the nature of the fusion protein sequence which may itself influence the insertion of each hydrophobic segment into the bilayer membrane. Therefore the structural information of presenilin in its native state is still required to understand the mechanism how γ-secretase functions and furtherly the mechanism of AD disease.

1.6 Objective of this study

Given the biological importance of presenilin protein and the lack of its native structural information at atomatic level, the objective of this study was to heterologously express human PS2 and its N-terminal fragment as well as its C-terminal fragment in *E.coli* via *in vivo* or *in vitro* expression. The isolated protein was to be purified and characterised for subsequent structural studies through X-ray crystallography or NMR spectroscopy.

2 Materials and methods

2.1 Materials and their source

All chemicals for experimental purpose were purchased from Sigma, Calbiochem, Merck, Applichem, BMA, Fluka, and Affymetrix.

2.1.1 Kits

Zero Blunt Cloning Kit	Invitrogen
Rapid Ligation Kit	Fermentas
Thermo Sequence Fluorescent Labeled Primer Cycle Sequencing Kit with 7-Diaza- dGTP	GE-Healthcare
Nucleospin Plasmid	Macherey-Nagel
Plasmid Mini kit	Qiagen
In vitro translation kit	Qiagen
Gel Extraction Kit	Qiagen
Bio-Rad protein assay kit	Bio-Rad
Color Silver Stain Kit	Pierce
SEC calibration kit	Sigma
Initial screening suits for crystallization	Qiagen and Emerald
Membrane protein crystallization kit	Qiagen

2.1.2 Molecular biology materials

Phusion Hot Start DNA-polymerase	New England Biolabs
Restriction enzymes	Fermentas
Antarctic Phosphatase	New England Biolabs
Buffer QX1, Solubilization Buffer	Qiagen
Agarose	BMA

MassRuler™ High Range DNA Ladder	Fermentas
MassRuler™ Middle Range DNA Ladder	Fermentas
MassRuler™ Low Range DNA Ladder	Fermentas
PageRuler™ Prestained Protein Ladder	Fermentas
BenchMark™ Protein Ladder	Invitrogen

2.1.3 Resins and columns

Ni-NTA Agarose	Qiagen
Strep-tactin superflow high capacity resin	IBA BioTAGnology
Macro-prep High Q media	Biorad
HiLoad 10/30 Superose 6 ana column	GE Healthcare
HiLoad 16/60 Superdex 6 pg column	GE Healthcare
HiLoad 10/30 Superdex 200 ana column	GE Healthcare
HiLoad 16/60 Superdex 200 pg column	GE Healthcare

2.1.4 Instruments

Thermomixer compact	Eppendorf
PCR Thermo Cycler	PTC-200 (MJ research)
DNA-Sequencer:	Long Redair 4200 (MWG Biotech, Ebersberg, Germany)
Shaker	INFORS
Cell disruptor	EmulsiFlexC3 (Avestin Europe GmbH) Constant Cell Disruption System (Constant Systems, Northants, UK)
Micro-Centrifuge	5417R (Eppendorf)
Optima ™ Ultracentrifuge	TL-100CE (BECKMAN)
Avanti-Centrifuge	J-20XP (BECKMAN)

Optima ™ Ultracentrifuge	L-70K (BECKMAN)
Automated protein purification platform	ÄKTA Explorer (GE Healthcare)
Electrophoresis apparatus	BIO-RAD & GE Healthcare
Absorption Spectrometer	UV2101PC Spectrophotometer (Shimadzu, Germany)
UV 2401 PC Spectrophotometer	(Shimadzu, Germany)
Fluorescence Spectrometer	Spectrofluorophotometer QM-7 (Photon Technology International, Birmingham, NJ, USA)
RF 1501 Spectrofluorophotometer	(Shimadzu, Duisburg, Germany)
Circular Dichroism Spectrometer	J-810-Spectropolarimeter (Jasco)
Dynamic Light Scattering	Protein Solution (DynaPro)

2.1.5 Bacterial strains, vectors and plasmids

E.coli strain (manufacturer)	Genotype	Purpose
Top 10 (Invitrogen)	F- mcr A Δ (mrr-hsd RMS-mcr BC) φ 80lac ZΔ M15 Δlac X74 rec A1 ara D139 Δ (araleu) 7697 gal U gal K rps L (Str^R) end A1 nup G	plasmid DNA amplification
BL21-CodonPlus(DE3)-RP (Agilent Technologies)	F-ompT hsdS(rB^- mB^-) dcm^+ Tetr gal λ(DE3) endA Hte [argU proL Camr]	protein expression
BL21 Star™ (DE3) (Invitrogen)	F- ompT hsdSB (rB- mB-) gal dcm rne131 (DE3)	protein expression
C41(DE3) (Lucigen)	F- ompT hsdSB (rB- mB-) gal dcm (DE3)	protein expression
C43(DE3) (Lucigen)	F- ompT hsdSB (rB- mB-) gal dcm (DE3)	protein expression

Table 2.1: Bacterial strains used.

Vector (manufcturer)	Marker	Purpose (genes cloned)
pQE2 (GENEART)	Kanamycin	Human presenilin2 full length and its N-terminal as well as C-terminal gen were cloned into pQE2 vector for protein expression.
PBlunt (Invitrogen)	Kanamycin	clone blunt PCR fragments; screen for positive clone

Table 2.2: Vectors used for cloning and expression.

Bacterial strains used in this work is listed **Table 2.1**. Vectors used for cloning and expression are listed in **Table 2.2**. Different PS2-constructs information is listed in **Table 2.3**. Oligonucleotides were ordered from Eurofins MWG, Ebersberg, Germany. Detailed protein sequence information is shown in appendix I.

Construct short name	Construct detailed information
His-PS2-FL	Full length human presenilin2 with N-His tag
His-PS2-FL-Strep	Full length human presenilin2 with N-terminal His tag and C-terminal Strep tag
His-PS2-FL-Strep	N-terminal fragment of human presenilin2 with N-terminal His tag and C-terminal Strep tag
His-PS2-FL-Strep	C-terminal fragment of human presenilin2 with N-terminal His tag and C-terminal Strep tag

Table 2.3: Different PS2-constructs.

2.1.6 Miscellaneous materials

Cuvettes	Hellma
Amicon Ultra centrifugal device	Millipore
Complete, EDTA-free Protease Inhibitor Cocktail Tablet	Roche Applied Science
Deoxyribonuclease-I from bovine pancreas	Sigma
GelRed Nucleic acid stain	Biotium Inc.

2.1.7 Media

Media	Recipe (/ L)	Purpose
LB	10 g Tryptone 5 g Yeast Extract; 10 g NaCl	Plasmid preparation
DYT	16 g Tryptone 10 g Yeast Extract 5 g NaCl	Transformation and Protein expression
TB	12 g Tryptone 24 g Yeast Extract 4 ml Glycerol 12.54 g K_2HPO_4 2.31 g KH_2PO_4	Protein expression

Table 2.4: Media used for cloning and expression.
All components are weighted and dissolved in Milli-Q water and autoclaved at 121 ℃ for 20 minutes before usage.

2.1.8 Buffers and solutions

Buffers for Agarose gel electrophoresis

TAE:	40 mM Tris, 1 mM EDTA, pH 8.0
Orange Loading buffer:	10 mM Tris.HCl, 0.15 % Orange G, 0.03 % Xylene cyanol FF, 60 mM EDTA

Buffers for DNA Sequencing

Sequencing gel:	21 g Urea, 32 ml Water, 5 ml 10xTBE, 500 µl DMSO, 4.3 ml Rapid Gel XL, 50 µl TEMED, 350 µl APS
10xTBE:	162 g Tris Base, 27.5 g Boric acid, 9.3 g EDTA pH 8.3-8.7
Licor Loading Dye:	95 % Formamide, 20 mM EDTA, 0.1 % Xylen cyanol FF

Buffers for SDS Polyacrylamide gel electrophoresis

Solution components	5 % Stacking gel (10 ml)
H_2O	6.8
30 % Acrylamide	1.7
1.0 M Tris, pH 6.8	1.25
10 % SDS	0.1
10 % ammonium persulfate	0.1
TEMED	0.01

Table 2.5: Solutions for preparing 5 % stacking gel.

Solution components	12 % Resolving gel (25 ml)	15 % Resolving gel (25 ml)
H_2O	8.2	5,7
30 % Acrylamide	10.0	12.5
1.0 M Tris, pH 6.8	6.3	6.3
10 % SDS	0.25	0.25
10 % APS	0.25	0.25
TEMED	0.01	0.01

Table 2.6: Solutions for preparing 12 or 15 % resolving gel.

SDS-Sample buffer:	62 mM Tris, 2 % (w/v) SDS, 5 % (v/v) β-Mercaptoethanol, 20%(w/v) Glycerol,

	0.2 % (w/v) Bromophenole blue
Running buffer:	25 mM Tris, 192 mM Glycine,
	0.1 % (w/v) SDS
Coomassie staining solution:	0.05 % (w/v) Coomassie blue R250,
	10 % (v/v) Acetic acid, 25% (v/v) Ethanol
Destaining solution:	10 % (v/v) Acetic acid

<u>Buffers for western blot</u>

Blot buffer:	39 mM Glycine; 48 mM Tris base; 20 % Methanol;
TBS buffer:	20 mM Tris base pH 7.6; 137 mM NaCl;
TBS-Tween buffer:	20 mM Tris base pH 7.6; 137 mM NaCl; 0.1 % Tween 20

<u>Buffers for Ni-NTA purification under denaturing condition</u>

Lysis buffer:	100 mM NaH_2PO_4; 10 mM Tris Cl; pH 8.0;
	10 % Glycerol; 20 mM β-mercaptoethanol;
	1mM PMSF; protease inhibitor ;
	1 mg/ml Lysozyme; DNAse;
Solubilisation buffer:	100 mM NaH_2PO_4; 10 mM Tris Cl; pH 8.0;
	10 % Glycerol; 20 mM β-mercaptoethanol;
	1 mM PMSF; 20 mM Imidazole; 6 M Urea
	1 % N-Lauroylsarcosine sodium salt;
Wash buffer:	100 mM NaH_2PO_4; 10 mM Tris Cl; pH 8.0;
	10 % Glycerol; 20 mM β-mercaptoethanol;
	1 mM PMSF; 25 mM Imidazole; 6 M Urea
	0.4 % N-Lauroylsarcosine sodium salt;
Elution buffer:	100 mM NaH_2PO_4; 10 mM Tris Cl; pH 8.0;
	10 % Glycerol; 20 mM β-mercaptoethanol;
	1 mM PMSF; 300 mM Imidazole; 6 M Urea
	0.4 % NLS;

<u>Buffers for Ni-NTA purification under native condition</u>

Lysis buffer:	20 mM Tris HCl; pH 8.0; 10 % Glycerol;

	Protease inhibitor (1 piece/ 50 ml buffer);
	1mM PMSF; 1 mg/ml Lysozyme; DNAse
	(5 mg/50 g cell pellet); 1mM TCEP;
	NaCl is added to 300 mM after cell opening.
Membrane wash buffer:	20 mM Tris-HCl; pH 8.0; 10 % Glycerol;
	300 mM NaCl; 1mM PMSF; protease inhibitor;
	1 mM TCEP;
Solubilisation buffer:	20 mM Tris-HCl; pH 8.0; 10 % Glycerol;
	300 mM NaCl; 1mM PMSF; protease inhibitor;
	1 mM TCEP; 1 % FC12; 10 mM imidazole;
Wash buffer:	20 mM Tris-HCl; pH 8.0; 10 % Glycerol;
	300-1000 mM NaCl; 1mM PMSF;
	Protease inhibitor; 1mM TCEP;
	0.094 % FC12; 10-25 mM imidazole;
Elution buffer:	20 mM Tris-HCl; pH 8.0; 10 % Glycerol;
	300 mM NaCl; 1mM PMSF; protease inhibitor;
	1 mM TCEP; 0.094 % FC12; 100 mM imidazole;

Buffers for Strep-Tactin purification under native condition

Strep-tag binding buffer:	20 mM Tris-HCl; pH 8.0; 10 % Glycerol;
	300 mM NaCl; 1mM PMSF; protease inhibitor;
	1 mM TCEP; 0.094 % FC12;
Strep-tag washing buffer:	20 mM Tris-HCl; pH 8.0; 10 % Glycerol;
	300 mM NaCl; 1mM PMSF; protease inhibitor;
	1 mM TCEP; 0.094 % FC12;
Strep-tag elution buffer:	20 mM Tris-HCl; pH 8.0; 10 % Glycerol;
	300 mM NaCl; 1mM PMSF; protease inhibitor;
	1 mM TCEP; 0.094 % FC12; 2.5mM desthiobiotin;

Buffer for Size exclusion chromatography under denaturing condition:

100 mM NaH_2PO_4; 10 mM Tris;6 M urea;
10 % Glycerol; 0.4 % NLS; 1 mM TCEP;
Protease Inhibitor, pH 8.0;

Buffer for Size exclusion chromatography under native condition:

20 mM Tris-HCl; pH 8.0; 10 % Glycerol;
300 mM NaCl; 1mM PMSF; protease inhibitor;
1 mM TCEP; 0.071 % FC12;

Buffers for Refolding of His-PS2-Strep：

Ni-NTA binding buffer:	100 mM NaH2PO4; 10 mM Tris pH 8.0;
	6 M urea; 30 % Glycerol; 0.4 % NLS;
	2 mM TCEP; Protease Inhibitor;
Refolding buffer:	100 mM NaH2PO4; 10 mM Tris; pH 7.4;
	30 % Glycerol; 2 mM TCEP, Protease Inhibitor,
Solubilization buffer:	10 mM NaH2PO4 pH 7.4; 10 % Glycerol;
	2 mM TCEP; Protease Inhibitor;
	0.043 % Cy 6 (or 0.073 % FC12);
Pellet solubilisation buffer:	20 mM Tris-HCl pH 8.0; 10 % Glycerol; 6 M Urea;
	1 mM TCEP; Protease inhibitor; 1 % SDS;
Ni-NTA elution buffer:	10 mM NaH2PO4 pH 7.4; 10 % Glycerol;
	1 mM TCEP; Protease Inhibitor;
	0.043 % Cy 6 (or 0.073 % FC12);
	300 mM imidazole;
PD-10 elution buffer:	10 mM NaH2PO4 pH 7.4; 10 % Glycerol;
	1 mM TCEP; Protease Inhibitor;
	0.043 % Cy 6 (or 0.073 % FC12);

2.2 Methods

2.2.1 Cloning

2.2.1.1 Principle

DNA cloning is defined as a process for faithfully reproducing DNA fragments via *in vivo* or *in vitro experiments*. *In vivo*, generally a vector carrying the DNA fragment of interest is used to bring the DNA into the host cell, a process which is called transformation. The transformed cell derives resistance to the certain antibiotic. Therefore only cells carrying the desired plasmid can be grown. The harvested cell was used to purify the desired plasmid. By doing this the required

plasmid is amplified. *In vitro*, the polymerase chain reaction (PCR) can be used. The cloning process normally is made up by four steps. Firstly, the gene of interest (insert) is digested with restriction enzymes from either a PCR product or a plasmid. Secondly, host plasmid (vector) is digested with same restriction enzymes producing the same type of end suitable for ligation of insert into vector. Thirdly, restriction enzymes digested insert and vector are ligated by an enzyme called ligase yielding a new plasmid carrying the gene of interest. Finally, the product plasmid is then transformed into bacterium cells to amplify identical copies (42, 43).

In this work, different restriction enzymes are used for each end of the insert. This will increase the possibility for correct direction of inserts. The vectors are dephosphorylated by alkaline phosphatase. This will reduce the self-ligation of vector which may produce false positive results. An additional screening method is also used to clone PCR product into pBlunt cloning vector whose multiple cloning site is located within a lethal gene. An introduction of insert into this gene will deactivate the lethal gene. Only with deactivation of this gene will the clone grow. The pBlunt plasmid was then purified and sequenced. The colony which gives the correct sequence information for the insert is used for ligation into expression vector (44).

2.2.1.2 Experiment

In this work, full length human presenilin 2 was cloned into pQE2 vector encoding an N-terminal his tag. To facilitate purification, furthermore a C-terminal strep tag was later introduced by cloning it into the His-PS2-FL plasmid. The N-terminal and C-terminal fragment of human presenilin 2 were also cloned with N-terminal his tag and C-terminal strep tag.

For introduction of the C-terminal strep tag into the pesenilin 2 proteins full length His-PS2-FL plasmid was used as the template. The part of the gene of interest was amplified by PCR using gene specific primers. The primer was designed to contain restriction site of Nde Ⅰ and Xho Ⅰ in the forward and reverse direction respectively (**Table 2.7**). The PCR setup and the cycling

condition are described in **Table 2.8** and **Table 2.9**, respectively. The PCR product was furtherly purified by agrose gel electrophoresis. The bands corresponding to the respective product was extracted using Gel Extraction Kit. The purified insert was then ligated into pBlunt vector using Zero Blunt Cloning Kit. The ligation mixture was transformed into Top 10 competent cell for amplification. The purified plasmid was subjected to restriction enzyme digestion and sequencing for confirmation of the insert. A positive colony was used for further ligation into pQE2 vector. The double digested insert and the pQE2 vector was ligated using rapid ligation kit. The prepared plasmid was subjected to restriction enzyme digestion and sequencing for confirmation of the insert.

Primers	Sequence (5'-3')	Usage
1	GG CAT ATG AAG CAC CAT CAT CAC CAT CAC CTG ACC TTT ATG GCG AGC GAT AGC	Forward primer for full length cloning
2	GG CTC GAG TTA TTT TTC GAA CTG CGG GTG GCT CCA AGC GCT AAT ATA CAG CTG ATG GCT GGC CAG G	Reverse primer for full length cloning
3	GG CAT ATG AAG CAC CAT CAT CAC CAT CAC GTG TGG ACC GTG GGC ATG GC	Forward primer for C-termianl cloning
4	GG CTC GAG TTA TTT TTC GAA CTG CGG GTG GCT CCA AGC GCT TGC GCT AGA ATA AAT CAG CGC CGG	Reverse primer for N-termianl cloning

Table 2.7: Primers used for cloning.
Red color represents the Nde Ⅰ site; green color represents the Xho Ⅰ site; blue represents his tag; pink represents strep tag.

Component	Volume / 50 µl reaction	Final conc.
Autoclaved milli-Q H_2O	add to 50 µl	
5x Phusion HF Buffer	10 µl	1x
10 mM dNTPs	1 µl	200 µM each
Primer A	1 µl	2 µM
Primer B	1 µl	2 µM
Template DNA	1 µl of 1.83 ng/µl	
DMSO 100 %	5 µl	10 %
Phusion Hot Start DNA Polymerase (2 U/µl)	0.5 µl	0.02 U/µl

Table 2.8:PCR setup.

Steps	PS2-FL	PS2-NTF	PS2-CTF
Initial denaturation	98 °C 30 s	98 °C 30 s	98 °C 30 s
Denaturation	98 °C 10 s	98 °C 10 s	98 °C 10 s
Annealing	66 °C 10 s	68 °C 10 s	72 °C 10 s
Extension	72 °C 21 s	72 °C 14 s	72 °C 7 s
Cycles	50		
Final extension	72 °C 5 min	72 °C 5 min	72 °C 5 min

Table 2.9: Cycling conditions.

2.2.2 Expression

1 µL of the respective plasmid (about 50 ng) was transformed into 100 µL C43 (DE3) competent cells. The transformation was spread on agar plates containing 50 µg/ml Kanamycin to select transformed cells. After over night incubation at 37 °C，several colonies were picked and inoculated into 250 ml TB medium containing 50 µg/ml Kanamycin and 2 % glucose. Cells were then grown over night at 37°C with shaking at 120 rpm to prepare the preculture. The next day twelve baffled flasks each containing 250 ml TB medium supplemented with 50 µg/ml Kanamycin were inoculated with 10 ml of the preculture. Cells were then grown at 30 °C to an OD_{600} of 0.8 to 1.0. Induction was then performed by adding IPTG to the final concentration of 0.2 mM. After induction, cells were grown at 18 °C 16 h at 120 rpm for protein expression. Cells were harvested by centrifugation (4 ℃, 7000 × g, 20 min) and subsequently subjected to osmotic shock (**Section 2.2.4.2**) before being opened for purification or frozen at -80 ℃ for storage.

2.2.3 Cell lysis and fractionation

Cell pellet was thawed and resuspended in 10 ml lysis buffer per g pellet with stirring at 4 ℃ in cold room. The suspension was then passed through the cell disruptor 3 times with a pressure of 15 000 to 20 000 psi. EDTA and NaCl were added into the cell lysate to 10 mM and 300 mM final concentration respectively. To remove unbroken cells, the suspension was centrifuged at a speed of 900 ×g for 15 min. Supernatant after 900 ×g was then centrifuged at a minimum speed of 7 000 ×g for 30 min to remove inclusion body. Supernatant from 7 000 ×g was centrifuged at a speed of 100 000 ×g for 1 h to collect the membrane fraction. For removal of the EDTA and the soluble proteins, the collected membrane was then resuspended and homogenized by glass porter with lysis buffer and pelleted down again for subsequent solubilsation. All centrifugations were performed at 4 ℃ (45, 46).

2.2.4 Purification

2.2.4.1 Immobilized metal affinity chromatography (IMAC)

2.2.4.1.1 Principle of IMAC

Immobilized metal affinity chromatography (IMAC) is a purification method based on the specific coordination of certain amino acids with metal ions immobilized onto the purification matrix. In this technique, metal ions such as cobalt, nickel and copper are often used. Amino acids such as histidine cysteine and tryptophan could specifically form complexes with metal ions immobilised onto the matrix.

A small poly-histidine tag which will not interfere the folding of target protein could be introduced to the protein of interest by recombinant DNA technology. Due to the higher affinity of his-tagged protein to the stationary phase immobilized with metal ions, any host proteins that bind non-specifically to the resin can be easily washed away without affecting the binding of tagged proteins therefore achieving purification purpose. Low concentrations of a histidine analogue, imidazole can be used to reduce the binding of unwanted impurities and to washed away the proteins which bind less strongly to the metal ions. Elution of the protein of interest can be achieved with higher imidazole concentrations **(Figure 2.1** and **Figure 2.2)**.

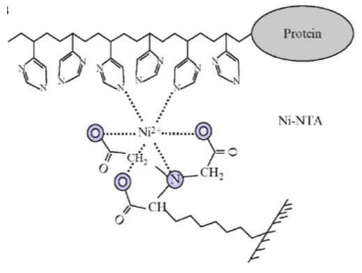

Figure 2.1:A model of interaction between the 6×His tag and Ni-NTA matrix.
Protein in grey with 6×His tag binding to immobilised Ni-NTA is shown (47).

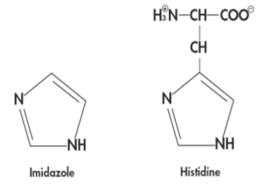

Figure 2.2: Chemical structures of histidine and imidazole.

The binding strength between a protein and a metal ion is affected principally by several factors, including the general properties of the affinity tag used, the accessibility of the affinity tag, the type of metal ion used, the pH and ionic strength of buffers. Thus, optimization of the above factors is crucial to the success of specific protein purification.

In *E.coli* expression systems, the recombinant soluble proteins are usually expressed at high levels, and the level of co-purifying contaminant proteins is relatively low. For membrane proteins, the expression level are generally low due to its toxicity therefore excessive matrix is needed to fully capture the low-expressed protein. However, the use of excessive matrix will also bring in more impurities. To this end, optimisation of the ratio between the matrix needed to the target protein should be carried out for a successful membrane protein purification. What's more, washing of the membrane pellet which will remove most of the soluble protein and loosely membrane associated protein is found to be very helpful for the final purity (47).

2.2.4.1.2 Ni-NTA and Co-NTA purification

In this work Ni-NTA and Co-NTA were used for purification in batch mode or on column mode. For column mode, briefly, the column which contains the relevant matrix is firstly equilibrated with 5 CV of binding buffer. Then the solubilised supernatant containing the target protein is passed through the column at a flow rate about 0.3 ml/min. The flow through is collected and reapplied to the column three times to allow more complete binding. Washing out of the impurities is achieved by passing through the column around 20 CV of wash buffer containing low concentration of imidazole. Elution of the target protein is realized by 5 ×1

CV of elution buffer containing high concentration of imidazole. The batch mode is more or less the same as described in column mode except that the binding is carried out outside the column by incubating the matrix with the solubilised protein for 2 h with gentle shaking at 4 ℃.

Co-NTA matrix is obtained by removing the Ni ions from the matrix and replacing then with Co ions according to the regeneration protocol (Qiagen). The purification procedure by Co-NTA is the same as described above.

2.2.4.2 Removal of periplasmic fraction by osmotic shock

2.2.4.2.1 Principle

It is reported that under stress conditions (such as protein overexpression) *E. coli* will produce highly specific metal chelators which are mainly located within the periplasmic space of *E. coli.* These metal chelators will cause metal ions leakage from the column hence significantly reduced the binding capacity of the column. Furthermore, it will also cause the migration of His-tagged protein on IMAC column which will reduce the efficiency of purification. Therefore, the purification of low abundance protein can be improved significantly after removal of the periplasmic fraction (48).

2.2.4.2.2 Experiment

For the above reason, the periplasmic fraction was removed before IMAC purification: Immediately after expression, harvested cell pellet was resuspended in 5 ml/g sucrose buffer (50 mM HEPES, 20% sucrose, 1 mM EDTA pH 7.9). After resuspension, cells were pelleted by centrifugation at 7,000 x g for 30 min at 4 °C. The supernatant was discarded and the pellet was resuspended in 5 ml/g of 5 mM $MgSO_4$ and incubated on ice for 10 min. Cells were finally pelleted down by centrifugation at 4,500 x g for 20 min at 4 °C. The supernatant was discarded and the pellet was resuspended in 7 ml/g pellet lysis buffer and thereby subjected to cell lysis.

2.2.4.3 Strep-Tactin purification

2.2.4.3.1 Principle

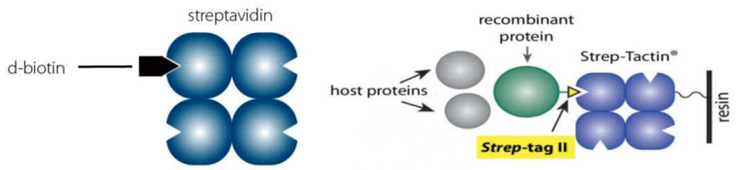

Figure 2.3: Schematic illustration of Strep-tag purification system.
Binding of biotin to streptavidin (left) and Strep-tag II to Strep-Taction (right) (49).

The Strep-tag purification system is principally based on the binding of biotin to streptavidin. After systematic optimization, Strep tag II and Strep-Tactin system has been proved to be a reliable protein purification technique. Strep tag II is an 8 amino acids (WSHPQFEK) peptide which could bind to the same position where the natural ligand D-biotin is bound with steptavidin. Strep-Tactin is an engineered steptavidin with nearly 100 times higher binding capacity compared to steptavidin. It is found that Strep tag II generally has negligible effect on the recombinant protein folding and bioactivity and can be introduced by cloning to either N- or C-terminus of the gene of interest. Therefore Strep tag II and Strep-Tactin system can be applied for the efficient purification of corresponding fusion proteins on affinity columns with immobilized Strep-Tactin **(Figure 2.3)** (50).

2.2.4.3.2 Purification

A strep tag purification cycle consists of load, wash, elution and regeneration steps. The cell lysate containing protein with fused Strep tag II peptide is loaded to a column with immobilized Strep-Tactin. For better binding, the flow through is recollected and reapplied to the column twice. Removal of host proteins is achieved by washing the column with 5 CV of wash buffer. Elution of Strep tag II fused protein is achieved via competition with 2.5 mM D-desthiobiotin which is an inexpensive, reversibly binding and stable analog of biotin. D-desthiobiotin can be removed from the Strep-Tactin by application of a HABA (2-[4'-hydroxy-benzeneazo] benzoic acid) solution via an indication of colour change from yellow-orange to red. For regeneration of the column, HABA is

washed out with a small volume of binding buffer. The disappearance of the red colour indicates that the column is ready for next purification run.

2.2.4.4 Ion Exchange Chromatography (IEX)

2.2.4.4.1 IEX Principle

Ion exchange chromatography (IEX) is a purification technique that allows the separation of biomolecules based on their net surface charges. Positively charged biomolecules could be absorbed by the negatively charged exchanger in cation exchange chromatography and vice versa.

A typical IEX purification consists of equilibration, absorption, washing, and elution steps. The binding and the binding strength depends on to a great extent the net surface charge of a biomolecule. Biomolecules may vary considerably in their net charge properties under different buffer conditions. Hence, the pH and ionic strength of the equilibration buffer are critical for the absorption of target proteins and the prevention of the binding of impurities to the medium. After absorption of the target protein, the unbound or loosely bound protein is washed away with the same equilibration buffer. Elution of the bound protein is often carried out via a linear gradient of increasing ionic strength in the elution buffer. The elution volume of the certain protein is depending on the strength of the interaction between the protein and the medium. At a given pH, the stronger the interaction the higher the ionic strength that is needed for elution and therefore the higher the elution volume. In this way proteins binding to the matrix with different strength are eluted differentially achieving purification purpose (51, 52).

2.2.4.4.2 IEX purification

After Ni-NTA purification, poor purity was obtained for His-PS2-FL. His-PS2-FL has a PI of 4.80 and therefore is negatively charged at pH 8.0. Hence, an anion exchanger Macro-Pre High Q support matrix was used for further purification.
Before upscale purification, the optimal matrix to target protein ratio and NaCl concentration for binding was determined by small scale experiments. Briefly,

Ni-NTA elutes corresponding to equal amount of cell pellet were incubated with 10 50 and 100 µl of IEX-matrix respectively with gentle mixing for 1 h at 4℃. After centrifugation, the supernatant (named flow through) was collected and aliquoted for analysis. The bound protein was then eluted from the matrix by adding equal volume of elution buffer containing 2 M NaCl. Samples corresponds to the same part of cell pellet was loaded onto a 12 % SDS-PAGE. His-PS2-FL was detected by coomassie staining and western blot.

After determination of the matrix to target protein ratio, Ni-NTA elution fractions corresponding to equal amount of cell pellet were incubated with the chosen matrix volume at the identical condition except for the addition of NaCl to 0, 100, 200, 300, 350, 400, 450 and 500 mM respectively. After centrifugation, only the flow through was collected and aliquoted for analysis. In this way, the optimal NaCl concentration for binding was determined.

2.2.5 Ammonium sulphate precipitation (ASP)

2.2.5.1 Principle

Ammonium sulfate precipitation is a classic protein purification and concentration method based on the salting out effect of salt on solutes. The solubility of different proteins varies at a given ionic strength of the solution (53). Therefore, as salt concentration gradually increases, protein with increasing solubility will precipitate out of the solution sequentially. At each concentration step, after the reaction reach equilibrium, centrifugation will be performed to separate the supernatant and pellet fraction hence achieving purification of certain protein from a protein mixture.

Due to bound lipids or detergents, some membrane pellet precipitated by ammonium sulfate has lower density than protein only precipitates. During centrifugation, these precipitates will often float to the top of tube rather than forming a pellet.

2.2.5.2 Experiment

200 µl (corresponds to 40 mg cell pellet) of the solubilised His-PS2-FL was mixed with indicated volume of buffer and 100 % saturated Ammonium sulphate (AS) solution to get the desired degree of saturation of AS (Table 2.10). Each 1 ml reaction in 1.5 ml eppendorf tubes was kept at 4 ℃ cold room with stirring for 1 h for full equilibration. Centrifugation at 22 000 ×g for 30 min at 4 ℃ was performed to separate supernatant and pellet. The supernatant after AS precipiatation was then removed carefully with a 1 ml syringe (27 G diameter needle) and submitted to TCA precipitation to separate AS from protein for SDS-PAGE analysis. The pellet after AS precipiatation was dissolved in 400 µl pellet solubilisation buffer by stirring for 5 h at 4 ℃.

Groups	Percent of saturated $(NH_4)_2SO_4$ solution %	Volume of saturated $(NH_4)_2SO_4$ added µl	Volume of buffer added µl	Volume of solubilised His-PS2-FL µl	Final Volume of each reaction µl
1	10	100	700	200	1000
2	20	200	600	200	1000
3	30	300	500	200	1000
4	40	400	400	200	1000
5	50	500	300	200	1000
6	60	600	200	200	1000
7	70	700	100	200	1000
8	80	800	0	200	1000

Table 2.10: Ammonium sulphate precipitation experiment setup.

Floating pellets was observed for group 6, 7 and 8 where AS concentration was 60, 70 and 80 % respectively. Supernatant from those groups was directly poured out into another tube and subjected to centrifugations to separate the supernatant from the floating pellet. The obtained floating pellet was dissolved in 400 µl pellet solubilisation buffer by stirring for 3 h at RT. After TCA precipitation, the pellet was dissolved in 400 µl pellet solubilisation buffer with stirring for 3 h at RT. Samples from each fraction in each group was analyzed by SDS-PAGE and Western blot analysis for the presence of His-PS2-FL.

2.2.6 Size exclusion chromatography (SEC)

2.2.6.1 Principle of SEC

Size exclusion chromatography (SEC) is a chromatographic purification method based on the size of the biomolecules. Usually, gel matrix with certain size cut-off is used to separate biomolecules. Molecules will diffuse into the beads to greater or lesser extent base on their size. Molecules which have a smaller size than the cut-off of the matrix could diffuse more into the pores of the beads and therefore move through the bed more slowly (with higher elution volume), while larger molecules enter less or not at all and thus move through the bed more quickly (with lower elution volume). Given these characteristics, SEC can be used for group separation (desalting, buffer exchange), fractionation (purification) and size analysis (homogeneity).

For globular protein, Superpose 6 matrix can achieve high-resolution separations across exceptionally an broad molecular weight range (5 000 to 5 000 000 Da) which makes it suitable for studying membrane proteins given their preference to form aggregates and oligomers. Superdex 200 matrix exhibits good resolution at the Mw range from 10 000 up to 600 000 Da for globular proteins and it is suitable for a polishing step in purification. In this study, superpose 6 and superdex 200 analytical columns were used for protein detergent complex molecular weight determination and the investigation of their stability as well as their homogeneity. Superdex 200 prepare grade columns was used for His-PS2-NTF-Strep upscale purification. PD-10 column which has a Sephadex G-25 matrix was used for buffer exchange and desalting (54, 55).

2.2.6.2 Column calibration

For calibration, the column was equilibrated with 2 CV of the gel filtration buffer. 0.1 ml of the protein standards as listed in **Table 2.11** dissolved in gel filtration buffer (at a concentration of 0.2 mg/ml) was injected into a 0.1 ml loop and the protein was eluted with 1.5 CV of gel filtration buffer at a flow rate of 0.3 ml/min.

Elution profiles of proteins standards were shown in **Figure 2.4** and **Figure 2.6**. Calibration curves were obtained by plotting Lg (Mw) versus *Kav* and Lg (nm) versus *Kav* as shown in **Figure 2.5** and **Figure 2.7**. Mw is the molecular weight of the protein standard and nm is its radius. *Kav* of each protein was calculated using the following formula:

$K_{av} = (V_e - V_0)/ (V_t - V_0)$

Where V_e is the elution volume, V_0 is the void volume and V_t is the total column volume. Therefore *Kav* represents the fraction of stationary column volume available for diffusion of a given bimolecular.

Proteins standards	**MW (Da)**	**Radias by DLS (nm)**	**Elution volume on superpose 6 (ml)**	**Elution volume on superdex 200 (ml)**
Acetone	58		21.53	20.96
Cytochrome c, horse heart	12 400	1.80	18.8	17.31
Carbonic Anhydrase, bovine erythrocytes	29 000	2.60	17.9	15.86
Albumin from chicken egg white	44 287	3.10	17.07	14.60
Albumin from bovine serum	66 000	3.70	16.32	13.42
Alcohol Dehydrogenase, yeast	150 000	4.50	15.71	12.18
β-Amylase, sweet potato	200 000	5.90	15.00	11.25
Ferritin peak Ⅲ	443 000	6.90	14.06	9.99
Thyroglobulin from porcine thyroid gland	670 000	8.70	12.12	
Ferritin peak Ⅱ	886 000	9.40	12.25	
Blue dextran	2000 000	44.10	7.55	7.86
Ferritin peak Ⅰ	32000 000	50.10	7.43	7.80

Table 2.11: MW, radius and the elution volume for each proteins standard.

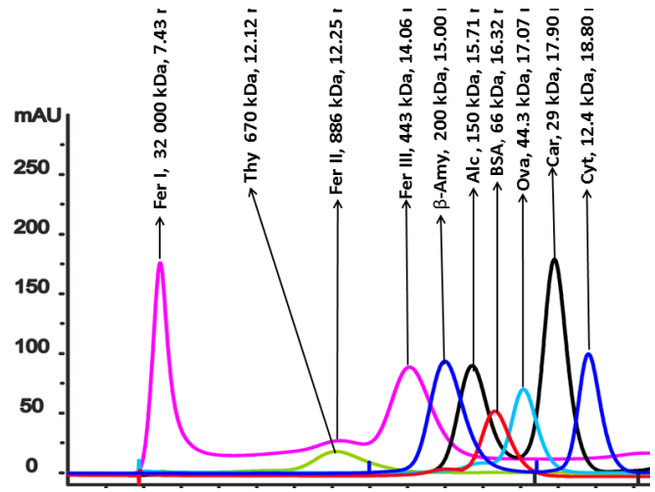

Figure 2.4: SEC profiles of the protein standards on superpose 6 analytical column.
Each color represents one single run. Protein standards short name (the first three letters of the full name) and the molecular weight as well as the elution volume are shown above the peak. Ferritin peak I was eluted at 7.43 ml, this value was taken for the V_0.

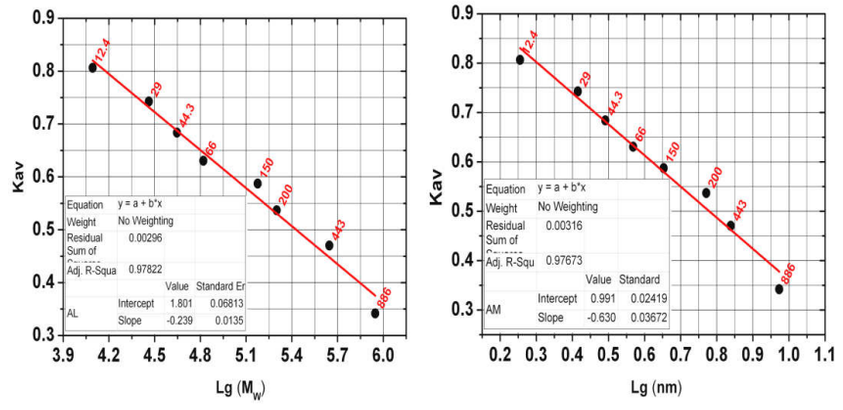

Figure 2.5: Calibration curves of superpose 6 analytical column.
Plot of Lg (Mw) versus *Kav* (left) and Lg (nm) versus *Kav* (right).

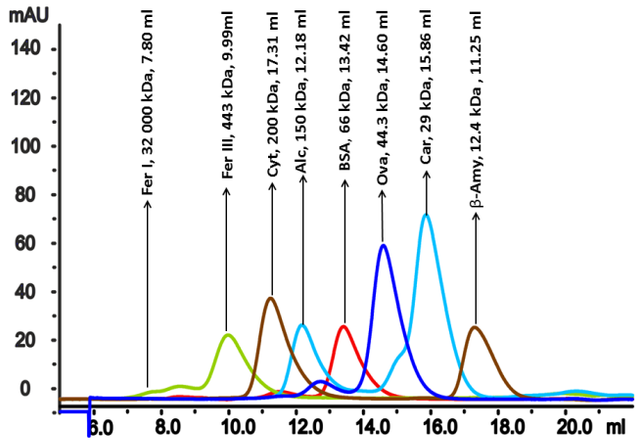

Figure 2.6: SEC profiles of the protein standards on superdex 200 analytical column.
Each color represents one single run. Protein standards short name (the first three letters of the full name) and the molecular weight as well as the elution volume are shown above the peak. Ferritin peak I was eluted at 7.80 ml, this value was taken for the V_0.

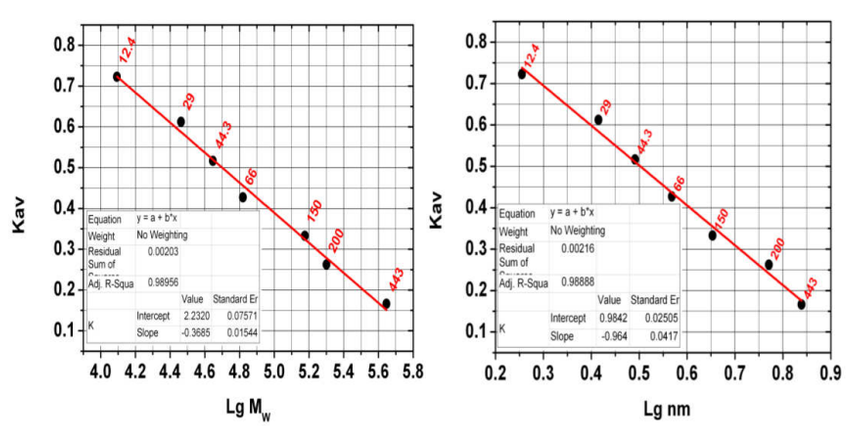

Figure 2.7: Calibration curve of superdex 200 analytical column.
Plot of Lg (Mw) versus *Kav* (left) and Lg (nm) versus *Kav* (right).

2.2.6.3 SEC measurements

To investigate the molecular weight of a protein detergent complex, the purified protein was eluted with the gel filtration buffer containing the relevant detergent. The same running conditions were used as for calibration.

2.2.7 Mass spectrometry (MS)

2.2.7.1 Principle of MS

Mass spectrometry (MS) is an analytical method for the determination of biomolecule mass. A typical MS measurement consists of two basic processes. Firstly, the sample is ionised to generated charged molecules or molecule fragments. Secondly, the mass-to-charge ratios of these ionised species are measured from which their masses are calculated. (56).

As illustrated, a MS spectrometer consists of an ion source, a mass analyser and a detector (**Figure 2.8**). The ion source is used to convert biomolecules into ions which will fly under the magnetic field; the mass analyser functions in sorting the ions by their masses; while the detector measures the abundance of each mass species.

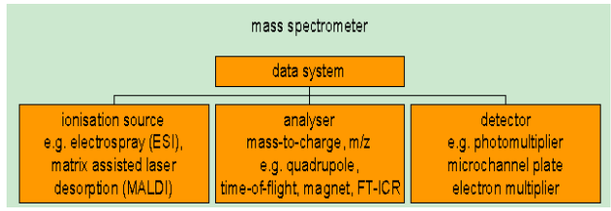

Figure 2.8: Simplified schematic of a mass spectrometer.
An ion source, a mass analyzer and a detector are shown (57).

A matrix assisted ionization technique (Matrix Associated Laser Desorption Ionization-Time of Flight, MALDI-TOF) is very often applied for the ionisation of sample. Briefly, the protein sample is mixed with an organic matrix. The mixture is then applied to a metal sample plate and dried at room temperature. The plate was then loaded into the MS spectrometer. After evaporation of water, the resulting sample crystals are subjected to laser pulses to excite the matrix. The sample is then ionised via proton transfer by excited matrix. The ionised sample is mainly singly charged. When a magnetic field is applied, the charged ions will obtain an amount of energy to drive the ions to the detector. Ions of lower mass will travel to the detector with a higher speed than the heavier ones. The distance the ion needs to reach the detector is constant therefore the time required for each ion to reach the detector mainly depends on its mass. In this

way, the molecular masses can be determined, using the fact that the mass of a molecule is proportional to the square of the flight time (58). For accurate mass determination, calibration with known standards is necessary. For samples requiring further separation, tandem MS (MS/MS) can be applied. One or several parental ions from the first MS will be fragmented into smaller ions and separated again by their mass-to-charge ratio (59).

For a given protein, the amino acid sequence is unique. The masses species and abundance of the digested fragments by a known protease will therefore provide a fingerprint. Hence, a protein finger print data base could be set up. The measured MS data of the protein of interest will provide the information such as the quantity, the modifications and the mass of the peptides fragment with nano-gram sensitivity. When searching against the data base, the matching peptide masses could be used for protein identification. The most commonly used MS method to identify proteins is a combination of peptide mass fingerprinting and amino acid sequencing via tandem MS (59).

Experimentally, proteins of interest are firstly separated via gel electrophoresis. The protein band or spot of interest is excised, reduced and alkylated and then digested by protease with high specificity such as trypsin. Next, the supernatant of digested peptides is then collected and applied to a mass spectrometer. The peptide mass fingerprinting of the studied protein is measured. The measured peptide masses are then used for searching against the online protein finger print database (Swiss-Prot or NCBInr). The commonly used searching program is Mascot or ProFound. The matching result consists of a list of possible protein identifications along with the probability. By performing tandem MS on one or several of the parental peptides, the identification accuracy could be significantly increased **(Figure 2.9)**.

Figure 2.9: Example of the process of protein identification.
The protein of interest is excised digested and extracted. The masses of the peptides in the extract are then measured by MS to obtain the peptide mass fingerprint. The peptide with m/z = 2574 (labeled with an arrow) was then selected and fragmented. Finally, both the MS and tandem MS data were searched against protein databases to determine the protein identity (60).

2.2.7.2 Experiment

In this work Ni-NTA purified protein were subjected to peptide mass fingerprinting and MS/MS for identification. After separation by a 12 or 15 % SDS-PAGE, the protein was visualized by coomassie brilliant blue. Bands of interest were excised and the gel pieces were cut, destained, dehydrated and digested as described in the Trypsin Profile IGD Kit (SIGMA).

Briefly, gel pieces were cut into 1 to 1.5 mm sizes and placed into a 1.5 ml Eppendorf tube. 200 µl of de-staining solution (200 mM ammonium bicarbonate and 40 % acetonitrile) was added into the tube to de-stain the gel. De-staining

was performed twice for 30 min. After centrifugation, the supernatant containing the dye was removed. To dry the gel pieces in the pellet, the sample was subjected to Speed Vac for 15-30 min. Protein digestion was initiated by addition of 20 µl (0.4 µg of trypsin) of the prepared trypsin solution and 50 µl of the trypsin reaction buffer (40 mM ammonium bicarbonate and 9 % acetonitrile) into the tube. Digestion was allowed to proceed overnight at 37 ℃ with gentle mixing. The mixture was then centrifuge and the supernatant was collected and transferred into another clean tube. Trifluoroacetic acid was added with a final concentration of 0.1 % (v/v) to the supernatant containing digested peptides for acidification. For sample application, an aliquot of 0.5 µl of the digested peptide solution was mixed with 0.5 µl of matrix solution (50 mM 2, 5-dihydroxybenzoic acid in acentonitrile and 0.1% (w/v) trifluoric acid) on the sample plate. The sample matrix mixture was dried at room temperature before loading onto the Ultraflex III TOF/TOF mass spectrometer (Bruker Daltonics, Bremen, Germany).

For MS measurement, sample was ionized and separated according to the m/z ratio. MALDI-TOF and MS/MS were performed. Baseline correction and mass peak detection was performed using the software flex Analysis Version 3.0 (Bruker Daltonics, Build 92). Several ion peaks from matrix were used as internal standards to check the calibration. Finally, both the MS and tandem MS data were searched against protein databases (NCBInr or Swiss-Prot) for identification.

2.2.8 Refolding of His-PS2-FL

2.2.8.1 Principle

Refolding by quick dilution due to its simplicity is one of the commonly used methods for refolding. The solubilized protein can be directly diluted into a buffer containing no denaturing reagent. However, in order to avoid aggregation during refolding, the protein concentration needs to be as low as possible. Therefore, a high dilution factor is used to reduce the chance for the molecule to meet each other during refolding. This makes the dilution method buffer consuming and restrains its usage mainly to small scale refolding study (61, 62).

On column refolding is a process in which the denatured protein is bound to the matrix and subsequently the buffer is exchanged into renaturing buffer. The advantage of this is that the matrix bound protein is spatially constrained during refolding process. Hence, the possibility for aggregation is reduced when the protein is in a partially folded state (63).

Involvement of lipids or detergent in refolding buffer during dilution is reported to be helpful for membrane protein refolding. However, detergent may bind to the refolding intermediate and hence hinders the refolding process (49).

In this work, we combined the on column refolding and the quick dilution method. Briefly, purified His-PS2-FL under denaturing condition was bound to Ni-NTA matrix and the loaded matix was then quickly diluted into a buffer containing no urea and detergent to allow the protein to refold. The refolded protein was then solublised and eluted from the column.

2.2.8.2 Experiment

After SEC, fractions which were free of Sly D were pooled and used for refolding by quick dilution. To perform refolding, His-PS2-FL was first bound to Ni-NTA matrix in batch mode and then loaded to a column containing preequilibrated matrix. To ensure sufficient binding, the flow through was reloaded twice. In order to reduce hydrophobic interactions, the retained matrices were washed with binding buffer. The washed matrices were then quickly diluted into refolding buffer and incubated for 30 min before being loaded back again to the column. Solubilization buffer was passed through the column to solubilize the refolded His-PS2-FL. Finally elution of the target protein was achieved by passing through elution buffer containing 300 mM imidazole. The eluted His-PS2-FL was passed through PD-10 column to remove imidazole before being subjected to CD spectroscopy or concentrated for crystallization. (All the buffers used are described in **section 2.1.8**).

2.2.9 Protein concentration determination

2.2.9.1 Ultraviolet/Visible (UV/Vis) Spectroscopy

Visible and ultraviolet spectroscopy is a biochemical method commonly used to determine biomolecule concentration. Proteins can absorb ultraviolet light with absorbance maxima at around 280 and 200 nm. Aromatic amino acids (phenylalanine, tyrosine, and tryptophan) in proteins are responsible for the absorbance peak at 280 nm. Absorption around 200 nm is due to the peptide bond.

According to Beer-Lambert law of absorption, the light which is absorbed by a given biomolecule is proportional to its concentration and the thickness of the sample solution,

$A = -\log (I/I_0) = \varepsilon * c * l$

Where A is absorption (optical density, OD), I is the intensity of the transmitted beam which could be measured by the detector; I_0 is the intensity of the primary beam already known; ε is the molar extinction coefficient or molar absorptivity which is biomolecule specific (l/mol/cm); c is the concentration of the biomolecules (mol/l); l is the length that the light travels across the sample (cm).

For purified protein with known extinction coefficient, the protein concentration can be determined by measuring its absorption at 280 nm. The molar absorption coefficients at 280 nm used in this study are summarized in **Table 2.12** (all Cys residues are assumed to be reduced).

Protein	Ext. (M^{-1} cm^{-1})	Ext. (g l^{-1})	MW (Da)
His-PS2-FL	76780	1.503	51091.4
His-PS2-FL-Strep	82280	1.573	52298.6
His-PS2-NTF-Strep	60850	1.703	35732.6
His-PS2-CTF-Strep	26930	1.437	18742.3

Table 2.12: Extinction coefficient and MW used in this work.
Calculated extinction coefficients and the MW of the respective protein obtained from the protein sequence using the ProtParam tool (64).

2.2.9.2 The Bradford assay

The Bradford assay is based on the binding of coomassie brilliant blue G-250 dye (CBBG) to proteins at arginine, tryptophan, tyrosine, histidine, and phenylalanine residues. Among these amino acids, CBBG exhibits nearly eight times stronger binding affinity than the other residues. CBBG free dye (green or red) has an absorbance maximum at 470 nm. After binding with protein (blue color), the maximum shifted to 595 nm. Therefore the concentration of the protein present in the solution could be determined by measuring the absorption at 595 nm (65). It is found that hydrophobic proteins tend to precipitate and will appear as dark blue clumps after the addition of CBBG. These clumps will cause light scattering and hence influence the assay reliability. However, addition of a tiny amount of sodium hydroxide before adding CBBG dye reagent will help to solubilize the hydrophobic protein and relieve this problem to some extent. Detergent containing samples are not compatible with the Bradford assay unless a very small volume of the sample is used so that the final concentration after dilution is negligible (65, 66).

2.2.9.3 Experiment

For purified protein the concentration is determined by measuring OD_{280} using calculated extinction coefficient described in **Table 2.12**. For unpurified proteins (lysate, inclusion body, membrane fraction), their concentrations are determined by Bradford's assay. Micro-assay procedure was followed as described in Bio-Rad protein assay kit (Bio-Rad) where 200 µl of Bradford reagent was mixed with 800 µl of water as blanks. For samples, 1-10 µl was added mixed and incubated with Bradford reagent at room temperature for 5 min (the volume of the buffer used was correspondingly decreased to ensure that the total volume of buffer and sample is 800 µl). The absorbance was measured at 595 nm against a blank after 5 min. All the measurements were done within 30 min. The protein concentration was estimated from a calibration curve using BSA as the standard protein.

2.2.10 Gel electrophoresis

2.2.10.1 Principle

Electrophoresis is defined as the migration of the charged biomolecules in solution in the presence of a spatially uniform electric field. Usually the sample is run in a supporting matrix such as agarose or polyacrylamide gel. Within these supporting matrixes are the porous gels functioning as a sieve for retardation. Molecules with different sizes will exhibit different motilities due to different degree of retardation. Agarose gel provides large pore size therefore is used to separate larger macromolecules such as nucleic acids, large proteins and protein complexes (67). While polyacrylamide gel is used to separate proteins and small oligonucleotides (68).

While running, DNA samples are usually mixed with loading dye such as Xylene cyanol and Bromophenol blue to avoid the running out of sample. Xylene cyanol and Bromophenol blue have the same mobility as DNA fragment of 5 000 bp and 300 bp respectively. Nucleic acids remain negatively charged at any pH used for electrophoresis. The mobility of nucleic acids therefore is solely depended on the DNA molecule size. Hence, different conformations of a plasmid will exhibit different mobility on an agarose gel (in slowest to fastest order: nicked or open circular, linearized, supercoiled plasmid).

Protein samples are often mixed with SDS sample buffer containing sodium dodecyl sulfate (SDS) and β-mercaptoethanol (β-ME). To ensure the interaction of SDS to protein, normally protein sample are heated before loading. SDS which is a hash detergent is used to denature the protein into a linear form conferring polypeptide chain with negative charges. β-ME is a reducing reagent and is involved to break the inter or intra molecular disulfide bonds. In this way, the protein is maintained as an extended monomeric form during electrophoresis. Collectively, the mobility of the protein molecule is solely depended on the size (molecular weight).

After separation of biomolecules, the sample needs to be visualized to determine the mobility. The most common dye used to visualise DNA bands is ethidium bromide (EtBr). It fluoresces under UV light when incorporated into DNA. EtBr is a known mutagen due to its cell membrane permeability. While GelRed is a safe alternative to EtBr. GelRed has almost identical absorption and emission spectra as EtBr (excitation peak at around 300 nm and emission peak at around 595 nm). Therefore when illuminated with an ultraviolet light, the DNA complexes with gel red will fluoresces red making it easy for detection.

The two most commonly used staining methods for proteins are coomassie and silver staining. It is found that coomassie staining mechanism for protein is via a combination of hydrophobic interactions and heteropolar bonding with mainly basic amino acids (65). The staining process allows the binding of the dye with protein. However, the gel will also absorb dye which will provide strong blue background. The excessive coomassie could be washed and destained in destaining solution (normally 10% acetic acid) to remove the background colour. With proper destaining, the protein bands will appear as blue against a clear background. The sensitivity of coomassie staining is around 100 ng.

Silver staining is a more sensitive protein staining method with a sensitivity of 2–5 ng. The visualisation process consists of impregnation, reduction of silver ions to elemental silver and fixation. After developing, the silver ions are reduced into insoluble silver near the protein molecules. Therefore the protein bands with enough abundance will appear as a dark brown or black band on the gel.

2.2.10.2 Experiment

For agarose gel electrophoresis, 1 or 1.5 % agarose gels containing gel red (1:10 000 dilution) was used for DNA separation. DNA sample was mixed with appropriate volume of loading dye before running the gel under 100 V for 30 min. MassRuler™ High Range DNA Ladder was used as a marker.

For sodium dodecyl sulfate polyacrylamide gel electrophoresis (SDS-PAGE), protein samples are mixed with 5×SDS sample buffer vortexed and heated at 46 ℃

for 30 min before being loading to a 10 to 15 % SDS-PAGE. The separation was performed under 50 V for 15 min followed by 200 V for about 50 min until the bromophenol blue dye reaches the bottom edge of the PAGE. The SDS-PAGE was then incubated with Coomassie staining solution for 5-30 min with gentle shaking. The stained gel was then gently agitated in destaining solution until the background becomes clear. A folded paper towel was placed in the destaining solution to soak up excessive stain.

2.2.11 Western blot

2.2.11.1 Principle

The western blot is an analytical technique used to detect specific proteins in a given sample based on the antibody-antigen specific interaction. It firstly uses gel electrophoresis to separate native or denatured proteins by the length of the polypeptide (denaturing conditions) or by the 3-D structure of the protein (native/non-denaturing conditions). The separated proteins are then transferred to a membrane (typically nitrocellulose or PVDF), where they are probed using a specific antibody against the target protein (69).

2.2.11.2 Experiment

In this work, protein samples are firstly separated on 10-15 % SDS-PAGE following by being transferred to a PVDF membrane by semi-dry blotting. The gel and membrane are sandwiched between two stacks of filter paper that have been pre-wet with transfer buffer. The membrane is placed near the anode, and the gel is placed near the cathode. SDS-coated, negatively charged proteins are transferred to the membrane when an electric current is applied. Transfer efficiency is checked by staining proteins on the membrane using Ponceau S.

The membrane is then placed in blocking buffer with agitation at 4 ℃ over night in order to reduce non-specific protein interactions between the membrane and the antibody. This is achieved by placing the membrane in a solution containing bovine serum albumin (BSA) and non-fat dry milk (NFDM). Next day anti-his tag antibody is added into the blocking buffer and binding is

performed with gentle agitation at RT for 1 h. Unbound antibody is washed away by 3 times with TBS + 0.01% Tween 20 and one time with TBS. The enzyme substrate is then added to the membrane and incubated with the membrane for 5 min. Bands corresponding to the protein of interest will appear as dark regions on the developed film. Alternatively the protein of interesting can also be visualized by gel doc system.

2.2.12 Fluorescence spectroscopy

2.2.12.1 Principle

Fluorescence is defined as the emission of longer wavelength light by a substance called fluorophore due to its absorption of short wavelength light. Typically fluorescence happens within the nanosecond time range. During this time range, a three-stage process occurs. The three-stage process is illustrated by the simple electronic-state diagram (Jablonski diagram) shown in **Figure 2.10.**

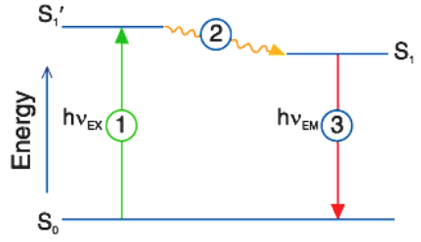

Figure 2.10: Schematic illustration of different electronic transitions.
In stage 1, an excited electronic singlet state (S_1') is generated by absorption of a photon of energy $h\nu_{EX}$ by fluorophore. In stage 2, the fluorophore undergoes conformational changes and is also subjected to many possible interactions with its miro-environment. Consequently, a relaxed singlet excited state (S_1) is generated from S_1'. In Stage 3, the emmison of a photon of energy $h\nu_{EX}$ occur after which the fluorophore returns back to the ground state S_0. Due to energy loss from S_1' to S_1, the emitted spectrum is always shifted (named as Stokes shift) to longer wavelength as compared with the absorption spectrum (70).

In protein, there are three aromatic amino acids (tryptophan, tyrosine and phenylalanine) contributing to the protein intrinsic fluorescence. However, only tyrosine and tryptophan are used experimentally due to their higher quantum yields. Tryptophan has a maximum absorption near 280 nm and an emission peak ranging from around 300 to 350 nm depending on the polarity of the local

environment. When exited at wavelength of 280 nm, both tryptophan and tyrosine will be exited. Pure emission from tryptophan can be obtained only by excitation at wavelengths above 295 nm.

Tryptophan fluorescence can be quenched in the presence of other residues to a great extent. Also, energy transfer between aromatic amino acids is possible. Thereby the investigation of protein structure by intrinsic fluorescence is practically limited to cases with only one tryptophan, or several with the same known local environment. For proteins with different tryptophan micro-environments, analysis becomes tedious since each tryptophan will yield a different emission spectrum collectively making the analysis difficult (71, 72).

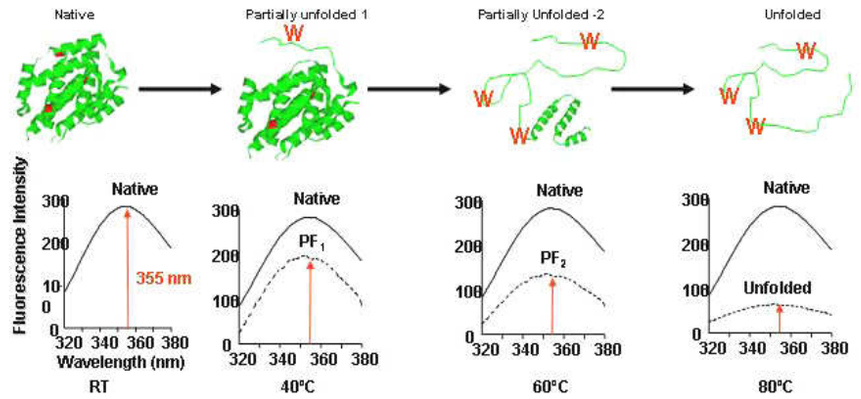

Figure 2.11: Illustration of protein thermal unfolding.
Protein unfolding by temperature (upper) and tryptophan emission spectra (lower) at each temperature (33).

Since tryptophan fluorescence emission maximum is sensitive to its microenvironment, this feature could be applied to steady or kinetic state protein unfolding studies. In a thermal unfolding process, the protein is unfolded by increasing temperature. For each temperature, tryptophan fluorescence spectrum is measured (**Figure 2.11**). Fluorescence intensity (FI) will change upon unfolding. In some cases, the maximum emission wavelength (λ max) will also change into longer wavelength when protein is unfolded. Plotting FI or λ max against the change of temperature will yield the unfolding curve from which the melting temperature could be extracted to investigate the protein thermal

stability (**Figure 2.12**). This is steady state study. In kinetic study, the temperature is set to be constant and the unfolding process is investigated by a function of time (**Figure 2.12**).

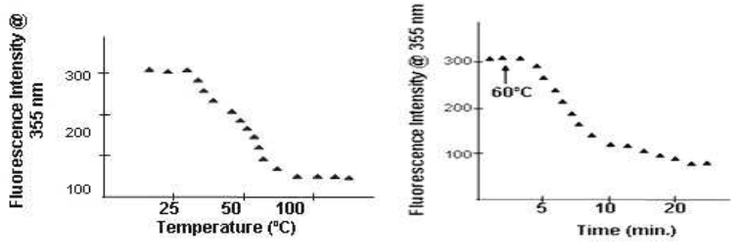

Figure 2.12: Steady and kinetic state protein unfolding.
Steady state (left) investigation of unfolding monitored by tryptophan fluorescence as a function of temperature; Kinetic state (right) investigation of unfolding monitored by tryptophan fluorescence as a function of time (33).

2.2.12.2 Experiment

In this work, refolded His-PS2-FL (0.058 mg/ml) was denatured by 6 M urea and 8 M GndHCl as well as by heating to 40 ℃ and 60 ℃ respectively in the presence of 8 M GndHCl. The samples and the buffer were filtrated through a 0.2 centrifugation filter before the measurement. The corresponding fluorescence spectra were collected in a 1 cm^2 rectangular quartz cell with an integration of 0.1 s, a step size of 1 nm, a scanning speed of 100 nm/min, and an average of 3 spectra. Excitation wavelength used is 295 nm and emission spectra from 300 to 500 nm were collected.

Purified PS2-NTF was concentrated and glycerol was removed by buffer exchange through PD-10 column. The concentrated PS2-NTF (0.39 mg/ml) was diluted 10 times into 10 mM sodium phosphate; 1 mM TCEP; 1.5 CMC of the respective detergents or denaturing reagent (DM, DDM, Cy6, LDAO, FC12, 6 M Urea). After dilution, each sample was incubated for 2 h before being subjected to fluorescence spectroscopy.

For thermal unfolding of His-PS2-NTF-Strep, 0.84 µg/ml of purified His-PS2-NTF-Strep was unfolded by increasing temperature at a heating rate of 1

℃/min. For comparison, pure tryptophan fluorescence spectra were recorded between 20 and 80 ℃ every 5 degree was taken from using the same parameters as described above. For analysis, fluorescence intensity at 333 nm as a function of temperature was plotted against different temperatures.

2.2.13 Circular dichroism (CD) spectroscopy

2.2.13.1 Principle of CD

Plane polarized light can be viewed as a decomposition of the left and right handed circularly polarized light with identical amplitude. Right and left handed circularly polarized light will be absorbed differentially when plane polarized light interacts with asymmetric molecules (such as protein). Therefore the resulting plane due to differential absorption will be different as the initial plane and the light is considered to be optically rotated (**Figure 2.13**).

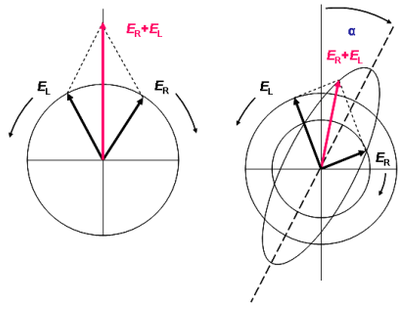

Figure 2.13: Principle of CD spectroscopy.
Linear polarized light (Left) can be viewed as a combination of left and right circular polarized light of same amplitude. Differential absorption (Right) of the left and right hand circular polarized light leads to ellipticity (Δε = εl - εr) and optical rotation (OR, shown as α) (74).

The phenomenon of the unequal absorption of left handed and right handed circularly polarized light by asymmetric molecules is defined as circular dichroism (CD). CD spectroscopy is a spectroscopic technique which measures the CD spectrum of a biomolecule. It is reported commonly in unit of mean residue ellipticity ($[\theta]_{MRE}$). $[\theta]_{MRE}$ has a unit of degrees· cm^2 ·$dmol^{-1}$. $[\theta]_{MRE}$ can be calculated by the following equation (73):

$[\theta]_{MRE} = MRW \cdot \theta / 10 \cdot d \cdot c$

where MRW equals to the molecular mass divided by N−1, N is the number of amino acids in the investigated protein, θ is the measured signal in degrees, d is the path length of the cuvette in cm and c is the sample concentration in g/ml.

There exist in protein three types of chromophores with different absorption wavelengths. Peptide bond has absorption below 240 nm (secondary structure); aromatic amino acid side chains have absorption between 260 to 320 nm (tertiary structure); disulphide bonds have a relatively weaker broad absorption centred at around 260 nm. Analysis of protein far and near UV CD spectra will therefore provide information about the protein secondary and tertiary structure respectively.

In the "far-UV" region (190-250 nm), the chromophore is the peptide bond. Only when the peptide bond is positioned in a regular, folded state will the differential absorption (CD) occur. Certain secondary structural element will yield a unique CD spectrum with specific shape and magnitude. A typical α-helical protein will yield a CD spectrum with negative peaks at 222 nm and 208 nm as well as a positive peak at around 193 nm. Proteins which are rich in β-sheets structure will exhibit negative bands at 218 nm and positive bands at 195 nm. While un-ordered proteins have very low CD signal above 210 nm and will produce negative peak near 195 nm (**Figure 2.14**).

Hence, the measured far UV CD spectrum of a given protein can be viewed as a combination of each of the above secondary structure elements in different proportion. The measured CD spectrum therefore can be deconvoluted and the secondary structural contents and percentage present in the protein under investigation can be subsequently calculated. DICHROWEB is an on-line analysis program established based on the CD spectra of soluble and membrane proteins of known structure to deconvolute the measured CD spectra into pure component spectra. Different secondary structure determination algorithms such as SELECON 3, CDSSTR and CONTIN as well as different reference sets

including soluble and membrane proteins together with native and denatured protein are available (75-78).

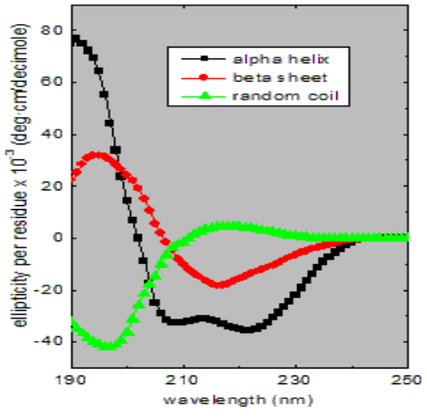

Figure 2.14: CD spectra of poly-L-lysine.
Alpha-helix (black square), beta-sheet (red dot) and random coil (green triangle) conformations are shown (79).

In the near UV region (250-350 nm), the CD spectrum of a protein is due to the aromatic amino acids side chains and disulfide bonds. The aromatic amino acids side chains of a protein in the state will be placed in a variety of asymmetric environments. Therefore they will absorb left and right polarised light to different extent and hence a CD signal will be recorded. The CD spectrum in the near UV region thus reflects the miro-environments of the aromatic amino acid side chains. When the protein exhibits a near UV CD signal, it is a good indication for the presence of a well-defined tertiary structure in the protein under investigation.

Each aromatic amino acid in its native state exhibits a specific near UV CD spectrum. Phenylalanine is responsible for the signals in the wavelength between 250 to 270 nm. Tyrosine contributes to the wavelength from 270 to 290 nm. Signals from 280 to 300 nm are due to tryptophan residues. Disulfide bonds however, yield a broad weak signal throughout the near UV region. In practice, the near UV CD spectrum of a given protein will be very often a combination of the unique spectra described above. When the protein contains only secondary

structure without the presence of tertiary structure, the signals in the near UV region will be nearly zero (80, 81).

2.2.13.2 CD measurements

For far UV CD spectra, 350 µl of 0.1-0.2 mg/ml of purified protein was placed in a quartz cuvette with a 0.1 cm path length and spectra were collected at 20 nm/min scan rate between 260 and 185 nm with a band width of 1 nm a response time of 8 s and a data pitch of 1 nm as well as an accumulation of 3 spectra. For near UV CD spectra, 700 µl of 0.7-1.0 mg/ml of purified protein was placed in a quartz cuvette with a 1 cm path length and spectra were collected at 20 nm/min scan rate between 340 and 250 nm with a band width of 1nm a response time of 8 s and a data pitch of 1 nm as well as a accumulation of 3 spectra. Baselines were corrected in the same way with buffer solutions, and spectra were buffer subtracted. All CD spectra were recorded at 4 ℃. For thermal unfolding experiment a scan rate of 50 nm / min and a response time of 2 s were used and the spectrum was recorded at every 5 ℃ with a heating rate of 1 ℃/min. Protein concentrations were determined from the absorbance at 280 nm using the calculated molar absorptivity as shown in **Table 2.12**.

Deconvolution of the raw CD spectra into pure component spectra was achieved using the algorithm SELECON 3, CDSSTR and CONTIN (82). The protein reference set used was Set 7. There are 48 different protein CD spectra, 5 of which are from denatured protein in this set. This database requires a wavelength range of 190 - 240 nm.

To demonstrate the deconvoluted component spectra, regular alpha helix (α_R), distorted alpha helix (α_D), regular beta sheet (β_R), distorted beta sheet (β_D), turn, and unordered (U) were used. Helix which is no more than four amino acids is classified into α_D helix. α_D helix also includes two amino acids from both ends of each helix. All remaining helical are defined as αR. For β_D, one residue from both ends of each β-sheet is included and it also includes all segments in a β-sheet that is less than two amino acids. All remaining β-sheet fraction belongs to β_R. The

turn class refers to the combination of the DSSP turn (T) and bend (S). The rest of the secondary structure contents which are not mentioned are considered to be the unordered fraction (83). The total secondary structure content is predicted using PSIPRED prediction (84).

The thermal stability of secondary and tertiary structure of PS2-NTD in FC12 was investigated by circular dichroism spectroscopy and Trp fluorescence spectroscopy respectively. The far UV CD spectrum and tryptophan fluorescence emission spectrum was recorded at every 5 ℃ with a heating rate of 1 ℃/min. As far UV CD spectra was over all shifted by 1 nm for membrane protein as compared with soluble protein, MRE at 221 nm instead of 222 nm was taken for fitting. Fluorescence intensity at 333 nm was taken for fitting. The equation used is as following (85, 86):

$$Y_{obs} = ((A1+M*x) + (A2+N*x)*\exp(E*(1/x0-1/x))) / (1+\exp(E*(1/x0-1/x)))$$

where Y obs is the observed signal, A1 is the ellipticity or fluorescence intensity at low temperature, A2 is the value at high temperature, M is the slope of the curve at low temperature, N is the slope of the curve at high temperature, E is equal to ΔH/R, ΔH is the van't Hoff enthalpy change of unfolding, R is the gas constant, x is the temperature, x0 is the melting temperature (Tm). Tm is defined as the midpoint of the transition where the fractions of folded and unfolded protein are equal. The above equation fits the thermal dependence of the far UV CD or Trp fluorescence signal into a two state unfolding transition (87). Total helix and strand content as a function of temperature were also fit to the above equation.

When assuming a two-state transition and no formation of the stable intermediate during thermal unfolding, the following equations could be applied,

$$f_F + f_U = 1,$$

where f F and f U represent the fraction of folded and unfolded protein fraction at equilibrium respectively. Therefore the observed y at a given temperature could be expressed as,

$$y = A1 * f F + A2 * f U$$

A combination of the above two equations will yield:

$$f U = (A1-y) / (A1-A2)$$

Therefore the equilibrium constant,

$$K = f U / 1- f U = (A1-y) / (y-A2)$$

The free energy changes ΔG at a given temperature could be calculated with the following equation:

$$\Delta G = - RT \ln K = - RT \ln (A1-y/y-A2)$$

Where R is the gas constant, T is the absolute temperature. As the in-meso phase crystallization experiment will be done at 20 ℃, the ΔG at this temperature is calculated to evaluate the protein thermal stability.

2.2.14 Dynamic light scattering

2.2.14.1 Principle

Dynamic light scattering (DLS) is a biophysical technique to determine the hydrodynamic radius (R_h) of a biomolecule in solution. During a DLS measurement, the intensity fluctuations of the light scattered by the biomolecules due to their diffusion properties in solution are monitored as a function of time.

Depending on the light wavelength and the particle size, light will be absorbed, reflected or scattered when interacting with particles. Under conditions where the particle size is smaller than the wavelength of the light, the light will be scattered in all directions. The scattered light will remain constant if the particle

remains still. However, due to the Brownian motion in solution, the distance between the particles is constantly changing with time. When a monochromatic and coherent light source interacts with the particles in the sample, the scattered light by the surrounding particles which are constantly moving will undergoes either constructive or destructive interference. Therefore a time-dependent fluctuation of the scattered light intensity will be recorded on the detector. Particle's size information (R_h) can be then extracted from the recorded signals during the measurement (88).

2.2.14.2 Measurements

Dynapro Titan system (Protein solutions) allows the control of temperature and humidity during measurement. To avoid the interference by contamination and big unwanted particles in solution, cuvettes were thoroughly cleaned by distilled water and ethanol. The samples were filtered through a 0.2 µm filter to remove dust and big aggregates before being measured. The sample was placed in a 50 µl quartz cuvette (Hellma, z = 8.5 mm, path length= 3 mm) and measured for at least 20 acquisitions of 3 to 10 s with a laser power of 70 to 90 %. Data acquisition and analysis was performed using the Dynapro software, Dynamics version 6.0 (Protein solutions).

2.2.15 Reconstitution and crystallization in monoolein (MO) cubic phase

2.2.15.1 Principle

Membrane protein crystallization in MO cubic phase is a method which uses MO-water based mesophases to crystalize membrane proteins. This system normally consists of lipids, water and proteins as well as other additives in certain proportions (89). Given the self-assembling property of lipids, under certain conditions, the mixture above will form a structured and transparent three-dimensional bi-continuous cubic phase interconnected by aqueous channels. Membrane proteins can be reconstituted passively or actively into the MO cubic phase within which they can diffuse laterally. Water soluble components can diffuse freely in the water channels. The phase behaviour of MO cubic phase can be easily controlled by adjusting the water content in the system.

What's more, phase identity was found to be stable with the addition of lipids (such as phosphatidylcholine and cholesterol) to different extent. This observation will meet the need of certain membrane proteins crystallization which requires special lipids for native state (90).

Investigation of bacteriorhodopsin crystallization in MO cubic phase uncovered the mechanism of nucleation, growth and transportation of *in meso* crystallization. During crystallization, it was found that nucleation happens at the place where the highly curved lipidic cubic phase transformed into lamellar phase which is a native membrane like structure. Growth of crystals occurs by transporting single protein molecule within the lamella phase to the nuclei (91, 92).

A controlled in meso phase crystallization system has been developed. This system is based on the fact that the formation of cubic phase doesn't require the active mixing of protein solution with dry monoolein (89). In the controlled system, the incorporation into lipidic phase happens passively. The crystallization is induced by addition of precipitant through dehydration of the system by vapour diffusion. This is an big advantage compared with the classic premixing experiment where active mixing is required which will produce a lot of heats resulting denaturing of the sensitive membrane protein (93).

2.2.15.2 Experiment

Because CD and fluorescence measurement require a homogeneous distribution of protein sample in cubic phase, the premixing of refolded His-PS2-FL with solid monoolein was achieved following the protocol described by Martin Caffrey (94). Briefly, 2 volume of refolded His-PS2-FL was mixed with 3 volume of MO generating a hydration level of about 40 % (wt/wt). The mixing is stopped when a transparent cubic phase was observed. The protein loaded cubic phase was then dispensed into a 0.1 mm path length quartz cuvette for CD measurement or a 1 cm^2 rectangular quartz cell for fluorescence measurement. The measurement parameter was the same as described in respective section.

A controlled in meso phase crystallization system was used for crystallisation of His-PS2-NTF-Strep. Brain polar lipids at a molar ratio of 5:1 to 10:1 (lipid: protein) was added into the concentrated protein solution before crystallization. Different crystallization conditions were monitored under a polarization microscope and a fluorescence microscope over time.

2.2.16 *In vitro* translation

2.2.16.1 Principle

In vitro translation system is protein expression system containing either a reconstituted reaction or the cellular crude extracts that includes all the bimolecular components required for transcription and translation. It separates the cell viability and protein translation therefore avoids the common problem encountered by *in vivo* protein expression. The commonly used extracts are *Escherichia coli*, wheat germ and rabbit reticulocytes. Generally *E.coli* based system produce better yield and homogeneity suitable for structural analysis (95, 96).

Although with higher cost per mg of protein, as compared with *in vivo* expression system, *in vitro* translation system has the following advantages (97): (i) Problems like protein targeting and translocation, post-translational modification, degradation, overloading of sorting and transporting systems and the toxicity upon membrane insertion can be avoided when *in vitro* system is used. (ii) Due to elimination of the tedious cellular process upon membrane protein expression, the success expression depends mainly on the complexity of mRNA secondary structure. (iii) The addition of membrane like substances such as detergent, peptide, liposomes and nanodiscs can produce functional and solubilised membrane protein directly within a short time period. (iv) *In vitro* system avoids the time consuming processes like expression, cell opening and solubilisation and has a very low background of hydrophobic proteins. It therefore facilitates the purification to a great extent. (v) The yield and quality always remains constant due to the simplicity which is of great importance for membrane protein structural analysis.

Based on the added membrane-mimicking substances, the *in vitro* translation of membrane proteins can be categorized into the following different modes: (i) Precipitation mode, where the membrane protein is synthesized in the absence of a membrane-like substances and the translated protein will precipitate after centrifugation. Proteins produced in this mode normally yield high purity after several washing steps without any further purification. However re-solubilisation is required for this mode and the homogeneity and function needs to be investigated (41). (ii) Detergent mode, where compatible detergents are added into the *in vitro* system to solubilise the translated membrane protein. Addition of detergents normally produces solublised membrane protein directly after translation (98-100). Therefore purification is required to remove the background proteins. (iii) Peptide mode, where artificial peptide surfactants are used for production of soluble and functional membrane proteins (101, 102). (iv) Nanodisc mode, in which the addition of nano-scale particles made of lipoprotein encircled membrane bilayer can be used to produce soluble functional and homogeneous membrane protein for structural analysis (103-106).

2.2.16.2 Experiment

Reaction components	Volume (µl)
E. *coli* Extract	8.75
RNase-free water	make up to 25
Reaction Buffer	10
IPTG (50 mM stock)	0.5
Plasmid DNA (0.35µg/µl stock)	1.5
Addition of membrane like substances	X
Total volume	25

Table 2.13: *In vitro* translation reaction setup.

In this work, *E.coli* based *in vitro* translation system was used to investigate the expression of His-PS2-FL-Strep and the expression as well as the homogeneity of in vitro translated His-PS2-CTF-Strep. In vitro reaction was setup as described in **Table 2.13**. Each reaction was incubated with 500 rpm shaking at 30 ℃ for 2 h. After 2 h incubation, reaction was then centrifuged at 20,000 ×g for 30 min. The supernatant and the pellet fractions were collected separately. Each pellet

fraction was solubilised in 25 µl of pellet solubilisation buffer. Equal volume of each fraction was used for western blot analysis.

For homogeneity analysis of *in vitro* translated His-PS2-CTF-Strep in different mode, 6×25 µl of reaction were used to produce enough protein. After centrifugation, the supernatant was collected, concentrated and filtered through a 0.2 µm filter before being injected onto either a superdex 200 analytical column or a superpose 6 analytical column. Running condition was identical as described in **Section 2.2.6**.

3 Results

3.1 Expression purification and biophysical characterization of His-PS2-FL

3.1.1 Expression

Different cell strains and different media were investigated to determine the condition where the best yield of His-PS2-FL is produced.

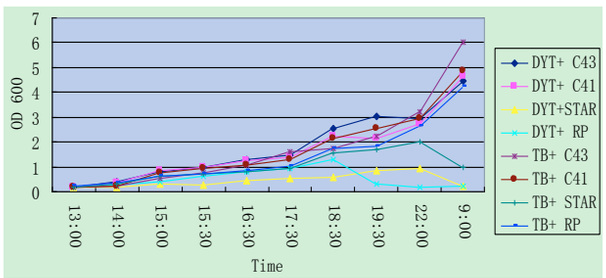

Figure 3.1: Growth curves of His-PS2-FL in different cells and media.
Shown are the growth curves of different cells transformed with His-PS2-FL in different media. OD_{600} is recalculated from a 10 times dilution of the actual sample and is plotted against time in every one hour after induction started from 13:00.

As shown in **Figure 3.1** and **Table 3.1**, TB+C43, TB+ C41, DYT+C41, DYT+C43 and TB+RP in decreasing order, yields reasonable OD_{600} and pellet amount after 16 h induction. Therefore cell from these groups were harvested and opened for protein yield analysis.

Groups	Induction OD_{600}	OD_{600} after 16 h	Pellet (gram)
DYT+ C43	0.81	4.45	1.01
DYT+ C41	0.83	4.63	1.09
DYT+STAR	0.83	0.22	
DYT+ RP	0.63	0.21	
TB+ C43	0.76	6.02	1.49
TB+ C41	0.78	4.88	1.25
TB+ STAR	0.63	0.99	
TB+ RP	0.62	4.23	0.93

Table 3.1: Expression of His-PS2-FL in different cells and media.
Shown are induction OD_{600} and the final OD_{600} as well as cell pellet amount after 16 h induction. Groups which have an OD_{600} lower than 1 was abandoned for analysis.

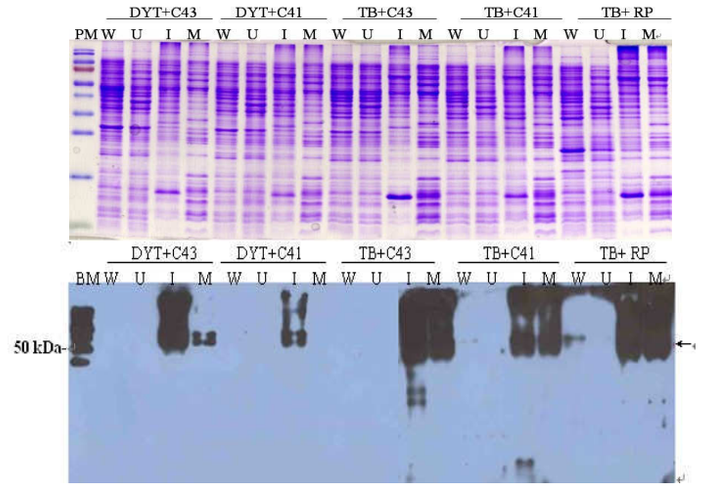

Figure 3.2: SDS–PAGE and western blot analysis of His-PS2-FL expression.
Coomassie staining (upper) and western blot (lower) showing the expression of His-PS2-FL. BM: bench marker; W: without plasmid control; U: uninduced control; I: inclusion body fraction; M: membrane pellet fraction. Black arrow indicates the monomer form of His-PS2-FL2. Media and cell strain are also indicated on the top of the page.

Western blot analysis **(Figure 3.2)** showed that no signal or very weak signals were detected for "without plasmid control" or "uninduced control" for all the five groups as expected. Almost equal intensity was observed in inclusion body and membrane fraction for TB+C43, TB+C41, TB+RP. For DYT+C43 stronger signal was detected in inclusion body fraction as compared with membrane fraction. For DYT+C41 only in the inclusion body fraction some signal was detected. In summary, TB+C43 yield the highest OD and cell pellet amount as well as the final yield of His-PS2-FL after overnight expression. Interestingly, coomassie staining detected the aggregation on the top of the gel in the inclusion body and membrane fraction. These aggregations are also western positive. This result indicates that the protein expression pattern changes upon induction.

3.1.2 Purification under denaturing condition

3.1.2.1 Ni-NTA purification

After proving the existence of His-PS2-FL, the protein yield was investigated by purification under denaturing condition. After cell lysis the inclusion body and membrane fraction was collected by centrifiguation as decscribed in **section**

2.2.3. Purification of the target protein from each fraction was described in **section 2.2.4**.

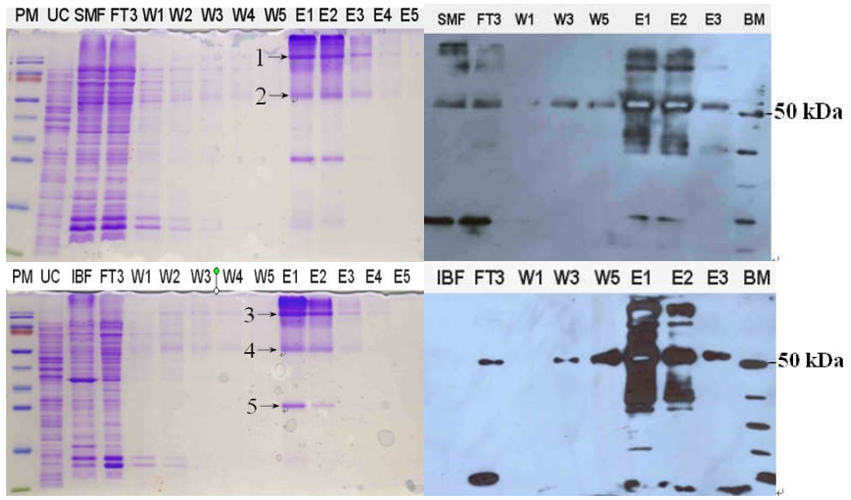

Figure 3.3: Purification of His-PS2-FL under denaturing condition.
Coomassie staining (left) and western blot (right) of Ni-NTA purification fractions. PM: prestained marker; BM: bench marker; UC: uninduced control; SMF: solubilised membrane fraction; IBF: Inclusion body fraction; FT3: flow through after 3 times reapply; W: wash; E: elution. Number and arrow indicate the bands which are subjected to mass spectrometry.

As shown in the **Figure 3.3**, from both membrane and inclusion body fractions similar bands were detected in Ni-NTA elution fractions which were western positive. Aggregation at the top of the SDS-PAGE was also observed. For comparison, in each lane samples corresponding to the same amount of cell pellet was loaded. As shown in coomassie staining, more His-PS2-FL from membrane fraction was detected as compared with the inclusion body fraction. Bands 1-4 as indicated in the figure were identified as His-PS2-FL while band 5 was determined as sly D protein by mass spectrometry.

3.1.2.2 Size exclusion chromatography

To remove the Ni-NTA co-purified slyD protein from His-PS2-FL, SEC was performed after Ni-NTA purification. As shown in the **Figure 3.4**, on Sephacryl S-200 HR column the Sly D protein was separated from PS2.

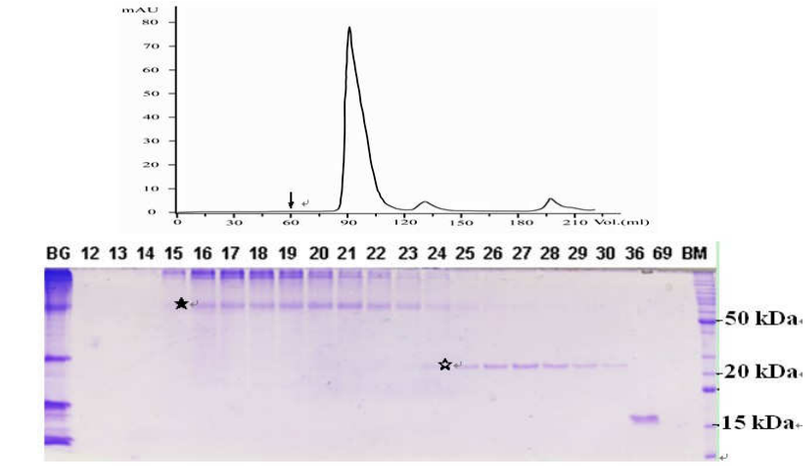

Figure 3.4: Separation of His-PS2-FL from Sly D by Sephacryl S-200 HR column.
SEC Profile of His-PS2-FL (Upper) and a 15 % SDS-PAGE (Lower) showing the separation of His-PS2-FL from Sly D. BG: His-PS2-FL before gel filtration; BM: bench marker; fraction numbers are shown above the page. Black arrow indicates the void volume of the column; filled star indicates the monomer form of His-PS2-FL; empty star indicates Sly D.

3.1.2.3 Refolding of His-PS2-FL

The refolding process of His-PS2-FL was monitored at each step. Silver staining showed the recovery of refolding and purity of the His-PS2-FL suitable for biophysical measurements as well as reconstitution experiments. Western blot identified the protein **(Figure 3.5)**.

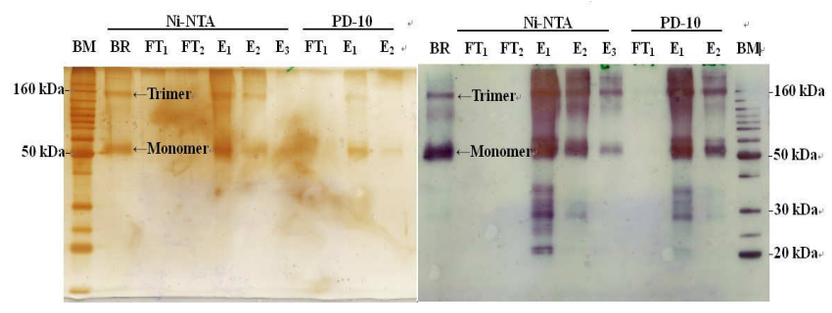

Figure 3.5: Refolding of His-PS2-FL by quick dilution.
Left: Silver staining of 12 % SDS-PAGE showing the refolded His-PS2-FL on Ni-NTA and PD-10 column. Right: Western blot of the same fractions. BM: bench marker; BR: before refolding; FT: flow through; E: elution. Monomer and trimer of His-PS2-FL were indicated with black arrows.

3.1.3 Purification under native condition

3.1.3.1 Comparison of Co-NTA and Ni-NTA

To determine the metal ion for IMAC purification, His-PS2-FL from the same amount of cell pellet was purified with equal amount of Co-NTA or Ni-NTA matrix respectively under otherwise identical conditions.

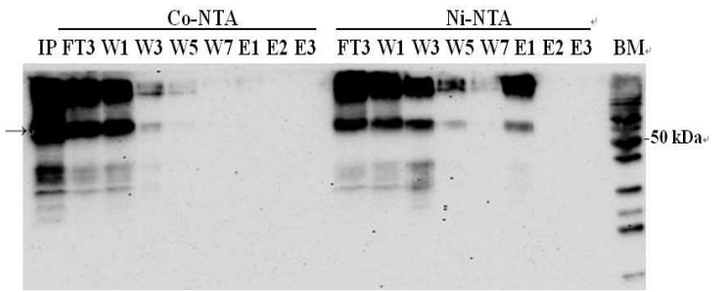

Figure 3.6: Purification of His-PS2-FL by Co-NTA and Ni-NTA under native condition. Western blots showing the His-PS2-FL purified by Co-NTA and Ni-NTA. IP: input; BM: bench marker; FT: flow through; W: wash; E: elution; Black arrow indicates the monomer of His-PS2-FL. For comparison, each lane corresponds to 2.4 mg cell pellet.

As shown in the **Figure 3.6**, with Ni-NTA in elution fractions a protein band corresponding to His-PS2-FL was detected while no signal was detected for Co-NTA in the same fraction. Therefore Ni-NTA was chosen for IMAC purification of His-PS2-FL.

3.1.3.2 Purification with different amount of Ni-NTA

The matrix volume used for IMAC is crucial for the yield and purity of each specific protein purification. Therefore, His-PS2-FL from the same amount of cell pellet was purified with different amounts of Ni-NTA matrix respectively to determine the optimal ratio of matrix to cell pellet.

As shown in the **Figure 3.7**, with increasing amount of matrix an increasing intensity of the bands corresponding to His-PS2-FL were detected in elution fractions in both coomassie staining and western blot. Western blot also showed that as the matrix amount increase, there was a decreasing tendency for the intensity of the band corresponding to His-PS2-FL in flow through fraction. It is

notes worthy that comparable yields and purities of the protein were observed in elution fractions for 250 and 500 µl matrix. Hence, for every 1 g cell pellet, 0.25 ml Ni-NTA matrix was chosen for purification.

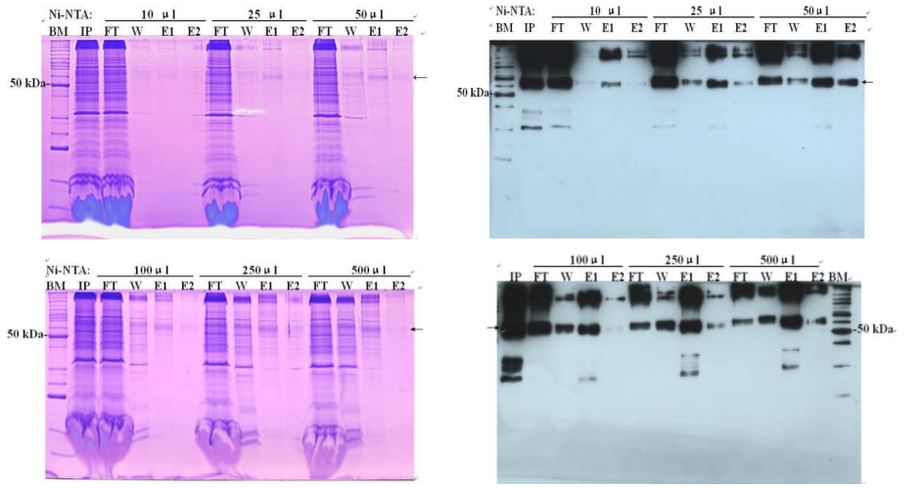

Figure 3.7: Purification of His-PS2-FL with different amount of Ni-NTA.
Coomassie staining (left) and western blot (right) showing the purification of His-PS2-FL with different amount of Ni-NTA matrix. BM: bench marker; FT: flow through of Ni-NTA; W: 5 CV wash with wash buffer; E: elution with 2×2.5 CV of elution buffer; Black arrow indicates the monomer of His-PS2-FL. For coomassie staining, each lane corresponds to 3.2 mg cell pellet; for western blot each lane corresponds to 2.4 mg cell pellet.

3.1.3.3 Ammonium sulphate precipitation

After Ni-NTA purification, impurities were observed in the elution fractions. Therefore ammonium sulphate precipitation of His-PS2-FL was performed before Ni-NTA purification to reduce the impurities as much as possible.

For groups where the AS concentration was higher than 60 %, there was an almost negligible amount of His-PS2-FL detected in supernatant by western blot compared with the intensity from input. For all groups there was an almost negligible amount of His-PS2-FL in the pellets compared to input. However, a considerable amount of His-PS2-FL was recovered in floating pellets where the AS concentration was 60, 70 and 80 percent (**Figure 3.8**) indicating the co-precipitation of lipids and detergents with membrane protein. Given these results, 70 % of AS was chosen to fully precipitate His-PS2-FL as a floating pellet.

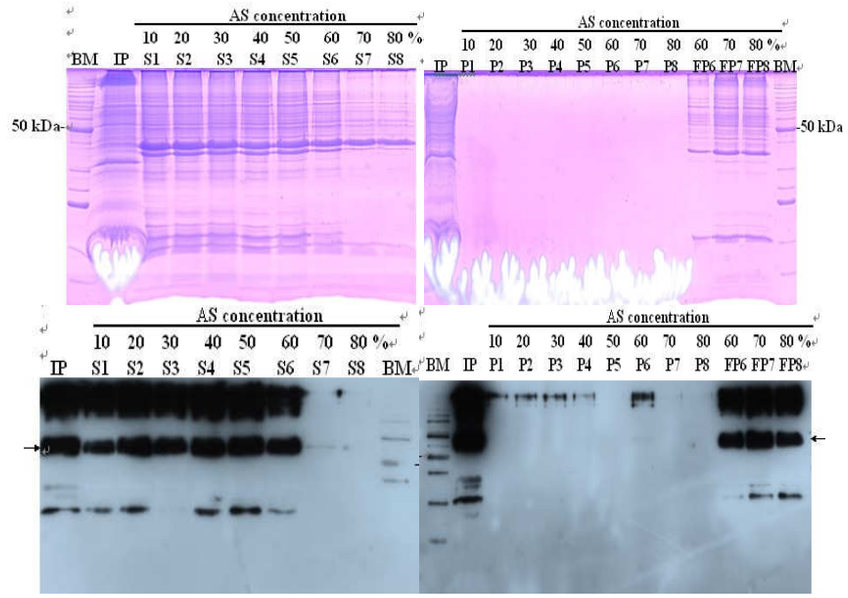

Figure 3.8: Ammonium sulphate precipitation of His-PS2-FL.
Coomassie staining (upper) and western blot (bottom) showing the concentration of ammonium sulphate to precipitate His-PS2-FL. AS: ammonium sulphate; BM: bench marker; IP: input; S: supernatant; P: pellet; FP: floating pellet. S1 to S8 and P1 to P8 correspond to the supernatant and pellet from 10 % to 80 % of saturated ammonium sulfate respectively. Black arrow indicates the monomer of His-PS2-FL. For coomassie staining, each lane corresponds to 3.2 mg cell pellet; for western blot each lane corresponds to 2.4 mg cell pellet.

3.1.3.4 Optimization of Purification

Different purification conditions like reducing agent, ionic strength and combination of ASP, on column and batch mode and a second purification by Ni-NTA were carried out respectively in order to improve the purity.

As shown in **Figure 3.9**, His-PS2-FL was co-eluted with impurities in the elution fractions with all the conditions investigated.

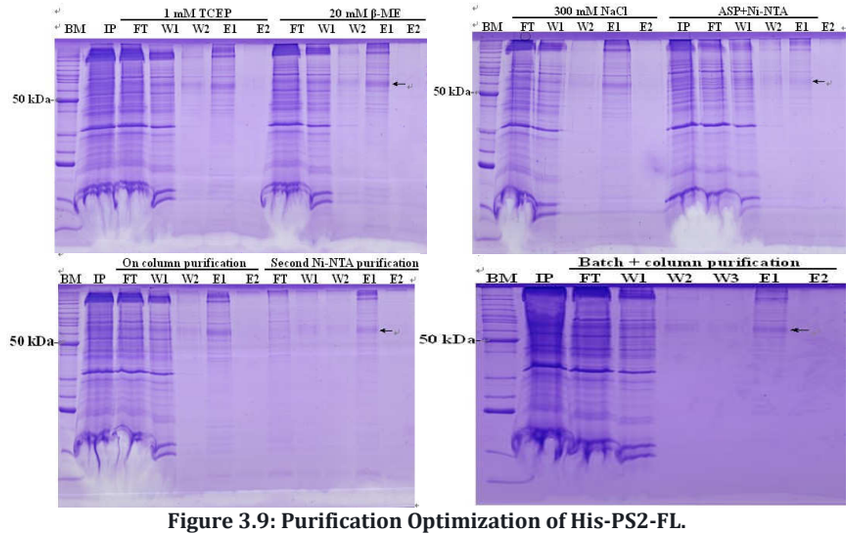

Figure 3.9: Purification Optimization of His-PS2-FL.
Coomassie staining showing the Ni-NTA purification fractions of His-PS2-FL under different conditions. BM: bench marker; IP: input. Black arrow indicates the monomer of His-PS2-FL. For coomassie staining, each lane corresponds to 3.2 mg cell pellet; for western blot each lane corresponds to 2.4 mg cell pellet.

3.1.3.5 Anion exchange chromatography

Because of the purity problem, anion exchange chromatography was performed after Ni-NTA purification. To determine the optimal matrix volume needed for purification, His-PS2-FL samples corresponding to the same amount of cell pellet were purified with different amount of Macro-Pre High Q support matrix respectively. Binding experiments were performed in presence of different NaCl concentration with the chosen matrix volume to determine the optimal NaCl concentration.

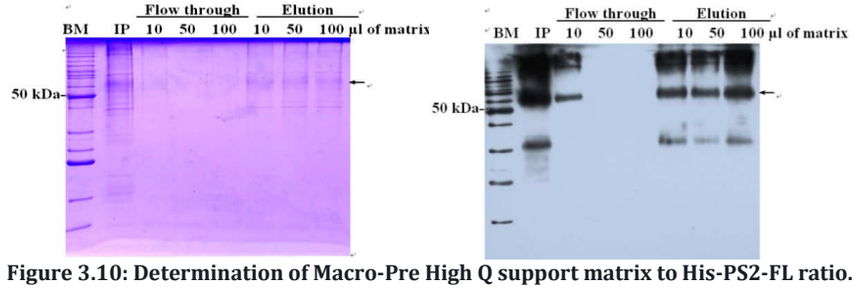

Figure 3.10: Determination of Macro-Pre High Q support matrix to His-PS2-FL ratio.
Coomassie staining (left) and western blot (right) showing the amount of Macro-Pre High Q support matrix required for capturing His-PS2-FL. BM: bench marker; IP: input. For coomassie staining, each lane corresponds to 3.2 mg cell pellet; for western blot each lane corresponds to 2.4 mg cell pellet.

As shown in **Figure 3.10**, in elution fractions, only 100 µl of matrix yields the comparable intensity with input. Therefore for 1 g cell pellet, 1 ml Macro-Pre High Q support matrix was chosen for purification.

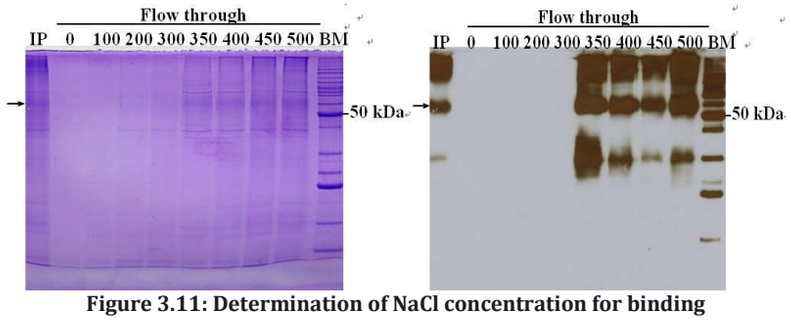

Figure 3.11: Determination of NaCl concentration for binding to High Q support matrix.

Coomassie staining (left) and western blot (right) showing the concentration of NaCl for binding of His-PS2-FL to Macro-Pre High Q support matrix. BM: bench marker; IP: input. NaCl concentration is given in mM. Black arrow indicates the monomer of His-PS2-FL. For coomassie staining, each lane corresponds to 3.2 mg cell pellet; for western blot each lane corresponds to 2.4 mg cell pellet.

As shown in **Figure 3.11**, with up to 300 mM NaCl no signal corresponding to His-PS2-FL was detected from western blot. For this reason 300 mM NaCl was added to the binding buffer. It is notes worthy that the protein purity in 500 mM NaCl elution does not improve significantly compared with input sample.

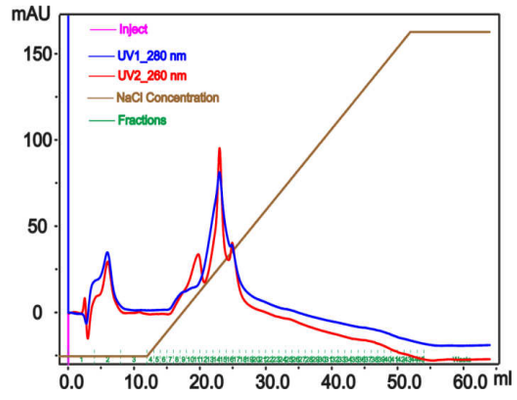

Figure 3.12: Elution profile of His-PS2-FL on Macro-Pre High Q support matrix.

Elution profile of His-PS2-FL on Macro-Pre High Q support matrix monitored by ÄKTA revealed that no separation between the proteins of interest and the impurities occurred (**Figure 3.12**).

3.1.3.6 Size exclusion chromatography

To improve the purity after Ni-NTA, Ni-NTA elutes was loaded onto a Superose 6 pg column.

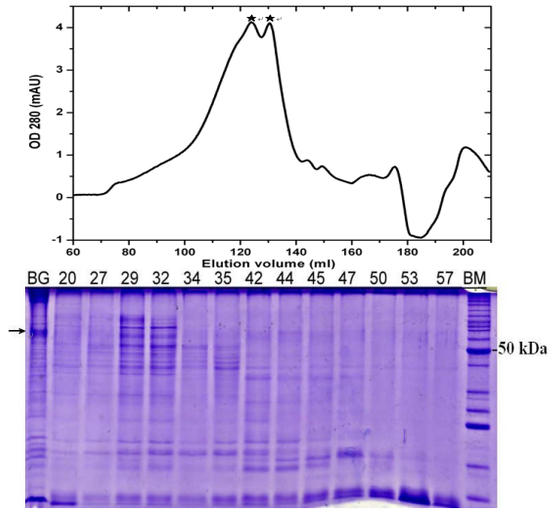

Figure 3.13: Purification of His-PS2-FL by SEC after Ni-NTA.
SEC profile (upper) of His-PS2-FL on superose 6 pg and coomassie staining of elution fractions (lower). BG: corresponds to the pooled Ni-NTA elution fraction; BM: bench marker. Black stars indicate the peak which contains His-PS2-FL; Black arrows indicate the His-PS2-FL monomer; the fraction number is indicated above the page (Each fraction is 2 ml; void volume of the column is 60 ml; fraction was collected after the void volume).

SEC profile and SDS-PAGE analysis (**Figure 3.13**) showed that there was no clear separation between the His-PS2-FL and impurities (Fraction 29 and Fraction 32).

3.1.4 Biophysical characterization

The refolded His-PS2-FL showed reasonable purity and yields suitable for biophysical studies. Therefore the protein was subjected to MS, CD, fluorescence spectroscopy and SEC analysis.

Bands	Protein name	% of the sequence coverage	Mascot score
1	PS-2	14 %	71
2	PS-2	14 %	79
3	PS-2	11 %	47
4	PS-2	14 %	73
5	slyD	40 %	86

Table 3.2: Identification of His-PS2-FL and copurifying proteins by mass spectrometry.
Protein short names along with the mass spectrometric parameters (% of the sequence coverage and the Mascot score (107) are summarized for each band. Bands 1 to 5 are indicated in **Figure 3.3**.

3.1.4.1 Mass spectrometry

As shown in **Table 3.2** and **Figure 3.14** bands 1 to 4 from **Figure 3.3** were identified as PS2. Band 5 was identified as slyD.

Band 1
1 MLTFMASDSE EEVCDERTSL MSAESPTPRS CQEGRQGPED GENTAQWRSQ
51 **ENEEDGEEDP DR**YVCSGVPG RPPGLEEELT LKYGAKHVIM LFVPVTLCMI
101 VVVATIKSVR FYTEK**NGQLI YTTFTEDTPS VGQR**LLNSVL NTLIMISVIV
151 VMTIFLVVLY KYRCYKFIHG WLIMSSLMLL FLFTYIYLGE VLKTYNVAMD
201 YPTLLLTVWN FGAVGMVCIH WKGPLVLQQA YLIMISALMA LVFIKYLPEW
251 SAWVILGAIS VYDLVAVLCP KGPLR**MLVET AQER**NEPIFP ALIYSSAMVW
301 TVGMAKLDPS SQGALQLPYD PEMEEDSYDS FGEPSYPEVF EPPLTGYPGE
351 ELEEEEERGV KLGLGDFIFY SVLVGKAAAT GSGDWNTTLA CFVAILIGLC
401 LTLLLLAVFK KALPALPISI TFGLIFYFST DNLVRPFMDT LASHQLYI
Band 2
1 MLTFMASDSE EEVCDERTSL MSAESPTPRS CQEGRQGPED GENTAQWRSQ
51 **ENEEDGEEDP DR**YVCSGVPG RPPGLEEELT LKYGAKHVIM LFVPVTLCMI
101 VVVATIKSVR FYTEK**NGQLI YTTFTEDTPS VGQR**LLNSVL NTLIMISVIV
151 VMTIFLVVLY KYRCYKFIHG WLIMSSLMLL FLFTYIYLGE VLKTYNVAMD
201 YPTLLLTVWN FGAVGMVCIH WKGPLVLQQA YLIMISALMA LVFIKYLPEW
251 SAWVILGAIS VYDLVAVLCP KGPLR**MLVET AQER**NEPIFP ALIYSSAMVW
301 TVGMAKLDPS SQGALQLPYD PEMEEDSYDS FGEPSYPEVF EPPLTGYPGE
351 ELEEEEERGV KLGLGDFIFY SVLVGKAAAT GSGDWNTTLA CFVAILIGLC
401 LTLLLLAVFK KALPALPISI TFGLIFYFST DNLVRPFMDT LASHQLYI
Band 3
1 MLTFMASDSE EEVCDERTSL MSAESPTPRS CQEGRQGPED GENTAQWRSQ
51 ENEEDGEEDP DRYVCSGVPG RPPGLEEELT LKYGAKHVIM LFVPVTLCMI
101 VVVATIKSVR FYTEK**NGQLI YTTFTEDTPS VGQR**LLNSVL NTLIMISVIV
151 VMTIFLVVLY KYRCYKFIHG WLIMSSLMLL FLFTYIYLGE VLKTYNVAMD
201 YPTLLLTVWN FGAVGMVCIH WKGPLVLQQA YLIMISALMA LVFIKYLPEW
251 SAWVILGAIS VYDLVAVLCP KGPLR**MLVET AQER**NEPIFP ALIYSSAMVW
301 TVGMAKLDPS SQGALQLPYD PEMEEDSYDS FGEPSYPEVF EPPLTGYPGE
351 ELEEEEERGV KLGLGDFIFY SVLVGKAAAT GSGDWNTTLA CFVAILIGLC
401 LTLLLLAVFK KALPALPISI TFGLIFYFST DNLVRPFMDT LASHQLYI
Band 4
1 MLTFMASDSE EEVCDERTSL MSAESPTPRS CQEGRQGPED GENTAQWRSQ
51 **ENEEDGEEDP DR**YVCSGVPG RPPGLEEELT LKYGAKHVIM LFVPVTLCMI
101 VVVATIKSVR FYTEK**NGQLI YTTFTEDTPS VGQR**LLNSVL NTLIMISVIV
151 VMTIFLVVLY KYRCYKFIHG WLIMSSLMLL FLFTYIYLGE VLKTYNVAMD
201 YPTLLLTVWN FGAVGMVCIH WKGPLVLQQA YLIMISALMA LVFIKYLPEW
251 SAWVILGAIS VYDLVAVLCP KGPLR**MLVET AQER**NEPIFP ALIYSSAMVW
301 TVGMAKLDPS SQGALQLPYD PEMEEDSYDS FGEPSYPEVF EPPLTGYPGE
351 ELEEEEERGV KLGLGDFIFY SVLVGKAAAT GSGDWNTTLA CFVAILIGLC
401 LTLLLLAVFK KALPALPISI TFGLIFYFST DNLVRPFMDT LASHQLYI
Band 5
1 MKVAKDLVVS LAYQVRTEDG VLVDESPVSA PLDYLHGHGS LISGLETALE
51 GHEVGDK**FDV AVGANDAYGQ YDENLVQR**VP K**DVFMGVDEL QVGMRFLAET**
101 **DQGPVPVEIT AVEDDHVVVD GNHMLAGQNL KFNVEVVAIR** EATEEELAHG
151 HVHGAHDHHH DHDHDGCCGG HGHDHGHEHG GEGCCGGKGN GGCGCH

Figure 3.14: Peptides identified by MALDI-MS analysis.
Matched peptides shown in **Bold Red**.

3.1.4.2 Circular dichroism spectroscopy

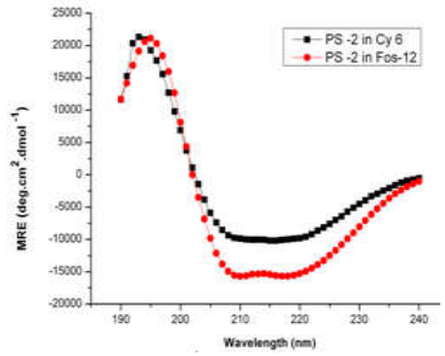

Figure 3.15: CD spectra of refolded His-PS2-FL in FC12 and Cy6.

Detergents	Helix 1	Helix 2	Strand1	Strand2	Turns	Unordered
FC12	0.31	0.19	0.11	0.06	0.16	0.18
Cy6	0.23	0.16	0.13	0.10	0.17	0.21

Table 3.3: Secondary structure contents of refolded His-PS2-FL in FC12 and Cy6.
Deconvolution of the raw CD spectra into pure component spectra.

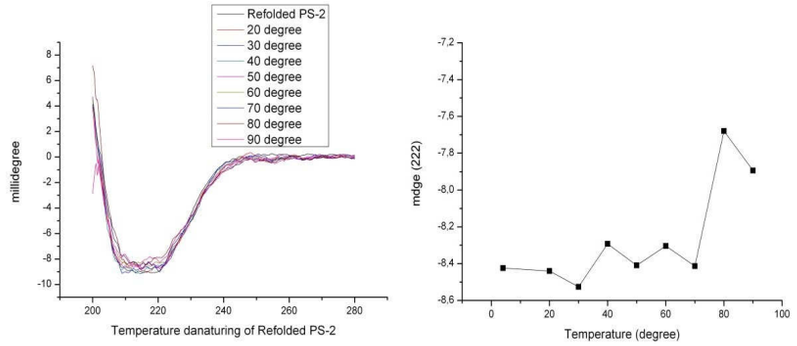

Figure 3.16: Thermal unfolding of refolded His-PS2-FL monitored by CD spectroscopy.
CD spectra of refolded His-PS2-FL at different temperatures (left) and the plot of 222 nm signal against different temperatures (right).

Purified His-PS2-FL was refolded in FC12 and Cy6 and subjected to circular dichroism spectroscopy to study the effect of detergents on secondary structure (**Figure 3.15** and **Table 3.3**). Thermal unfolding of refolded His-PS2-FL in FC12 was also investigated by CD spectroscopy. Refolded His-PS2-FL displays the characteristics of a predominantly α–helical protein. Deconvolution shows a helical content of 50 % in FC12 and 39 % in Cy6 indicating that FC12 favors the formation of α–helical structure. As shown in **Figure 3.16**, as temperature

increases, a decreased CD signal was observed. The plot shows that at 80 ℃, a significant decrease of signal at 222 nm was observed.

3.1.4.3 Fluorescence spectroscopy

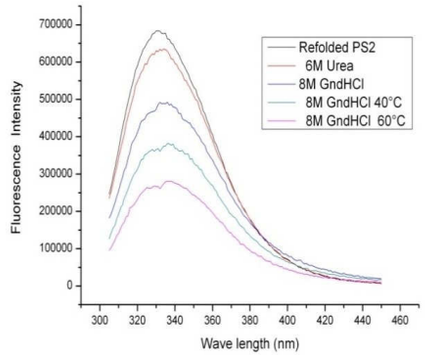

Figure 3.17: Unfolding of refolded His-PS2-FL monitored by fluorescence spectroscopy.

Refolded PS2: Refolded PS2 (0.058 mg/ml) in refolding buffer (10 mM NaH_2PO_4, 10 % Glycerol, 0.073 % (w/v) FC12, 2 mM TCEP, Protease Inhibitor, pH 7.4). 6 M urea: Refolded PS2 in refolding buffer supplemented with 6 M urea. 8 M GndHCl: Refolded PS2 in refolding buffer supplemented with 8 M GndHCl. 8 M GndHCl 40 ℃: Refolded PS2 in refolding buffer supplemented with 8 M GndHCl was heated to 40 ℃ for 30 min. 8 M GndHCl 60: Refolded PS2 in refolding buffer supplemented with 8 M GndHCl was heated to 60 ℃ for 30 min.

Unfolding of refolded His-PS2-FL in FC12 was also investigated by fluorescence spectroscopy (**Figure 3.17**). As compared with refolded PS2, a decreased emission was observed for PS2 denatured by urea and GndHCl. However, no significant red shift was observed indicating the microenvironment of trptophan remained stable.

3.1.4.4 Reconstitution into MO cubic phase

To investigate how refolded His-PS2-FL behaves biophysically in lipidic cubic phase, His-PS2-FL was reconstituted into MO cubic phase and subject to CD and fluorescence spectroscopy.

Reconstitution of refolded His-PS2-FL showed the characteristics of a predominantly α–helical protein in MO cubic phase with negative peaks between 208 nm to 223 nm and a cross over point at around 205 nm. The positive peak at

around 190 to 192 nm was not recorded due to the higher HT value caused by MO lipids. The tryptophan fluorescence of reconstituted His-PS2-FL after refolding was also measured. After subtraction the MO signal (red) from PS2 reconstituted MO signal (green), the pure PS2 tryptophan fluorescence signal (blue) was obtained. The spectrum had an emission maximum around 335 nm as shown in **Figure 3.18.**

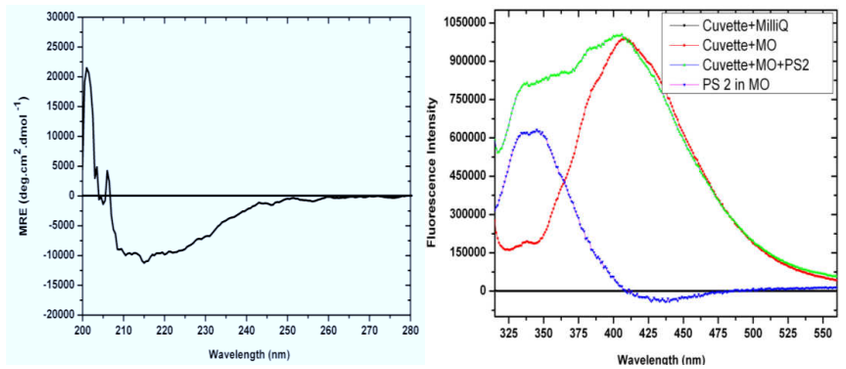

Figure 3.18: Reconstitution of refolded His-PS2-FL into MO cubic phase.
CD (left) and fluorescence spectra (right) of refolded His-PS2-FL reconstituted into MO cubic phase.

3.1.4.5 Size exclusion chromatography

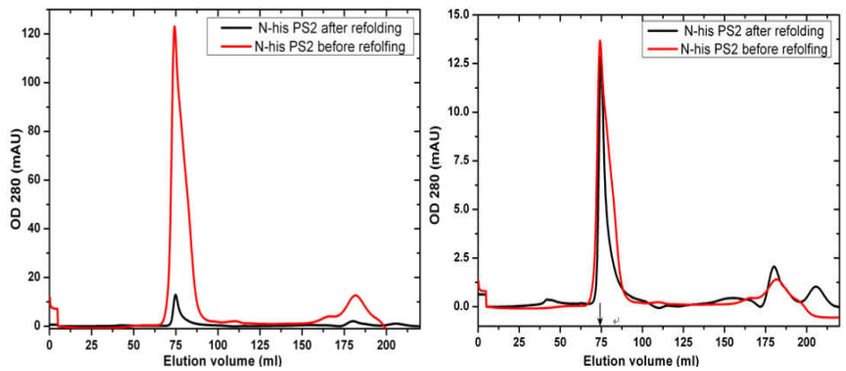

Figure 3.19: SEC analysis of before and after refolding of His-PS2-FL.
SEC profiles of His-PS2-FL before (red) and after (black) refolding on Superose 6 pg column. The picture on the right side is the SEC profiles of normalized intensity to show the elution volume differences. Black arrow indicates the void volume of the column which corresponds to elution volume of blue dextrin (74.50 ml; 2000 kDa).

To test the homogeneity and oligomerization state after refolding, refolded His-PS2-FL was concentrated and loaded onto a Superose 6 pg column. As shown in **Figure 3.19**, no significant difference of the elution volumes between before and after refolding was observed. The elution volume is 74.89 ml which is very close to the void volume (74.50 ml).

3.2 Cloning, expression, purification and characterization of PS2-proteins

3.2.1 Cloning and expression

Because of the failure in obtaining pure PS2-FL natively and the aggregation problem for refolded PS2-FL with N-his tag, a C-strep tag was introduced to the C-terminal of the PS2. At the same time, N-terminal fragment (PS2-NTF) and C-terminal fragment of PS2 (PS2-CTF) were also cloned using PS2-FL as a template. All these three constructs are N-terminally his and C-terminally strep tagged. The cloned constructs were confirmed by sequencing. Expressions of the protein of interests were investigated via small scale expression.

As shown in **Figure 3.20**, total protein fraction, except for CTF, aggregation on the top to the page was observed only for induced cells but not for uninduced cells. In the inclusion body fraction, a weak signal was detected for NTF with uninduced cells. While for induced cells except for the case of CTF expression, which showed a very weak signal, strong signals were observed for the other three proteins. In the membrane fraction, with uninduced cells, FL2 and NTF showed weak signals, and no signals were detected for the other two cases. However for induced cells, all four proteins showed western signals, although for CTF the signal is weak. Interestingly, with total protein for induced cells, all the signals were located on the top of separation PAGE indicating that protein has aggregated, possibly because of a lack of SDS. The observed aggregation was weaker when cells were fractioned into inclusion body and membrane fraction before subjecting the fraction to SDS-PAGE analysis.

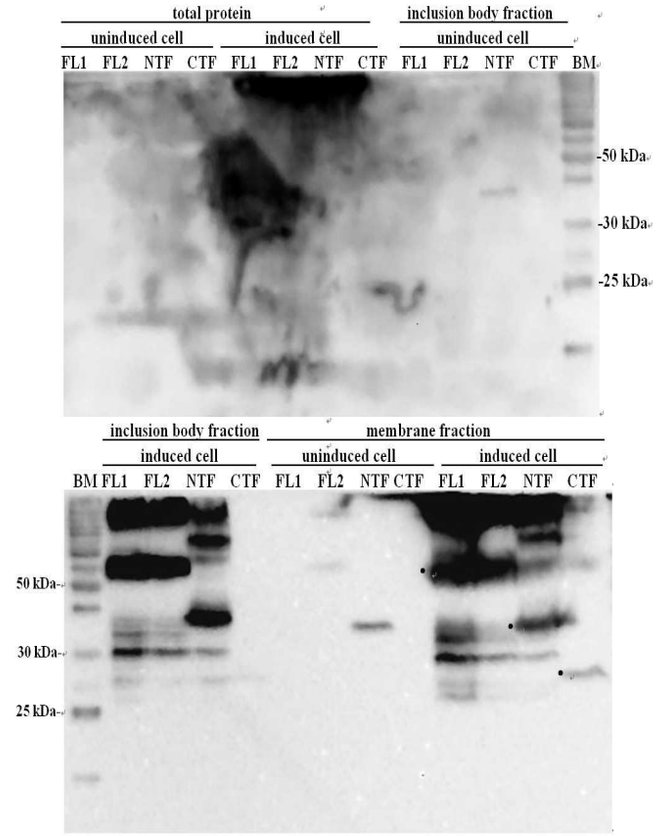

Figure 3.20: Expression of PS2-constructs.
Western blots showing the distribution of proteins of interest in different cell fraction. FL 1: full length PS2 with N-6 his; FL 2: full length PS2 with N-6 his and C-strep; NTF: N-terminal fraction of PS2 with N-6 his and C-strep; CTF: C-terminal fraction of PS2 with N-6 his and C-strep; BM: bench marker; Black dots indicate the monomer of the proteins of interest. Note that for FL 2 and NTF "leaky expression" were observed with un-induced control. However, full induction is achieved only in the presence of IPTG inducer.

3.2.2 Solubilisation

3.2.2.1 Solubilisation with different detergents

Membrane protein purification often requires the solubilisation of the target protein by detergents (108). To investigate the effect of detergents on the solubilisation of the respective proteins, membrane suspension corresponding to the same amounts of cell pellet was incubated with the solubilisation buffer

containing the respective detergents, as indicated in **Table 3.4**. After overnight incubation, each reaction was centrifuged at 100 000 × g for 1 h to separate the supernatant and the pellet fraction. The differently treated samples from the same amount of cell pellet were analysed by western blot.

Similar results were obtained for PS2-FL NTF and CTF. Figure 3.21 shows the remaining membrane pellet after detergent extraction. Similar to the experiment with OG and NG, a brownish membrane pellet was observed. For groups which contain FC12, 14, and 16 as well as NLS a clear transparent pellet were observed. Pellet after DM, DDM, Cy6, LDAO, CHAPS, and CTAB extraction yielded the slightly brownish pellet. CHPSO precipitated because of the temperature.

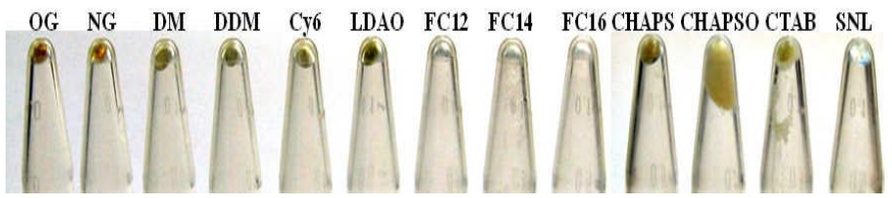

Figure 3.21 Residual membrane pellet upon solubilization with different detergents. 100 mg membrane was solubilised with different detergents respectively. Detergent name is listed above each tube. Shown is the remaining pellet (in brown grey or transparent) from 1 h 100 000 ×g centrifugation after detergent extraction.

Western blot analysis of the target protein revealed that for groups which contain OG and NG, very weak signals were detected in supernatant. For group which contains DM, DDM, Cy6, LDAO, CHAPS and CHAPSO, less intensity from the protein of interest were detected in supernatant as compared with the intensity from pellet except for His-PS2-NTF-Strep in LDAO, where more intensity in the supernatant was observed. However aggregation on top of the PAGE was also observed. The intensity in the supernatant is comparable with the intensity in the suspension only for groups which contain FC12, 14, and 16 as well as NLS as shown in **Figure 3.22**. Interestingly, it was the observed that the less brown the colour of the pellet after detergent extraction, the more efficient the detergent solubilised.

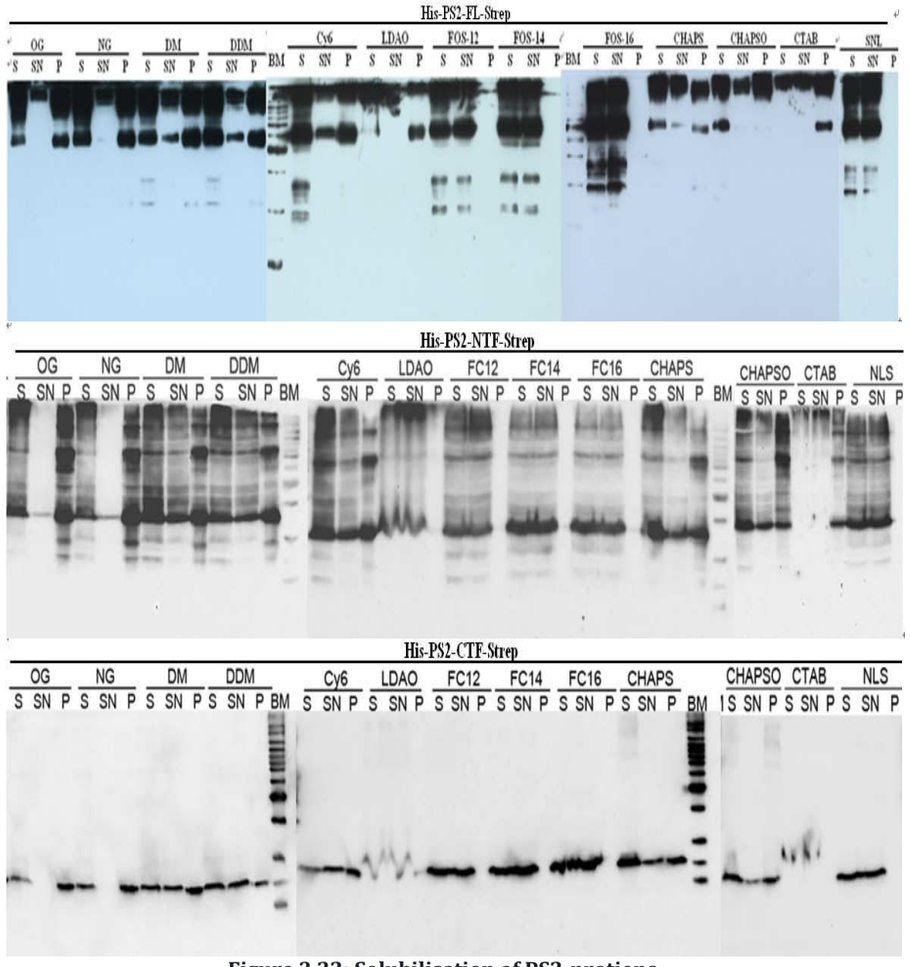

Figure 3.22: Solubilisation of PS2-protiens.

Effect of detergents on solubilisation of His-PS2-FL-Strep (top) His-PS2-NTF-Strep (middle) and His-PS2-CTF-Strep (bottom). S: suspension before 100 000×g; SN: supernatant after 100 000×g; P: pellet after 100 000×g; BM: bench marker. Detergents short names are indicated respectively. Shown is the western blot analysis of solubilisation.

Detergent used for solubilisation	Abbreviation	Type	Micell Molecular weight (KDa)	Concentration for solubilisation (% W/V)
n-Octyl-ß-D-glucopyranoside	OG	N	24.55	2
n-Nonyl-ß-D-glucopyranoside	NG	N	40.75	1
n-Decyl-ß-D-maltopyranoside	DM	N	33.29	1
n-Dodecyl-ß-D-maltoside	DDM	N	50.04	1
6-Cyclohexylhexyl β-D-maltoside	Cy 6	N	46.28	1
N,N-Dimethyldodecylamine *N*-oxide	LDAO	Z	17.43	1
FOS-choline-12	FC12	Z	18.98	1
FOS-choline-14	FC14	Z	40.98	1
FOS-choline-16	FC16	Z	72.53	1
3-[(3-Cholamidopropyl) dimethylammonio]-1-propanesulfonate	CHAPS	Z	6.14	2
3-([3-Cholamidopropyl] dimethylammonio)-2-hydroxy-1-propanesulfonate	CHAPSO	Z	6.93	2
Hexadecyltrimethylammonium bromide	CTAB	C	61.95	1
N-Lauroylsarcosine sodium salt	Sarkosyl NL	A	0.58	1

Table 3.4: Detergents used for solubilisation.
N stands for Non-ionic detergent; Z stands for Zwitterionic detergent; C stands for Cationic detergent; A stands for Anionic detergent.

3.2.2.2 Double extraction with same detergent

To increase solubilisation efficiency of the mild detergents, double extraction with the same detergent was performed.

For all the three protein investigated, the observed intensity for the pellet fraction was still comparable with the intensity for suspension as shown in **Figure 3.23,** except for LDAO where the signal is negligible when compared with suspension before centrifugation.

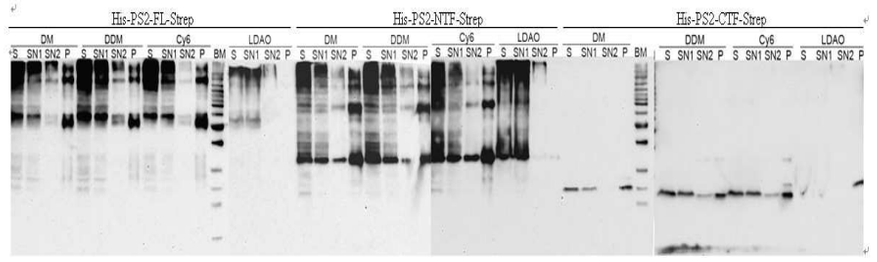

Figure 3.23: Effect of double extraction with same detergent on solubilisation of PS2-proteins.
S: suspension before 100 000×g; SN1: supernatant after first 100 000×g centrifugation; SN2: supernatant after second 100 000×g centrifugation; P: pellet after second 100 000×g centrifugation; BM: bench marker. Shown is the western blot analysis of solubilisation.

3.2.2.3 Double extraction with different detergents

To increase the solubilisation efficiency of a mild detergent, double extraction with different mild detergents was also performed. Briefly, the membrane was firstly incubated with NG which is found to exhibit poor solubilisation efficiency towards the target protein. After 3 h incubation, the membrane pellet was collected by centrifugation and resuspended by sonication with solubilisation buffer containing the second detergent.

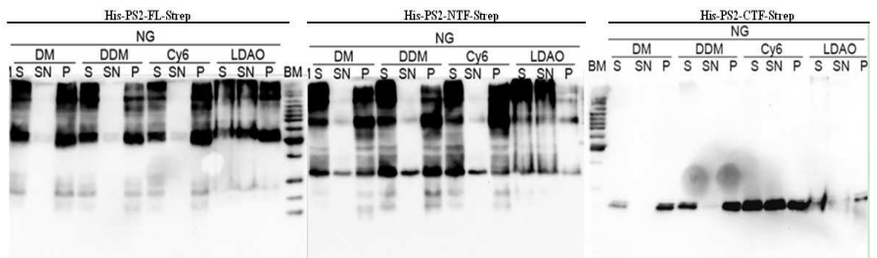

Figure 3.24: Effect of double extraction with different detergents on solubilisation of PS2-proteins.
S: suspension before 100 000×g; SN: supernatant after 100 000×g; P: pellet after 100 000×g; BM: bench marker. Shown is the w**estern blot analysis o**f solubilisation.

As shown in **Figure 3.24**, for His-PS2-FL-Strep, of all the four detergents studied, only for LDAO some signal for the supernatant was observed. For His-PS2-NTF-Strep in the supernatant fraction the strongest signal was observed for LDAO. The next stronger were DDM and Cy6, while DM produced the weakest

signal. For PS2-CTF, only in the Cy6 group reasonable signal was observed when compared with the signal from the suspension and the pellet. In conclusion, the efforts to solubilise the respective protein by mild detergents failed: None of the detergents studied were able to maintain the majority of the protein in supernatant.

3.2.2.4 Solubilisation with different amounts of FC12 micelles

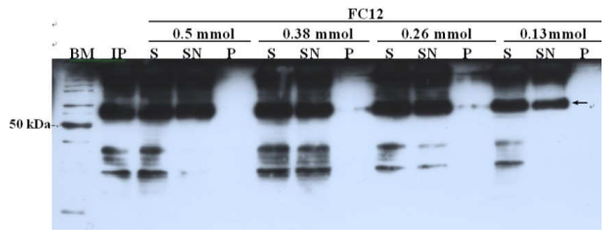

Figure 3.25: Effect of different amount of FC12 micelles on solubilisation of His-PS2-FL-Strep.

IP: input represents sample mixed with SDS sample buffer at zero time; S: suspension before 100 000×g centrifugation; SN: supernatant after 100 000×g; P: pellet after 100 000×g; BM: bench marker. FC12 micelle amount is given in mmol; black arrow indicates the His-PS2-FL-Strep monomer. Shown is the western blot analysis of solubilisation.

Of the 13 detergents tested for solubilisation, FC12 are one of the several detergents which can achieve total solubilisation. Therefore the effect of different amounts of FC12 micelles on the solubilisation of His-PS2-FL-Strep was studied.

With all amounts of detergent investigated, negligible signal was detected for pellet fractions. However, with 0.13 mmol a decreased intensity for the monomer band was observed. This indicates that there were not enough micelles to maintain the protein in a monomer form (**Figure 3.25**).

3.2.2.5 Solubilisation with different time durations

After determination of the amount of FC12 micelles for a given amount of cell pellet, the effect of increasing time on the solubilisaiton of His-PS2-FL-Strep was investigated.

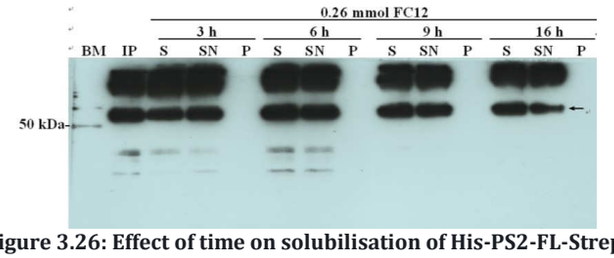

Figure 3.26: Effect of time on solubilisation of His-PS2-FL-Strep.
IP: input represents zero time sample mix with SDS sample buffer; S: suspension before 100 000×g; SN: supernatant after 100 000×g; P: pellet after 100 000×g; BM: bench marker. FC12 micelles amount was indicated as mmol; solubilisatin time was indicated in hour; black arrow indicates the His-PS2-FL-Strep monomer. Shown is the western blot analysis of solubilisation.

For 0.1 g cell pellet in 0.5 ml of 1 % FC12 for 3 h of solubilisation no signal from the protein of interest was detected in the pellet fraction as shown in **Figure 3.26.** The signal for the supernatant was comparable with the signal for the suspension and input indicating complete solubilisation of the target protein.

3.2.3 Purification

3.2.3.1 Ni-NTA purification with different detergents

Effect of detergents on the binding of the respective proteins to Ni-NTA was investigated by performing purification in presence of each detergent after solubilisation.

As shown in **Figure 3.27, f**or His-PS2-FL-Strep almost no detectable signals from the protein of interest were observed in the flow-through fractions and the wash fractions. However for His-PS2-NTF-Strep and His-PS2-CTF-Strep, signal corresponding to small part of the respective protein was found in the flow through and wash fractions. For all the 3 proteins, FC 12 produced the strongest signal in the elution fraction among all the 5 detergents, although the LDAO group also showed reasonable signals.

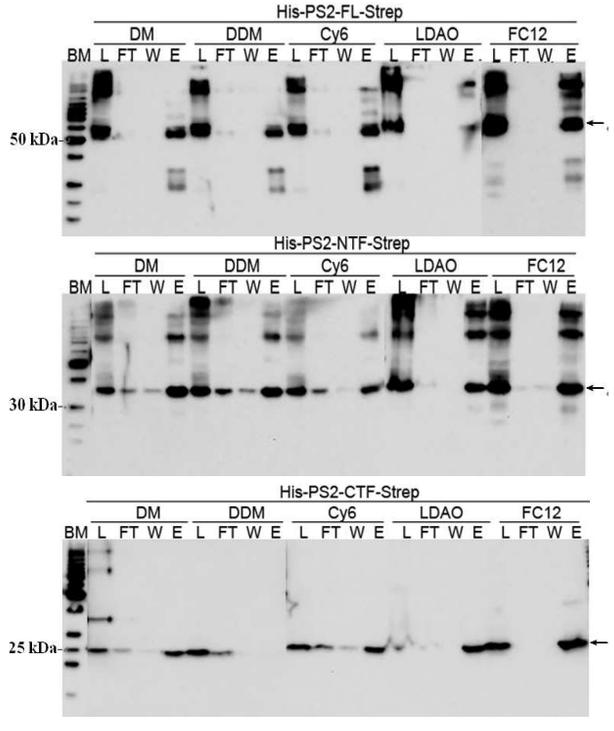

Figure 3.27: Ni-NTA purification with different detergents.
Effect of detergents on His-PS2-FL-Strep (top) His-PS2-NTF-Strep (middle) and His-PS2-CTF-Strep (bottom) purification by Ni-NTA. L: load; FT: flow through; W: wash; E: elution; BM: bench marker; Black arrows indicate the monomer form of the protein of interest respectively. Shown is the western blot analysis of purification.

3.2.3.2 Strep-Tactin purification with different detergents

Effect of detergents on the binding of respective protein to Strep-Tactin was also investigated by performing purification in presence of each detergent after solubilisation.

For PS2-FL and CTF, almost no detectable signals from the protein of interest were observed in elution fractions. Most of the signal was located in the flow-through and wash fractions. For His-PS2-NTF-Strep, amoung the five detergents tested, FC12 shows the strongest singal in elution fraction (**Figure 3.28**).

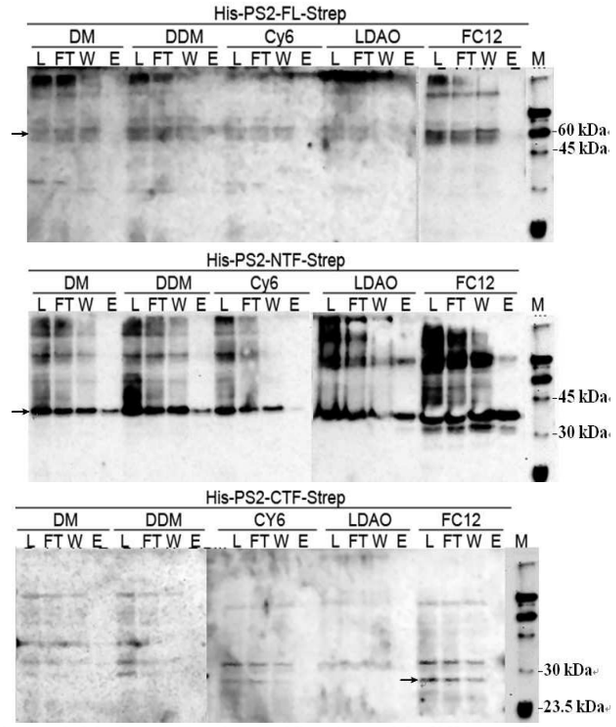

Figure 3.28: Strep-Tactin purification with different detergents.
Effect of detergents on His-PS2-FL-Strep (top) His-PS2-NTF-Strep (middle) and His-PS2-CTF-Strep (bottom) binding to Strep tag matrix. L: load; FT: flow through; W: wash; E: elution; M: Strep-tag Protein Ladder; Black arrows indicate the monomer form of the protein of interest respectively. Shown is the western blot analysis of purification.

3.2.3.3 Strep-Tactin purification with different FC12 concentrations

In order to optimize the FC12 concentrations during Strep-Tactin purification, the effect of FC12 concentration on the binding of His-PS2-NTF-Strep to Strep-Tactin was investigated.

For 0.1 % FC12 the intensity of the band corresponds to His-PS2-NTF-Strep gradually decreased from SMF to E2 to barely detectable intensity followed by a sudden increase in E3 to E5. However for 1 % FC12 the protein of interest was not sharply eluted, as shown by Figure 3.29.

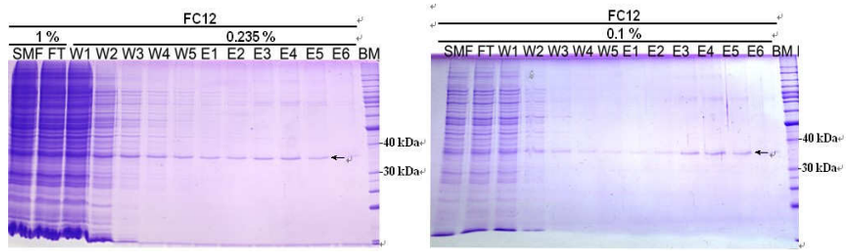

Figure 3.29: Effect of FC12 concentration on His-PS2-NTF-Strep binding to Strep matrix.
Coomassie staining showing the Strep-Tactin purification fractions in presence of 1 % (left) and 0.1 % (right) FC12. SMF: solubilised membrane fraction; FT: flow through; W: wash; E: elution; BM: bench marker; FC12 concentration was indicated on top of the SDS-PAGE.

3.2.3.4 Imidazole gradient elution

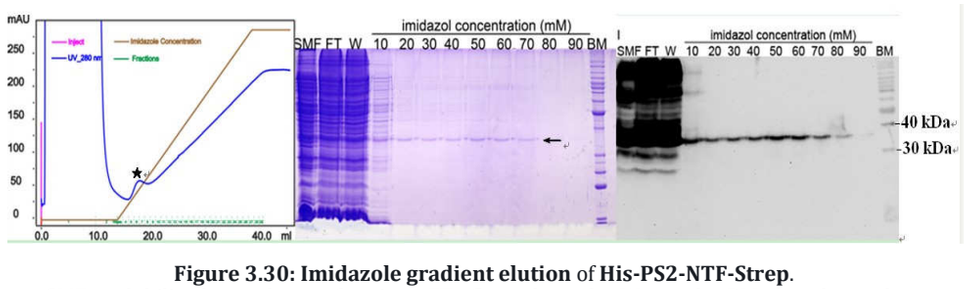

Figure 3.30: Imidazole gradient elution of **His-PS2-NTF-Strep**.
SMF: solubilised membrane fraction; FT: flow through; W: wash; BM: bench marker; imidazole concentration is given in mM. Black star indicates the elution peak which contains His-PS2-NTF-Strep. Black arrow indicates His-PS2-NTF-Strep monomer. Imidazole gradient elution profile of His-PS2-NTF-Strep (left) and coomassie staining (middle) as well as western blot (right) of different fractions are shown.

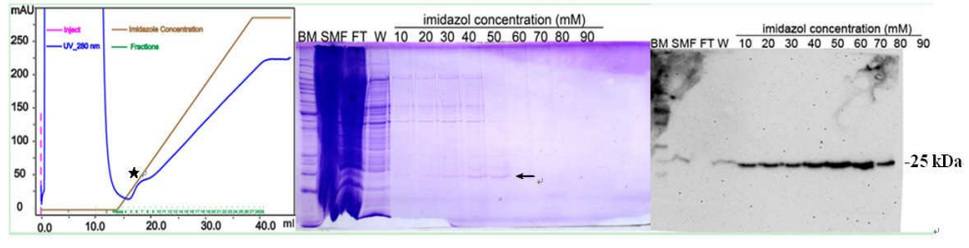

Figure 3.31: Imidazole gradient elution of His-PS2-CTF-Strep.
SMF: solubilised membrane fraction; FT: flow through; W: wash; BM: bench marker; imidazole concentration was also indicated as mM. Black star indicates the elution peak which contains His-PS2-CTF-Strep. Black arrow indicates His-PS2-CTF-Strep monomer. Imidazole gradient elution profile of His-PS2-CTF-Strep (left) and coomassie staining (middle) as well as western blot (right) of different fractions are shown.

Ni-NTA gradient elution was performed in order to determine the optimal imidazole concentration for Ni-NTA purification. As shown by **Figure 3.30** and **Figure 3.31**, His-PS2-NTF-Strep and His-PS2-CTF-Strep was eluted even with 10 mM imidazole. However the maximum intensity was observed with 50 to 60 mM. Similar results were observed for His-PS2-FL-Strep.

3.2.3.5 Ni-NTA purification

As shown in **Figure 3.32**, for all the three proteins, there are no significant differences between first and second Ni-NTA purification as far as the band intensity and the purity was concerned.

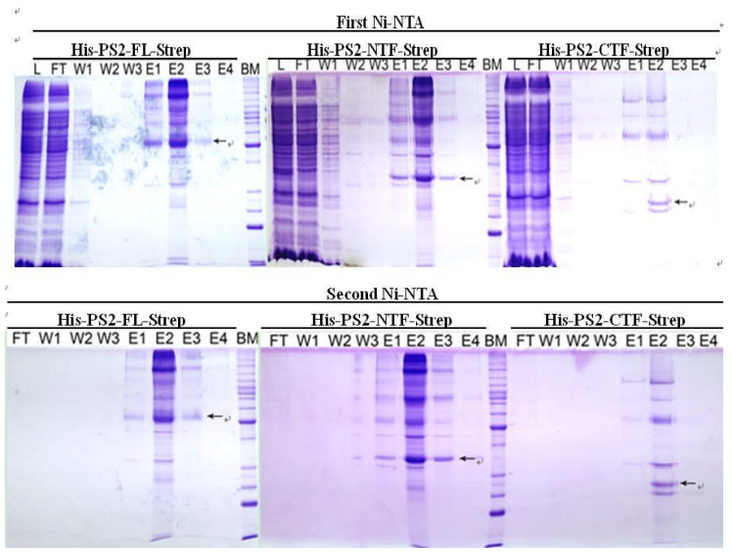

Figure 3.32: Double Ni-NTA purification of PS2-proteins.
SMF: solubilised membrane fraction; FT: flow through; W: wash; E: elution; BM: bench marker; Black arrows indicate the monomer forms of the proteins of interest. Shown are the coomassie staining of first (upper) and second (lower) Ni-NTA purification fractions.

3.2.3.6 Strep-Tactin purification after Ni-NTA

No signal corresponding to proteins of interest was detected in the elution fractions as shown by the **Figure 3.33**. Most of the protein was located in flow through fraction.

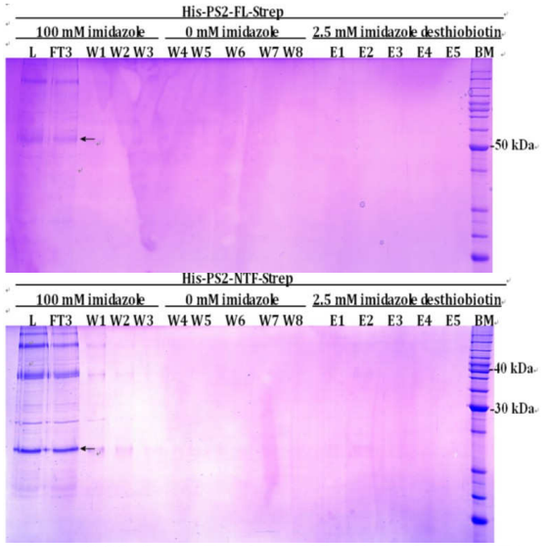

Figure 3.33: Strep-Tactin purification after Ni-NTA.

Coomassie staining of purification of His-PS2-FL-Strep (upper) and His-PS2-NTF-Strep (lower) by Strep tag. L: Ni-NTA elations; FT: flow through; W: wash; E: elution; BM: bench marker; Black arrows indicate the proteins of interest.

3.2.3.7 Removal of periplasmic fraction by osmotic shock

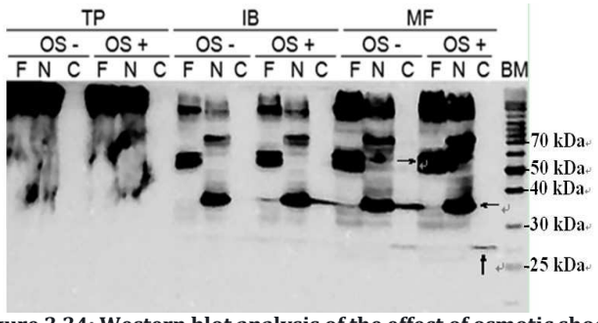

Figure 3.34: Western blot analysis of the effect of osmotic shock on protein distribution.

BM: bench marker; TP: total protein; IB: inclusion body; MF: membrane fraction; F: full length of PS2; N: N-terminal fraction of PS 2; C: C-terminal fraction of PS2; OS-: without osmotic shock; OS +: with osmotic shock. Black arrow indicates the monomer form of the protein in the membrane fraction.

As shown in **Figure 3.34**, addition of osmotic shock before cell opening didn't influence the distribution of any of the three proteins due to the fact that most of the protein was still located in the membrane fraction after osmotic shock.

3.2.3.8 Ni-NTA Purification after osmotic shock

As shown in **Figure 3.35**, removal of the periplasmic fraction before Ni-NTA purification improved purity for His-PS2-FL-Strep and His-PS2-NTF-Strep observably. However the purity of His-PS2-CTF-Strep didn't change (as compared with **Figure 3.32**).

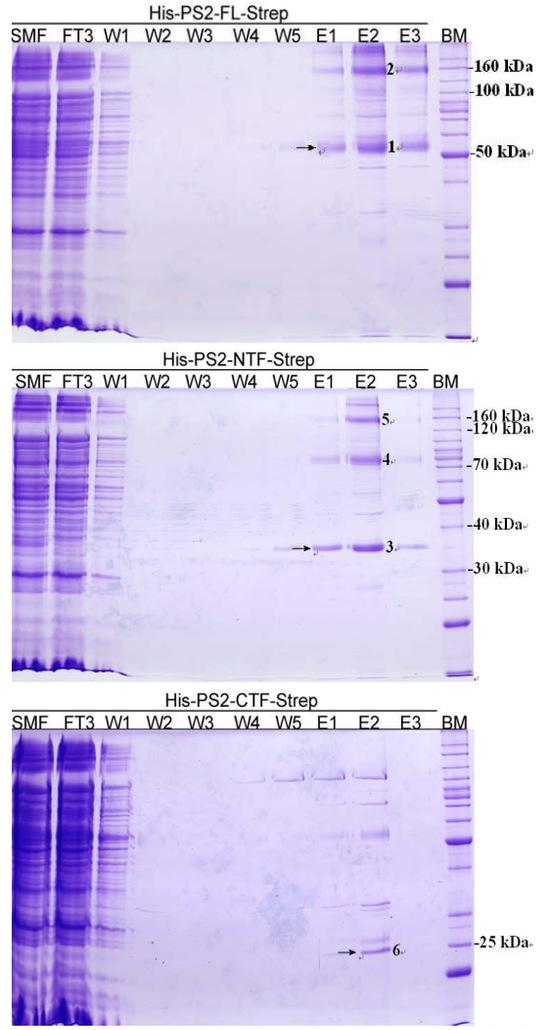

Figure 3.35: Ni-NTA Purification after osmotic shock.
SMF: solubilised membrane fraction; FT: flow through; W: wash; E: elution; BM: bench marker; Black arrows indicate the monomer forms of the proteins of interest. Coomassie staining of Ni-NTA purification fractions of His-PS2-FL-Strep (top) His-PS2-NTF-Strep (middle) and His-PS2-CTF-Strep (bottom) are shown. The numbers to the right side of the bands indicate the protein bands which are excised and subjected to Mass spectrometry.

3.2.3.9 Mass spectrometry

Bands (1-6) as indicated in Figure 3.35 were cut, destained, dehydrated and digested as described in the Trypsin Profile IGD Kit (SIGMA). The supernatant of the digested peptide was subjected to mass spectrometry. As shown in Table 3.5 and Figure 3.36, PS2-FL and PS2-NTF were significantly identified. However, for PS2-CTF only one peptide was detected.

Bands	Protein name	% of the sequence coverage	Score Swiss Prot
1	PS2-FL	10.3	238
2	PS2-FL	4.7	178
3	PS2-NTF	15.3	150
4	PS2-NTF	21.7	234
5	PS2-NTF	15.3	186
6	PS2-CTF	8.93	--

Table 3.5: Identification of PS2 proteins by mass spectrometry.

Protein score is -10*Log (P), where P is the probability that the observed match is a random event. Scores > 70 means the hit is significant. Search is performed in Swiss Prot against all organisms.

Band 1

1 HHHHHHHMLT FMASDSEEEV CDER**TSLMSA ESPTPR**SCQE GR**QGPEDGEN**
51 **TAQWRSQENE EDGEEDPDR**Y VCSGVPGRPP GLEEELTLKY GAKHVIMLFV
101 PVTLCMIVVV ATIKSVRFYT EKNGQLIYTP FTEDTPSVGQ RLLNSVLNTL
151 IMISVIVVMT IFLVVLYKYR CYKFIHGWLI MSSLMLLFLF TYIYLGEVLK
201 TYNVAMDYPT LLLTVWNFGA VGMVCIHWKG PLVLQQAYLI MISALMALVF
251 IKYLPEWSAW VILGAISVYD LVAVLCPKGP LR**MLVETAQE R**NEPIFPALI
301 YSSAMVWTVG MAKLDPSSQG ALQLPYDPEM EEDSYDSFGE PSYPEVFEPP
351 LTGYPGEELE EEEERGVKLG LGDFIFYSVL VGKAAATGSG DWNTTLACFV
401 AILIGLCLTL LLLAVFKKAL PALPISITFG LIFYFSTDNL VRPFMDTLAS
451 HQLYISAWSH PQFEK

Band 2

1 HHHHHHHMLT FMASDSEEEV CDERTSLMSA ESPTPRSCQE GR**QGPEDGEN**
51 **TAQWR**SQENE EDGEEDPDRY VCSGVPGRPP GLEEELTLKY GAKHVIMLFV
101 PVTLCMIVVV ATIKSVRFYT EKNGQLIYTP FTEDTPSVGQ RLLNSVLNTL
151 IMISVIVVMT IFLVVLYKYR CYKFIHGWLI MSSLMLLFLF TYIYLGEVLK
201 TYNVAMDYPT LLLTVWNFGA VGMVCIHWKG PLVLQQAYLI MISALMALVF
251 IKYLPEWSAW VILGAISVYD LVAVLCPKGP LR**MLVETAQE R**NEPIFPALI
301 YSSAMVWTVG MAKLDPSSQG ALQLPYDPEM EEDSYDSFGE PSYPEVFEPP
351 LTGYPGEELE EEEERGVKLG LGDFIFYSVL VGKAAATGSG DWNTTLACFV
401 AILIGLCLTL LLLAVFKKAL PALPISITFG LIFYFSTDNL VRPFMDTLAS
451 HQLYISAWSH PQFEK

Band 3

1 HHHHHHHMLT FMASDSEEEV CDER**TSLMSA ESPTPR**SCQE GR**QGPEDGEN**
51 **TAQWRSQENE EDGEEDPDR**Y VCSGVPGRPP GLEEELTLKY GAKHVIMLFV
101 PVTLCMIVVV ATIKSVRFYT EKNGQLIYTP FTEDTPSVGQ RLLNSVLNTL
151 IMISVIVVMT IFLVVLYKYR CYKFIHGWLI MSSLMLLFLF TYIYLGEVLK
201 TYNVAMDYPT LLLTVWNFGA VGMVCIHWKG PLVLQQAYLI MISALMALVF
251 IKYLPEWSAW VILGAISVYD LVAVLCPKGP LR**MLVETAQE R**NEPIFPALI
301 YSSASAWSH PQFEK

Band 4
1 HHHHHHHMLT FMASDSEEEV CDER**TSLMSA ESPTPR**SCQE GR**QGPEDGEN**
51 TAQWRSQENE EDGEEDPDRY VCSGVPGRPP GLEEELTLKY GAKHVIMLFV
101 PVTLCMIVVV ATIKSVRFYT EKNGQLIYTP FTEDTPSVGQ RLLNSVLNTL
151 IMISVIVVMT IFLVVLYKYR CYKFIHGWLI MSSLMLLFLF TYIYLGEVLK
201 TYNVAMDYPT LLLTVWNFGA VGMVCIHWKG PLVLQQAYLI MISALMALVF
251 IKYLPEWSAW VILGAISVYD LVAVLCPKGP LR**MLVETAQE R**NEPIFPALI
301 YSSASAWSH PQFEK
Band 5
1 HHHHHHHMLT FMASDSEEEV CDER**TSLMSA ESPTPR**SCQE GR**QGPEDGEN**
51 **TAQWRSQENE EDGEEDPDR**Y VCSGVPGRPP GLEEELTLKY GAKHVIMLFV
101 PVTLCMIVVV ATIKSVRFYT EKNGQLIYTP FTEDTPSVGQ RLLNSVLNTL
151 IMISVIVVMT IFLVVLYKYR CYKFIHGWLI MSSLMLLFLF TYIYLGEVLK
201 TYNVAMDYPT LLLTVWNFGA VGMVCIHWKG PLVLQQAYLI MISALMALVF
251 IKYLPEWSAW VILGAISVYD LVAVLCPKGP LR**MLVETAQE R**NEPIFPALI
301 YSSASAWSH PQFEK
Band 6
1 HHHHHHHMVW TVGMAKLDPS SQGALQLPYD PEMEEDSYDS FGEPSYPEVF
51 EPPLTGYPGE ELEEEEERGV K**LGLGDFIFY SVLVGK**AAAT GSGDWNTTLA
101 CFVAILIGLC LTLLLLAVFK KALPALPISI TFGLIFYFST DNLVRPFMDT
151 LASHQLYISA WSHPQFEK

Figure 3.36: Peptides identified by MALDI-MS analysis.
Matched peptides shown in **Bold Red**.

3.2.3.10 Size exclusion chromatography

To investigate the homogeneity and to remove the aggregated protein after Ni-NTA purification, Ni-NTA elution were concentrated and loaded onto a superose 6 analytical column. The running condition is as described in **Section 2.2.6**.

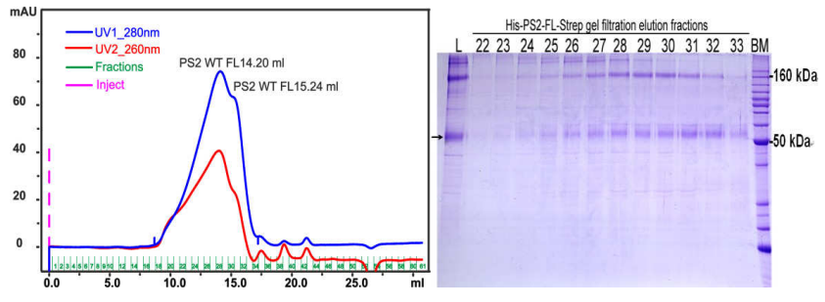

Figure 3.37: SEC analysis of His-PS2-FL-Strep.
BM: bench marker. L: load corresponds to the pooled Ni-NTA elution. Black arrow indicates the His-PS2-FL-Strep monomer. Gel filtration elution profile (left) on superose 6 analytical column and coomassie staining of elution fractions (right) are shown.

Gel filtration elution profile on superose 6 analytical and coomassie staining of elution fractions of the respective protein are shown in **Figure 3.37** (His-PS2-FL-Strep), **Figure 3.38** (His-PS2-NTF-Strep) and **Figure 3.39** (His-PS2-CTF-Strep).

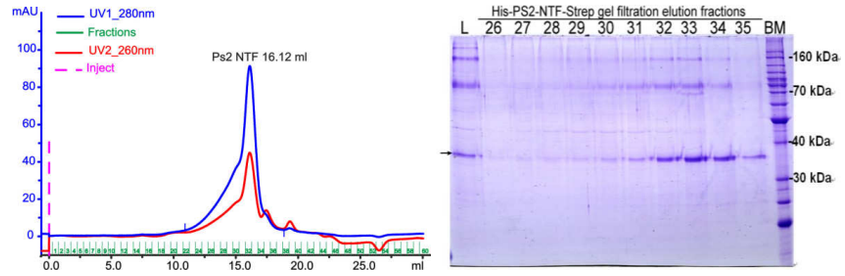

Figure 3.38: SEC analysis of His-PS2-NTF-Strep.
L: load corresponds to the pooled Ni-NTA elution; BM: bench marker. Black arrow indicate s the His-PS2-NTF-Strep monomer. Gel filtration elution profile (left) on superose 6 analytical column and coomassie staining of elution fractions (right) are shown.

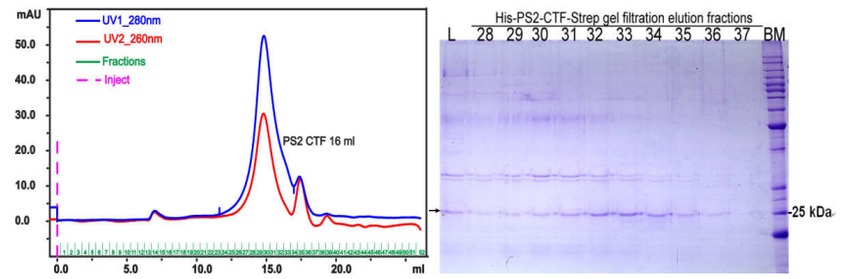

Figure 3.39: SEC analysis of His-PS2-CTF-Strep.
L: load corresponds to the pooled Ni-NTA elution; BM: bench marker. Black arrow indicates the His-PS2-CTF-Strep monomer. Gel filtration elution profile (left) on superose 6 analytical column and coomassie staining of elution fractions (right) are shown.

As shown in **Figure 3.40,** PS2-FL1 was predicted to have a MW of 338.15 kDa; PS2-FL2 was predicted at 166.15 kDa; His-PS2-NTF-Strep was predicted at 91.07 kDa; PS2-CTF was predicted at 98.85 kDa. By subtraction of the FC12 micelle MW from the observed molecular weight of the detergent protein complex it was calculated that the PS2-FL1 exists as a hexamer in FC 12 micelle ((338.15-18.98) / 52.3 = 6.10); PS2-FL2 as a trimer ((166.15-18.98) / 52.3 = 2.81); His-PS2-NTF-Strep as a dimer (91.07 -18.98) / 35.7 = 2.02); PS2-CTF as a tetramer (98.85 -18.98) / 18.7 = 4.27).

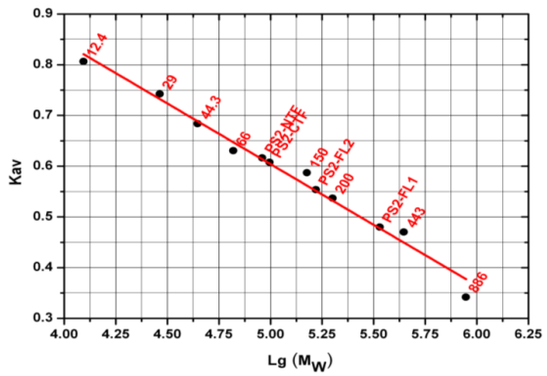

Figure 3.40: M_w determination of PS2 proteins by SEC.
In vivo expressed PS2-FL NTF and CTF molecular weight determination by superpose 6 analytical calibration curve. PS2-FL1 and PS2-FL2 represents the first and second peak respectively on elution profile.

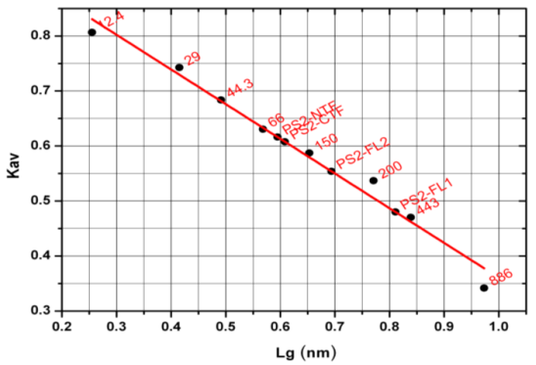

Figure 3.41: R_h determination of PS2 proteins by SEC.
In vivo expressed PS2-FL, NTF and CTF hydrodynamic radius determination by superpose 6 analytical calibration curve. PS2-FL1 and PS2-FL2 represents the first and second peak respectively on elution profile.

As shown in **Figure 3.41,** the first peak of His-PS2-FL-Strep was predicted at a hydrodynamic radius of 6.47 nm; the second peak was predicted as 4.94 nm; His-PS2-NTF-Strep was predicted as 3.93 nm; PS2-CTF was predicted as 4.06 nm.

3.2.3.11 Upscaled purification of His-PS2-NTF-Strep

It is reported that when glycerol is added into the *in meso* crystallization system, the lattice of the cubic phase becomes smaller, which doesn't support the membrane protein crystallization (109). Therefore glycerol is removed form the buffer by gel filtration which is the last purification step before crystallization.

As shown in **Figure 3.42**, the band corresponding to the His-PS2-NTF-Strep monomer was detected from fraction 28 to 49 indicating different oligomerisation state. However the intensity maximum was observed in fraction 45 and 46 which corresponds to the molecular weight of His-PS2-NTF-Strep dimer.

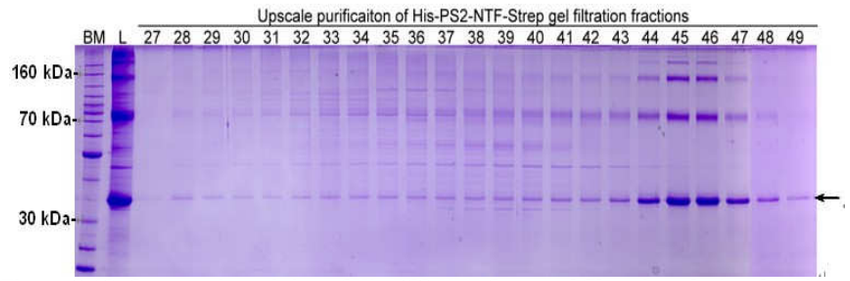

Figure 3.42: Coomassie staining of His-PS2-NTF-Strep gel filtration elution fractions.
L: load corresponds to the pooled Ni-NTA elution; BM: bench marker. Black arrows indicate the His-PS2-NTF-Strep monomer.

As shown in **Figure 3.43**, the absorption value and elution volume for first peak were nearly the same. The same elution volume was also observed for the second peak. However the chromatogram without glycerol had a lower absorption value than that with glycerol. For the third peak corresponding to the His-PS2-NTF-Strep dimer, higher absorption values and elution volumes were observed in the chromatography without glycerol. Given that the same amount of cells and an identical purification protocol were used, these results suggest that removal of glycerol increases the His-PS2-NTF-Strep dimer yield.

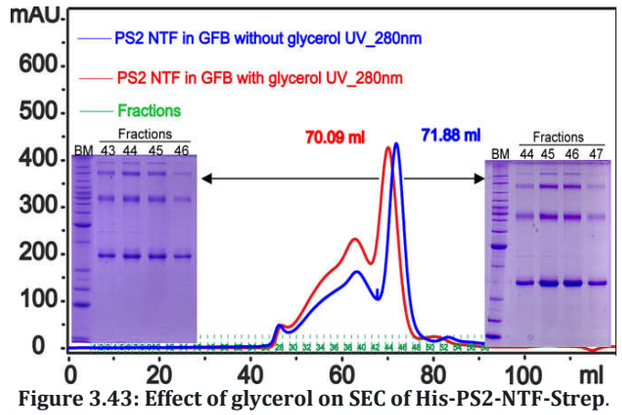

Figure 3.43: Effect of glycerol on SEC of His-PS2-NTF-Strep.
SEC profiles of His-PS2-NTF-Strep with (red) and without (blue) glycerol on superdex 200 pg column as well as the coomassie staining of peak fractions are shown.

By Ni-NTA and gel filtration, from 8 g cells (corresponding to 0.5 L TB culture), about 1 mg His-PS2-NTF-Strep can be purified with reasonable purity and homogeneity for crystallization screening.

3.2.4 Biophysical characterization of His-PS2-NTF-Strep

3.2.4.1 Size exclusion chromatography

3.2.4.1.1 His-PS2-NTF-Strep in different detergents

To investigate the oligomerisation state of His-PS2-NTF-Strep in different detergents, FC12 purified His-PS2-NTF-Strep was concentrated to 1.38 mg/ml and diluted 10 times into a buffer containing 1.5 CMC of DM, DDM, Cy6, LDAO, FC12 and 6 M urea respectively. The samples were then incubated at 4 ℃ with gentle mixing over night. Identical amount of protein was aliquoted and subjected to SDS-PAGE. Each sample was then concentrated and filtrated before being loaded onto a superdex 200 analytical column as described in **section 2.2.6**.

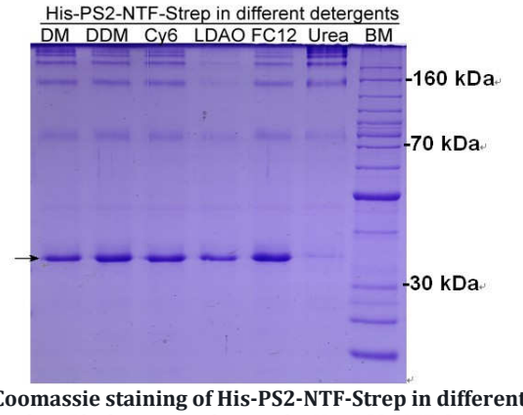

Figure 3.44: Coomassie staining of His-PS2-NTF-Strep in different detergents.
BM: bench marker. Black arrow indicates the His-PS2-NTF-Strep monomer.

As shown in **Figure 3.44**, in DDM, Cy6 and FC12 the intensity for the bands corresponding to His-PS2-NTF-Strep monomer were identical. While decreased intensity was observed for DM, LDAO and Urea. As intensity for the band corresponding to PS2-NTF monomer decreased the aggregation on top of the page increased for DM and Urea. For the LDAO group, a cloudy solution was

observed after overnight incubation, indicating that bigger aggregates form which did not enter the separation gel.

The SEC profile showed that only in FC12, His-PS2-NTF-Strep exhibits a single Gaussian-shaped peak indicating a monodispersed protein sample. In other detergents different oligomerisation were observed. His-PS2-NTF-Strep in LDAO however formed a cloudy solution and after concentrating and centrifugation a clear pellet was observed. Therefore for the supernatant no peak was detected by SEC (**Figure 3.45**).

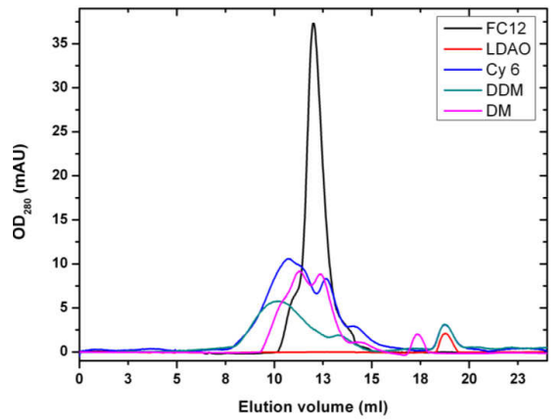

Figure 3.45: SEC profiles of His-PS2-NTF-Strep in different detergents.

3.2.4.1.2 His-PS2-NTF-Strep in different concentration of FC12

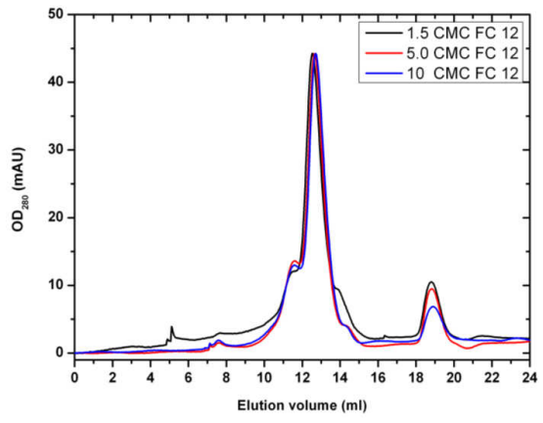

Figure 3.46: SEC profiles of His-PS2-NTF-Strep in different FC12 concentration.

To investigate whether the His-PS2-NTF-Strep dimer formation is due to an inadequate amount of detergent, purified dimer was run in presence of increasing concentration of FC12 during gel filtration. As shown in **Figure 3.46**, increasing concentration of FC12 did not change the elution volume of His-PS2-NTF-Strep.

3.2.4.1.3 His-PS2-NTF-Strep in different pH

Effect of pH on stability of His-PS2-NTF-Strep dimer was also investigated via gel filtration. As shown in **Figure 3.47**, except for pH 8, extra peaks were observed at about 7.8 ml which is close to the void volume of the column. The intensity for the peak near the void volume was higher in pH 6 than in pH 7 indicating a greater extent of protein aggregation.

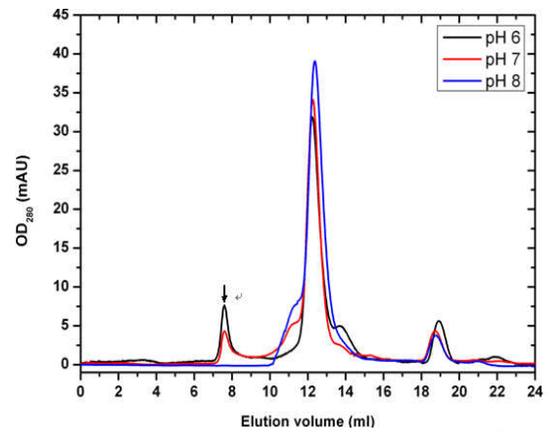

Figure 3.47: SEC profiles of His-PS2-NTF-Strep in different pH.
Black arrow indicates the void volume of the column.

3.2.4.1.4 His-PS2-NTF-Strep in different TCEP concentration

To investigate the effect of disulfide bond formation on the His-PS2-NTF-Strep dimer formation, purified dimer was run in presence of increasing concentrations of the reducing agent TCEP during gel filtration. Increasing concentration of TCEP did not change the elution volumn of His-PS2-NTF-Strep as shown in **Figure 3.48.**

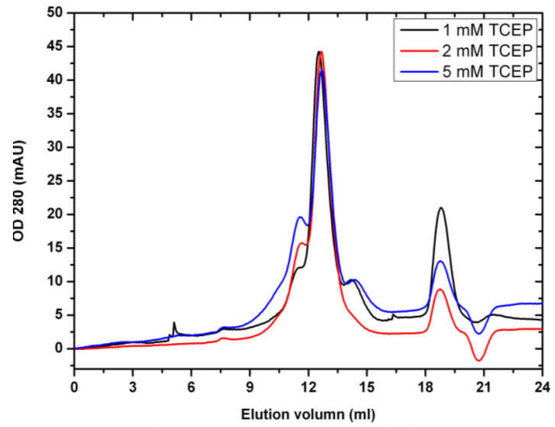

Figure 3.48: SEC profiles of His-PS2-NTF-Strep in different TCEP concentration.

3.2.4.2 CD spectroscopy analysis of His-PS2-NTF-Strep

3.2.4.2.1 Total secondary structure content prediction

According to PSIPRED software, the His-PS2-NTF-Strep was predicted to have a total helix content of 46.2 % and strand content of 14.6 % respectively (**Figure 3.49)**.

```
Conf: 9875311479832899400013345666678999999778987889998751123346 77
Pred: CCCCCCEEEEEECCCCCHHCCCCCCCCCCCCCCCCCCCCCCCCCCCCCCCCCCCCCCC
  AA: MKHHHHHHLTFMASDSEEEVCDERTSLMSAESPTPRSCQEGRQGPEDGENTAQWRSQENE
            10        20        30        40        50        60
Conf: 899999887757899999997201355532000001210011556777430166631111
Pred: CCCCCCCCCCCCCCCCCCCCCCCHHHHHHHHHHCHHHEEEEEHHHHHHHHHHHEEEEEEEE
  AA: EDGEEDPDRYVCSGVPGRPPGLEEELTLKYGAKHVIMLFVPVTLCMIVVVATIKSVRFYT
            70        80        90       100       110       120
Conf: 158707887200489971003332110024455677667778555332001457789999
Pred: CCCCEEEEEEECCCCCCCCHHHHHHHHHHHHHHHHHHHHHHHHHHHHHHHHHHHHHHHHH
  AA: EKNGQLIYTTFTEDTPSVGQRLLNSVLNTLIMISVIVVMTIFLVVLYKYRCYKFIHGWLI
           130       140       150       160       170       180
Conf: 98999999977999999988386670457999987511000476752286103579999
Pred: HHHHHHHHHHHHHHHHHHHHHHHCCCCCCCHHHHHHHHHHHHHHHHEEEEEEECCCCHHHHHHHH
  AA: MSSLMLLFLFTYIYLGEVLKTYNVAMDYPTLLLTVWNFGAVGMVCIHWKGPLVLQQAYLI
           190       200       210       220       230       240
Conf: 99999999962099315889999875301136447997389999998671999974135
Pred: HHHHHHHHHHHHHHHCCCHHHHHHHHHHHHHHCEEEEECCCCHHHHHHHHHHHHCCCCCCCEE
  AA: MISALMALVFIKYLPEWSAWVILGAISVYDLVAVLCPKGPLRMLVETAQERNEPIFPALI
           250       260       270       280       290       300
Conf: 51343358999999
Pred: EECCCCCCCCCCCC
  AA: YSSASAWSHPQFEK
           310
```

Figure 3.49: His-PS2-NTF-Strep total secondary structure prediction using PSIPRED. Conf: Confidence 0 =low 9 =high; Pred: Predicted secondary structure; AA: Target sequence; H =helix; E =strand; C =coil. A total helix content of 46.2 % and strand content of 14.6 % was predicted by PSIPRED predictions (110).

3.2.4.2.2 Far UV CD spectra of His-PS2-NTF-Strep in different detergents

To investigate the secondary structure of His-PS2-NTF-Strep in different detergents, FC12 purified His-PS2-NTF-Strep was concentrated to 1.38 mg/ml and diluted 10 times into a buffer containing 1.5 CMC of DM, DDM, Cy6, LDAO, FC12 and 6 M urea respectively. The samples were then incubated at 4 ℃ with gentle mixing over night. The CD spectra in different detergents were then recorded as described in **Section 2.2.13.**

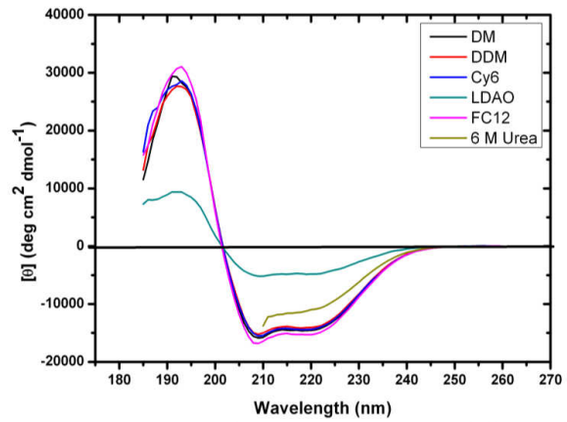

Figure 3.50: Far UV CD spectra of His-PS2-NTF-Strep in different detergents.

The far UV CD spectrum of His-PS2-NTF-Strep dimer solubilised in 2 CMC FC12, as shown in **Figure 3.50**, displays the characteristics of a predominantly α–helical protein with a negative bands at 219 to 223 and 208 to 211 nm, a positive band at 190 to 192 nm and a cross over point at 200 to 201 nm. The ideal values are 222, 208, 190 to 195 and 205 nm, respectively. Identical spectra were obtained for DM, DDM and Cy6. The spectrum in 6 M urea still shows the characteristics of an α–helical protein, although with decreased intensity. However, in LDAO a typical β-sheet spectrum was recorded.

Deconvolution of the measured far UV CD spectrum in FC12 yields 48.7 % α-helix, 11.5 % β-strand 15.5 % turn and 24.8 % unordered structure. Similar results were obtained for DM DDM and Cy6. In LDAO α-helix decreases to 16 % and β-strand increased to 31.2 %. The fraction for turns and unordered goes up to

19.3 % and 33.6 % respectively (**Table 3.6**). Among the 6 groups, FC12 shows the most helix signal.

Detergents	αR	αD	βR	βD	Turn	Unordered
DM	0.294 ±0.014	0.167 ±0.003	0.076 ±0.003	0.059 ±0.001	0.155 ±0.005	0.255 ±0.005
DDM	0.278 ±0.019	0.167 ±0.003	0.076 ±0.005	0.062 ±0.002	0.161 ±0.003	0.262 ±0.013
Cy 6	0.281 ±0.017	0.167 ±0.003	0.076 ±0.006	0.061 ±0.001	0.159 ±0.008	0.259 ±0.018
FC12	0.310 ±0.018	0.177 ±0.003	0.062 ±0.008	0.053 ±0.002	0.155 ±0.005	0.248 ±0.016
LDAO	0.074	0.086	0.203	0.109	0.193	0.336

Table 3.6: Deconvolution of His-PS2-NTF-Strep raw CD spectra in different detergents. Deconvolution of LDAO group was only possible with CONTIN.

3.2.4.2.3 Far UV CD spectra of His-PS2-NTF-Strep in different pH

γ-secretase has been found to localize in a variety of cell compartments. About 95 % of γ-secretase resides between the ER and Golgi, whereas only 5 % that displays activity localize at the plasma membrane or in endosome compartments(111). The pH varies from slightly neutral to acidic along the secretary pathway (112). Given that presenilins are presented in different cell compartments which have varying pH, the effect pH on secondary structure of His-PS2-NTF-Strep was investigated.

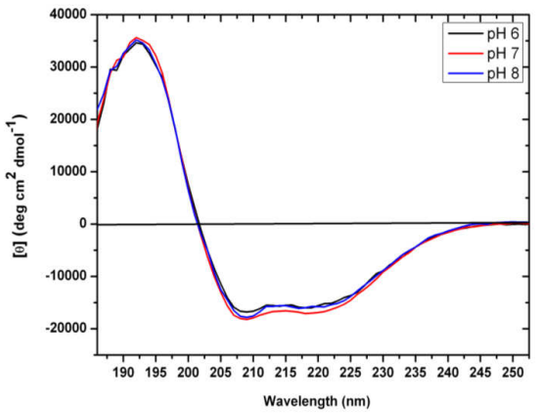

Figure 3.51: Far UV CD spectra of His-PS2-NTF-Strep in different pH.

As shown in **Figure 3.51** and **Table 3.7**, similar results were obtained for far UV CD spectra and component spectra for His-PS2-NTF-Strep in pH 8 and pH 6 (50.6 % helix and 11.6 % strand in pH 8; 49.8 % helix and 12.3 % strand in pH 6). However in pH 7 more helical and less strand signal and content was observed as compared with pH 6 and pH 8. Deconvolution of the spectrum of protein in pH 7 yields 53 % helix and 9.8 % strand.

pH	α_R	α_D	β_R	β_D	Turn	Unordered
pH 6	0.327± 0.020	0.171± 0.008	0.066± 0.003	0.056± 0.003	0.142± 0.010	0.237± 0.023
pH 7	0.345± 0.024	0.185± 0.005	0.051± 0.008	0.046± 0.008	0.151± 0.028	0.228± 0.024
pH 8	0.333± 0.023	0.173± 0.01	0.063± 0.006	0.052± 0.004	0.146± 0.030	0.228± 0.020

Table 3.7: Deconvolution of His-PS2-NTF-Strep raw CD spectra in different pH.

3.2.4.2.4 Far UV CD spectra of His-PS2-NTF-Strep upon thermal unfolding

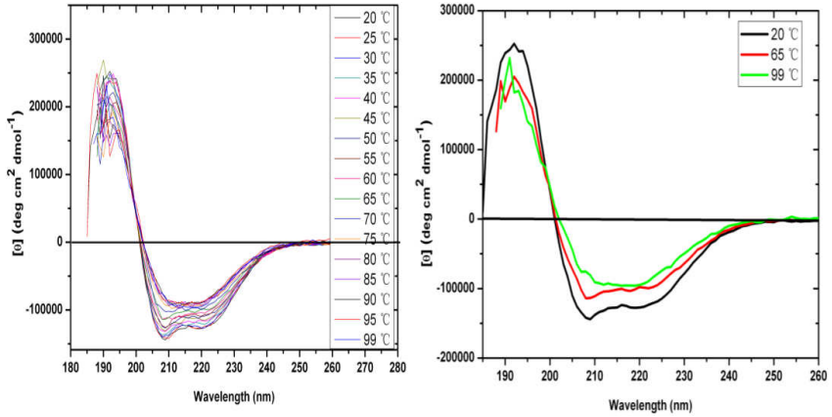

Figure 3.52: Far UV CD spectra of His-PS2-NTF-Strep upon thermal unfolding.
Far UV CD spectrum from 20 to 99 ℃ with 5 ℃ interval (left) and overlay of spectrum at 20 ℃, 65 ℃ as well as 99 ℃ (right).

Thermal stability of purified His-PS2-NTF-Strep was investigated via far UV CD. As shown in **Figure 3.52**, the far UV CD spectra of PS2-NTF unfolding by increasing temperature fall into three groups. The spectra before 55 ℃ belong to the first group while spectra after 75 ℃ belong to the third group. In between 55 and 75 ℃ is the second group. Overlay of far UV CD spectra at 20

65 and 99 ℃ shows a transition of typical α-helix spectrum at 20 ℃ to β-strand spectrum at 99 ℃.

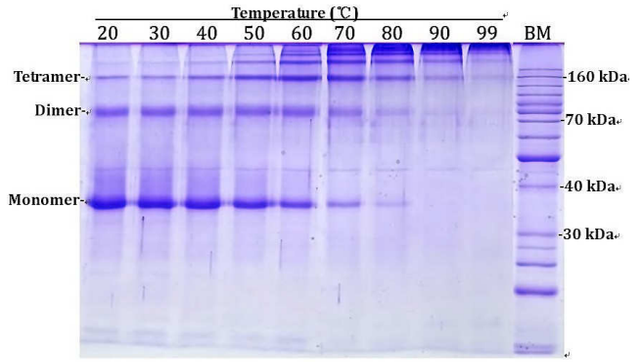

Figure 3.53: SDS-PAGE analysis of His-PS2-NTF-Strep upon thermal unfolding.
20 µl of PS2-NTF was subjected to the respective temperature for 20 min. SDS-sample buffer was added before loading to the SDS-PAGE. The protein was then visualized by coomassie staining.

SDS-PAGE analysis (**Figure 3.53**) revealed that from 20 to 70 ℃ a significant decrease of monomer signal and an increase of tetramer and higher oligomer signal were observed. However, the band intensity corresponding to the dimer remained constant until 60 ℃.

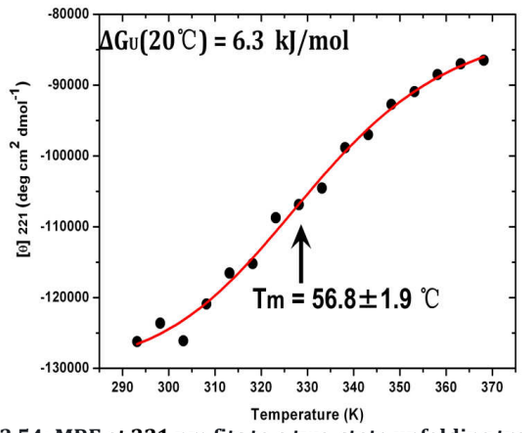

Figure 3.54: MRE at 221 nm fits to a two-state unfolding transition.

A plot of MRE at 221 nm as a function of temperature and a fit for a two-state unfolding transition are shown in **Figure 3.54**. The plot indicates that in FC12 the secondary structure of PS2-NTF is stable at elevated temperature with a T_m

of 56.8±1.9 ℃. The calculated unfolding free energy for secondary structure at 20 ℃ $\Delta G_{U(20℃)}$ is 6.3 kJ/mol.

Temperature (℃)	α_R	α_D	β_R	β_D	Turn	Unordered
20	0.27	0.17	0.07	0.06	0.16	0.28
25	0.27	0.17	0.07	0.06	0.16	0.28
30	0.26	0.17	0.07	0.06	0.17	0.28
35	0.26	0.16	0.08	0.06	0.16	0.28
40	0.26	0.17	0.07	0.06	0.18	0.27
45	0.25	0.16	0.10	0.08	0.17	0.25
50	0.23	0.16	0.08	0.07	0.17	0.28
55	0.22	0.17	0.07	0.06	0.18	0.28
60	0.21	0.15	0.10	0.08	0.19	0.27
65	0.21	0.14	0.11	0.08	0.18	0.28
70	0.20	0.14	0.13	0.09	0.19	0.24
75	0.18	0.13	0.13	0.10	0.20	0.26
80	0.14	0.11	0.16	0.11	0.22	0.26
85	0.14	0.11	0.16	0.10	0.21	0.28
90	0.13	0.07	0.18	0.12	0.24	0.26
95	0.14	0.08	0.19	0.12	0.20	0.27
99	0.13	0.07	0.20	0.13	0.21	0.27

Table 3.8: Deconvolution of His-PS2-NTF-Strep raw CD spectra in different temperatures.

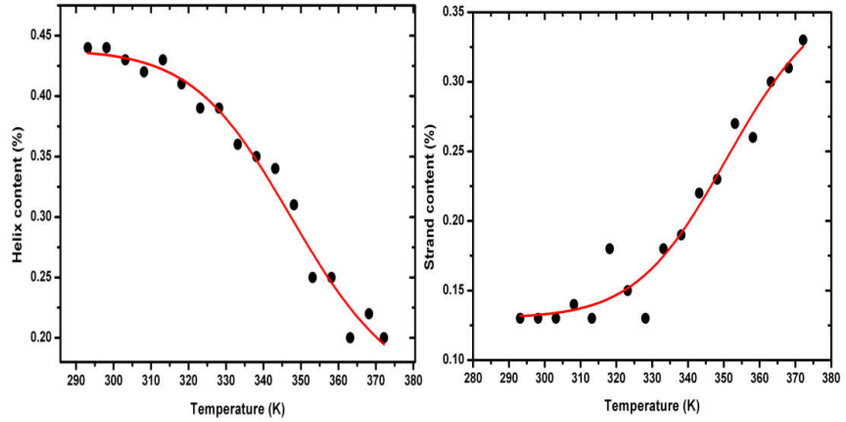

Figure 3.55: Temperature induced change of secondary structure of His-PS2-NTF-Strep.

Helix content (left) and strand content (right) as a function of temperature fit to a two-state unfolding transition are shown.

Deconvolution of the raw CD spectra into pure component spectra shows a decreasing of helix content from 44 % at 20 ℃ to 20 % at 90 ℃ and an increasing of strand content from 13 % at 20 ℃ to 34 % at 90 ℃. This corresponds to a refolding of about 62 amino acids from α-helix to β-strand structure when the

temperature increases from 20 ℃ to 90 ℃. Turn content increased slightly form 16 % to 21 % while unordered remained constant (**Table 3.8)**.

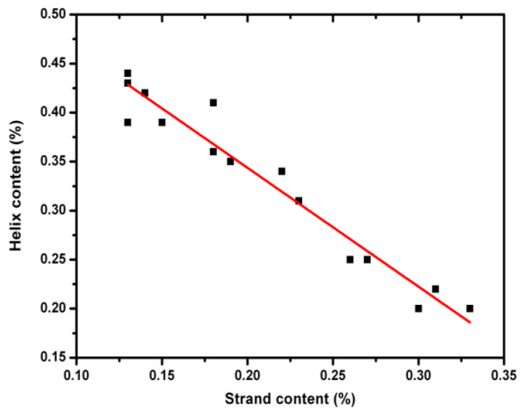

Figure 3.56: Corelation of helical and strand structure upon thermal unfolding.

Plots of temperature dependence of total helix and strand content (**Figure 3.55**) as a function of temperature showed a decreasing of total helix content and an increasing of total strand content. The correlation of the two is shown in **Figure 3.56**.

3.2.4.2.5 Near UV CD spectrum of His-PS2-NTF-Strep

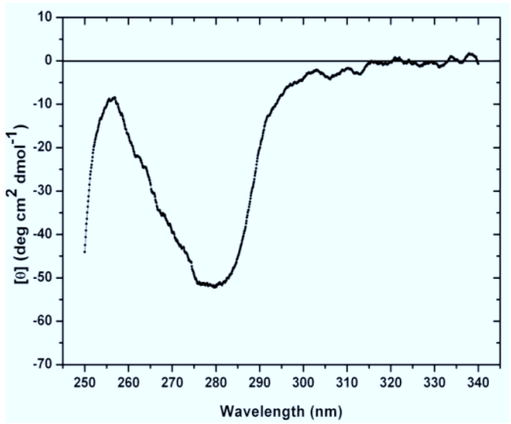

Figure 3.57: Near UV CD spectra of His-PS2-NTF-Strep in FC12.

To investigate the tertiary structure of His-PS2-NTF-Strep in FC12, purified His-PS2-NTF-Strep was concentrated and subjected to near UV CD**.** The near UV

CD spectrum of the PS2-NTF dimer purified in 2 CMC FC12, as shown in **Figure 3.57**, displays the characteristics of a distinct tertiary structure peak with a strong, well defined, negative bands between 255 and 300 nm with a maximum at around 280 nm.

3.2.4.3 Fluorescence spectroscopy

3.2.4.3.1 Tryptophan fluorescence of His-PS2-NTF-Strep in different detergents

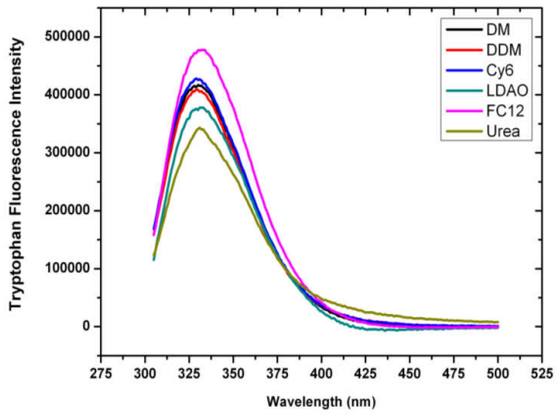

Figure 3.58: Tryptophan fluorescence of His-PS2-NTF-Strep in different detergents.

Tryptophan fluorescence reveals the microenvironment of tryptophan molecule and therefore it is a good indicator for the change of the protein tertiary structure. For this reason fluorescence spectroscopy was also applied for the investigation of His-PS2-NTF-Strep. As shown in **Figure 3.58**, like far UV CD spectra, His-PS2-NTF-Strep in FC12 again showed the strongest fluorescence intensity followed by DM, DDM and Cy6, whose emission maxima were very close to each other. The lowest intensity was observed with 6 M Urea, while LDAO was only slightly higher than for Urea.

3.2.4.3.2 Tryptophan fluorescence spectra of His-PS2-NTF-Strep in different pH

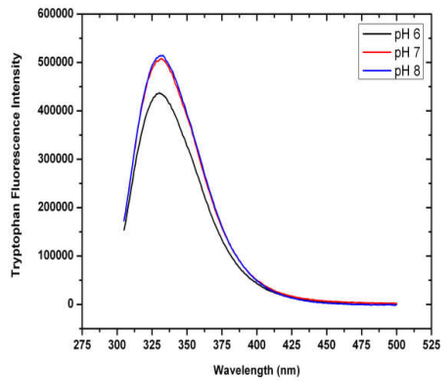

Figure 3.59: Tryptophan fluorescence of His-PS2-NTF-Strep in different pH.

Tryptophan fluorescence spectra in pH 7 and pH 8 were almost identical with emission maxima of 332 nm for pH 7 and 333 nm for pH 8. However, the intensity was much lower in pH 6 compared to the other two. The tryptophan emission maximum for pH 6 was 330 nm, 3 nm blue shifted as compared to pH 8 (**Figure 3.59**).

3.2.4.3.3 Tryptophan fluorescence of His-PS2-NTF-Strep upon thermal unfolding

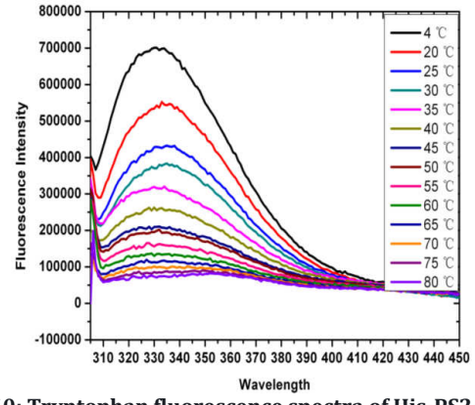

Figure 3.60: Tryptophan fluorescence spectra of His-PS2-NTF-Strep upon thermal unfolding.

The thermal unfolding of the PS2-NTF tertiary structure was also investigated by Trp fluorescence spectroscopy (**Figure 3.60** and **Figure 3.61**). When the

temperature increase with a heating rate of 1 ℃/min the fluorescence intensity was progressively quenched. A 2 nm red shift from 332 to 334 nm was detected with the emission maximum position at the temperatures above 60 ℃. Fluorescence intensity at 333 nm as a function of temperature was fitted into a two state transition with a T_m value of 31.8±0.7 ℃. The calculated unfolding free energy for tertiary structure at 20 ℃ $\Delta G_{U\,(20℃)}$ is 2.8 kJ/mol (Figure 3.61).

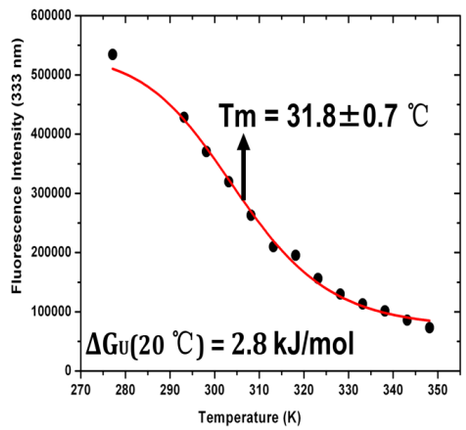

Figure 3.61: Fluorescence intensity at 333 nm as a function of temperature.

3.2.4.4 Dynamic light scattering

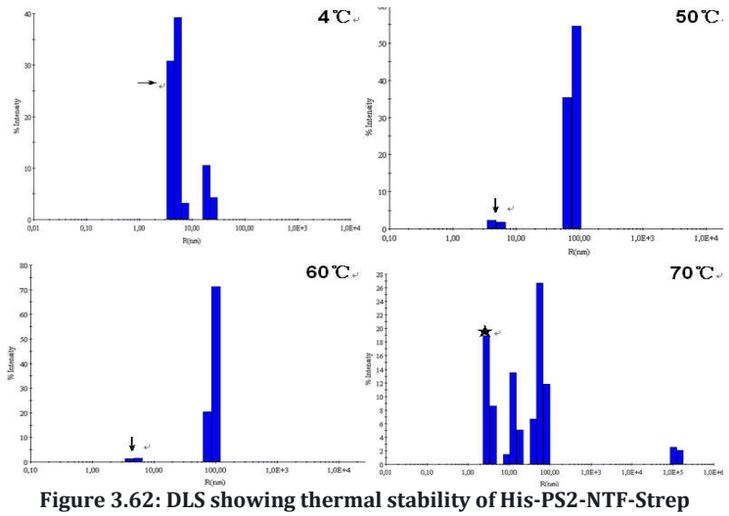

Figure 3.62: DLS showing thermal stability of His-PS2-NTF-Strep at different temperature.

Black arrow indicates the dimer; black star indicates the monomer.

DLS results showed that His-PS2-NTF-Strep dimer was stable up to 60 ℃ above which bigger radius species appeared (**Figure 3.62 and Table 3.9**).

Temperature (℃)	Radius (nm)	Polydispersity (%)
4	4.9	18.2
	21.2	15.1
50	4.8	17.2
	79.9	16.0
60	4.8	15.9
	96.8	12.3
70	3.3	18.4
	14.1	20.6
	61.9	23.4
	124995	18.8

Table 3.9: Peaks detected by DLS at different temperature.

3.2.5 Crystallization of His-PS2-NTF-Strep in MO lipidic cubic phase

As shown in **Figure 3.63**, His-PS2-NTF-Strep passively reconstituted into MO cubic phase at a time duration of 24 h. Under fluorescence microscope, after 72 h from the setup of the experiment, one of the conditions shows the condensed UV signal from the protein.

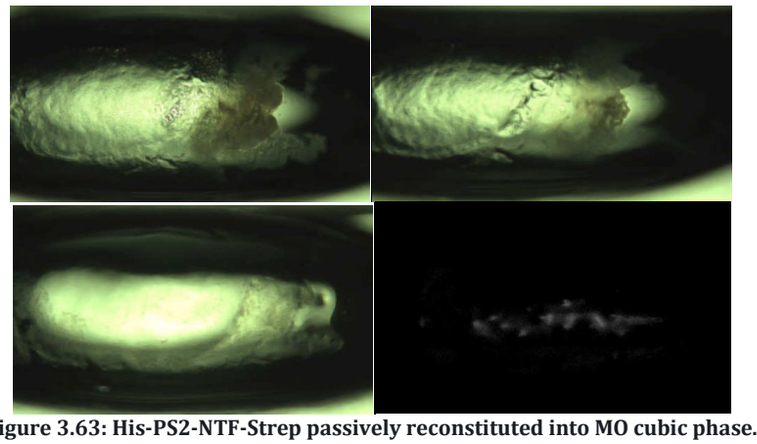

Figure 3.63: His-PS2-NTF-Strep passively reconstituted into MO cubic phase.
1 µl of His-PS2-NTF-Strep solution was added into a protein well coated with 132 µg MO. The formation of mesophase was monitored under a polarization microscope over time. Top left: o h; top right: 3 h; bottom left: 24 h; bottom right: 72 h under fluorescence microscope.

3.3 *In vitro* translation

In vitro translation system is also commonly used for membrane protein production. Different modes of *in vitro* translation as described in **Section 2.2.16** were carried out in order to obtain the best yield and homogeneity of the respective proteins.

3.3.1 *In vitro* translation of PS2-constructs

SDS-PAGE and western blot analysis (**Figure 3.64**) indicated the presence of FL1, FL2 and NTF in their respective pellet fraction whereas CTF was found to be in supernatant as well as in pellet fraction.

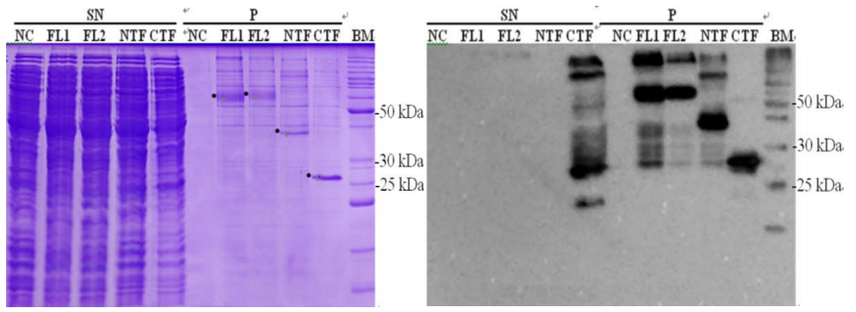

Figure 3.64: *In vitro* translation of PS2-constructs.
Coomassie staining (left) and western blot (right) showing the *in vitro* translated His-PS2-FL, His-PS2-FL-Strep, His-PS2-NTF-Strep and His-PS2-CTF-Strep locating in the pellet fraction. NC: negative control; FL 1: His-PS2-FL; FL 2: His-PS2-FL-Strep; NTF: His-PS2-NTF-Strep; CTF: His-PS2-CTF-Strep; BM: bench marker; Black dots indicate the monomer form the protein respectively.

3.3.2 *In vitro* translation of His-PS2-FL-Strep with detergents

Addition of detergent into *in vitro* translation reaction may produce soluble membrane protein directly. Therefore compatibility of different detergents with the *in vitro* translation system was investigated using His-PS2-FL-Strep as a model protein. Western blot analysis (**Figure 3.65**) showed the presence of His-PS2-FL-Strep only in supernatant fractions for the reactions containing Brij35, Brij58 and Brij98 . For group that containing Brij72, only in pellet fraction, there was signal detected. In experiments with DM, DDM, Cy6 or FC14 protein

signal was detected in both the supernatant and pellet fractions. For the detergents OG, LDAO, FC12 and CHAPS no signal indicating *in-vitro* translation could be detected at all.

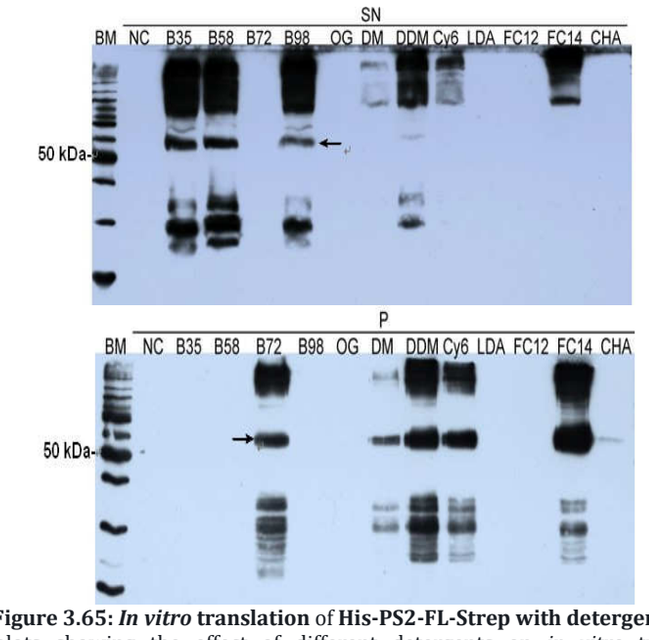

Figure 3.65: *In vitro* translation of **His-PS2-FL-Strep with detergents.**
Western blots showing the effect of different detergents on *in vitro* translation of His-PS2-FL-Strep. His-PS2-FL-Strep in supernatant (upper) and in pellet (lower) was detected by anti-his antibody. NC: negative control; B35: Brij 35; B58: Brij 58; B72: Brij 72; B98: Brij 98; LDA: LDAO; CHA: CHAPS; BM: bench marker. Black arrows indicate the monomer form of His-PS2-FL-Strep.

3.3.3 *In vitro* translation of His-PS2-FL-Strep with different detergent concentrations

From the initial *in vitro* translation experiments the detergent Brij35, DDM, Cy6 and FC14 were chosen for further optimization of their concentration to increase yield and solubilisation. Western blot analysis showed the signal of His-PS2-FL-Strep increased in the supernatant fractions and decreased in respective pellet fractions as Brij35 concentration increased. Whereas increasing concentration of DDM in respective reactions were found to decrease intensity of His-PS2-FL in both fractions. Reaction with only 0.224 % Cy6 showed the

presence of His-PS2-FL-Strep, most of which was found in the pellet fraction. No protein signal was found for the reactions with FC14 (**Figure 3.66**).

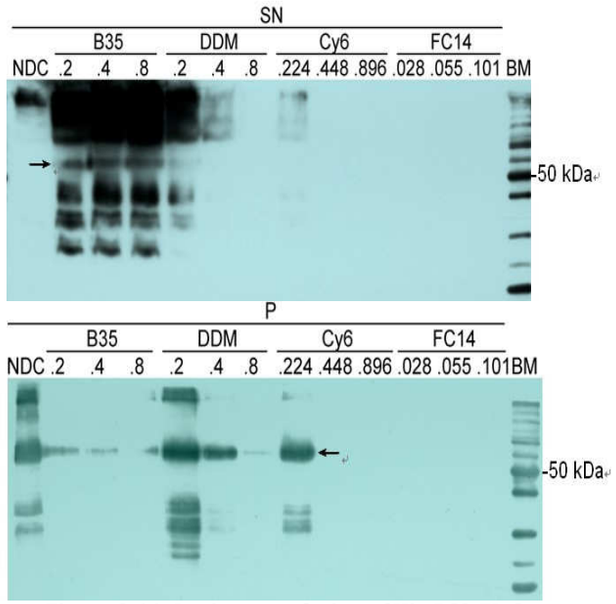

Figure 3.66: *In vitro* translation of His-PS2-FL-Strep with different detergent concentrations.
Western blots showing titration of *in vitro* translation system with different detergents concentration. NDC: no detergent control; B35: Brij 35; BM: bench marker; the percent concentration of detergent in each reaction was indicated under the detergents. Black arrows indicate the monomer form of His-PS2-FL.

3.3.4 *In vitro* translation of His-PS2-FL-Strep with peptides

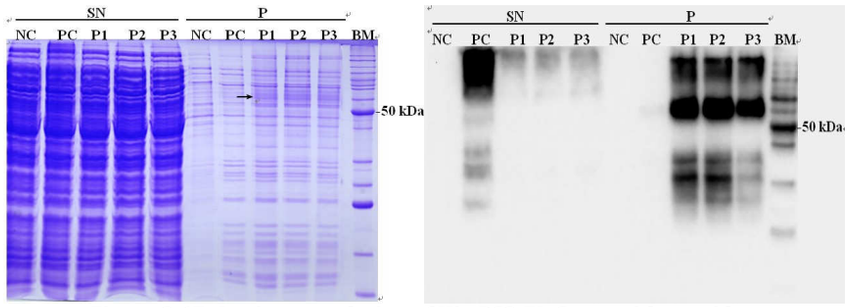

Figure 3.67: *In vitro* translation of His-PS2-FL-Strep with peptides.
Coomassie staining (left) and western blot (right) showing the *in vitro* translated His-PS2-FL-Strep in the presence of peptides. SN: supernatant; P: pellet; NTC: negative control; PC: positive control Brij 35; P1: AC6AD; P2: AC3VD; P3: AC3ID; BM: bench marker. Black arrow indicates the monomer form of His-PS2-FL-Strep.

The effect of peptidese on the solubility and yield of i*n vitro* translated His-PS2-FL-Strep was also investigated because they might be an alternative to detergents. As shown in **Figure 3.67, w**estern blot analysis indicated that none of the three peptides were able to maintain His-PS2-FL in the supernatant fraction even though no significant effect was seen on the yield of the protein.

3.3.5 *In vitro* translation of His-PS2-FL-Strep with peptides under oxidizing condition

The disulfide *in vitro* translation kit allows the formation of disulfide bond which may improve the folding of target protein and furtherly improve the protein yield and solubility. Hence, *in vitro* translation of His-PS2-FL-Strep in presence of peptide was carried out using disulfide kit.

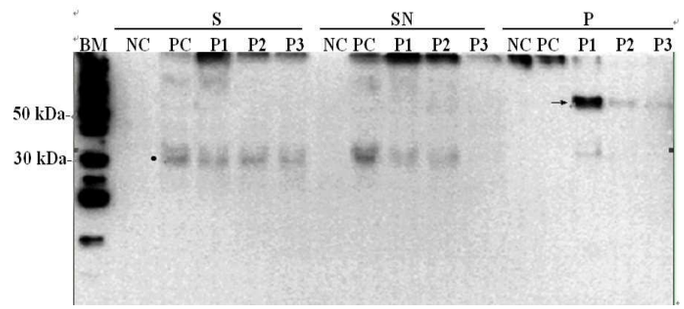

Figure 3.68: *In vitro* translation of His-PS2-FL-Strep with peptides under oxidizing condition.

Western blot showing the *in vitro* translated His-PS2-FL-Strep with peptides. S: suspension before 20 000×g; SN: supernatant after 20 000×g; P: pellet after 20 000×g; NC: negative control, where no plasmid was added; PC: positive control Brij 35; P1: AC6AD; P2: AC3VD; P3: AC3ID; BM: bench marker. Black arrow indicates His-PS2-FL-Strep full length while black dot indicates its N-terminal fragment. The sample in PC control overflow into NC control during loading therefore a signal is detected in pellet fraction.

The result showed that in suspension, no signal from the protein of interest was detected in the negative control reaction. For the other 4 reactions, aggregation on top of the PAGE was observed and a smear band corresponding to the MW of PS2-NTF was detected. Almost the same result was observed for supernatant fractions except for the P3 reaction which showed very weak signal. In the pellet fraction, of the three peptide investigated, P1 showed the strongest intensity of the bands which corresponds to the His-PS2-FL-Strep (**Figure 3.68**). This result

suggested that different peptide had different effect on the protein translation although their failure in maintaining the translated protein in supernatant.

3.3.6 *In vitro* translation of PS2-constructs with nanodiscs

Addition of nanodisc into *in vitro* translation reaction often results in the soluble membrane protein nanodisc complex directly after the translation. Hence the effect of nanodisc was also investigated. Different reaction components are listed in **Table 3.10**. For control reaction 1 and 2, no signal corresponding to the protein of interests was detected. For reaction 3 4 and 5, most of the protein was located in the supernatant as shown by **Figure 3.69**.

	Reactions				
Components	1 Control 1 (µl)	2 Control 2 (µl)	3 PS2-FL (µl)	4 PS2-NTF (µl)	5 PS2-CTF (µl)
E. coli Extract	8.75	8.75	8.75	8.75	8.75
RNase-free water	5.75	4.65	3.35	3.45	3.15
Reaction Buffer	10	10	10	10	10
IPTG (50 mM stock to 1 mM)	0.5	0.5	0.5	0.5	0.5
Nanodisc (31 µg/µl stock to 1.35 µg/µl)	0	1.1	1.1	1.1	1.1
Plasmid DNA (0.5 µg in 25 µl)	0	0	1.3	1.2	1.5
Total volume	25 µl				

Table 3.10: *In vitro* translation setup for nanodiscs mode.

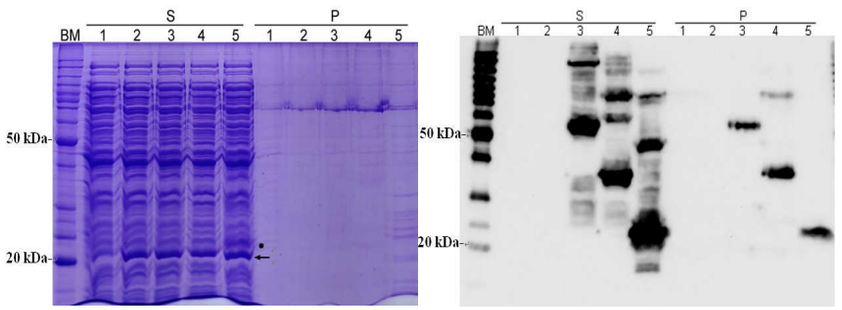

Figure 3.69: *In vitro* translation of PS2-constructs with nanodiscs.
Coomassie staining (left) and western blot (right) showing the *in vitro* translated His-PS2-FL-Strep, His-PS2-NTF-Strep and His-PS2-CTF-Strep in presence of nanodisc. 1-5 are different reactions as described in **Table 3.10**. BM: bench marker; Black dots indicate the CTF products; black arrow indicates the MSP (membrane scaffold protein). Note that CTF can be detected with Coomassie staining directly after translation.

3.3.7 Homogeneity of *in vitro* translated His-PS2-CTF-Strep

Structural investigation of membrane protein not only requires yield but also homogeneity. Therefore mid-scale screening was carried out to investigate the homogeneity of PS2-CTF produced by *in vitro* translation in different modes.

PS2-CTF produced as a precipitate did not yield a Gaussian shaped peak during gel filtration as shown in **Figure 3.70**. *In vitro* translated PS2-CTF in precipitate mode showed poor solution behaviour and yield as detected by gel filtration although the reasonable purity without any purification.

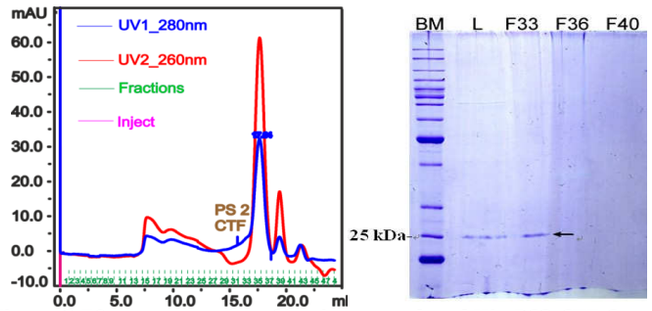

Figure 3.70: Homogeneity of in vitro translated His-PS2-CTF-Strep.
SEC profile (left) and Coomassie staining (right) of *in vitro* translated PS2-CTF. L: load; F: gel filtration fraction. BM: bench marker. Black arrow indicates His-PS2-CTF-Strep.

3.3.8 Homogeneity of *in vitro* translated His-PS2-CTF-Strep with detergents

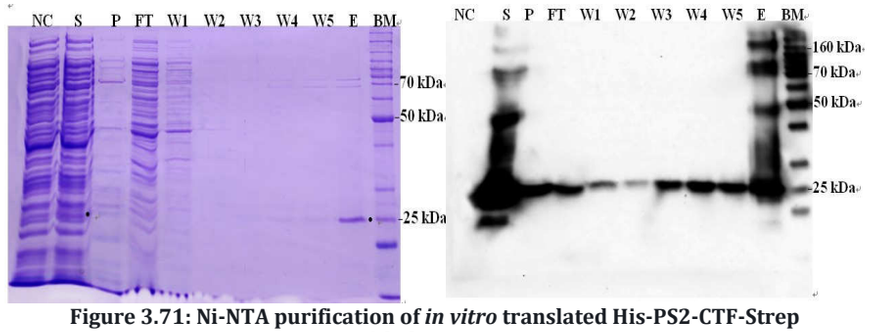

Figure 3.71: Ni-NTA purification of *in vitro* translated His-PS2-CTF-Strep with detergents.
Coomassie staining (left) and western blot (right) showing the Ni-NTA purification fractions of *in vitro* translated His-PS2-CTF-Strep. NC: negative control; S: supernatant after 20 000 ×g; P: pellet after 20 000 ×g; FT: flow through of Ni-NTA; W1: first 4 CV wash with binding buffer; W2: second 4 CV wash with binding buffer; W3:15 mM imidazole wash; W4: 20 mM imidazole wash; W5: 25 mM imidazole wash; E: elution with 100 mM imidazole; BM: bench marker; Black dots indicate His-PS2-CTF-Strep.

Unlike the precipitate mode, due to the addition of detergent the translated protein remains in the supernatant after the reaction. Therefore purification of the target protein from the *E coli* lysate is required. *In vitro* translated His-PS2-CTF-Strep in presence of Brij 35 was purified by Ni-NTA and was exchanged into FC12 (**Figure 3.71**). After purification, SEC analysis was performed (**Figure 3.72**). As showed in **Figure 3.73**, His-PS2-CTF-Strep was predicted to have a radius of 4.95 nm (upper) and a molecular weight of 162.31 kDa (lower). When subtracting the FC12 micelle MW from the detergent protein complex, PS2-CTF exists as an octamer in FC12 micelles ((162.31-18.98) / 18.7 = 7.7).

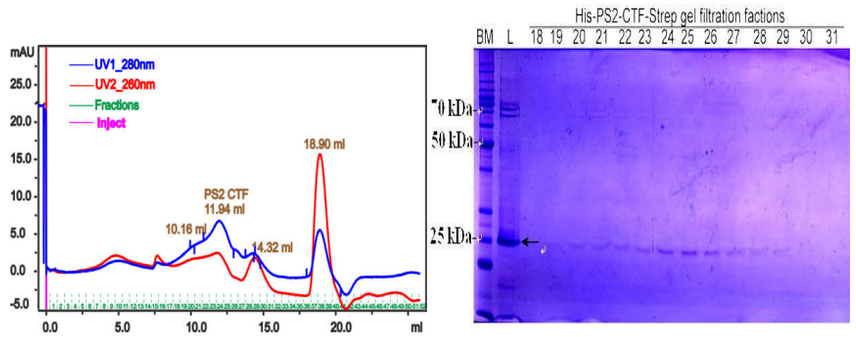

Figure 3.72: Homogeneity of of *in vitro* translated His-PS2-CTF-Strep with detergents. Gel filtration elution profile (left) and Coomassie staining (right) showing the homogeneity of *in vitro* translated His-PS2-CTF-Strep with detergents and an elution volume of 11.94 ml on superdex 200 analytical column.

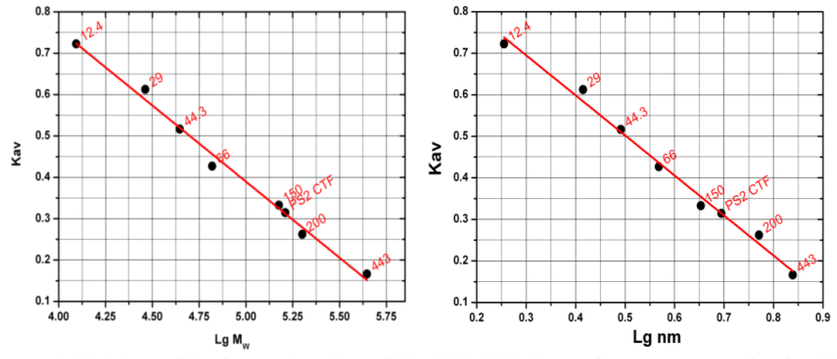

Figure 3.73: M_W and R_h determination of His-PS2-CTF-Strep-detergent complex by SEC.

3.3.9 Homogeneity of *in vitro* translated His-PS2-CTF-Strep with nanodiscs

Like the addition of detergent, soluble membrane protein nanodisc complex also requires the purification from the reaction mixture. In Ni-NTA elution fraction, His-PS2-CTF-Strep was co-eluted with MSP (**Figure 3.74**). The intensity ratio of His-PS2-CTF-Strep to MSP was about 4 to 1 as shown by coomassie staining **(Figure 3.75)**. Most of His-PS2-CTF-Strep was recovered in elution fraction although there was some loss in other fractions as shown by western blot. In the pellet fraction there was still a considerable amount of signal detected by western blot (**Figure 3.74**).

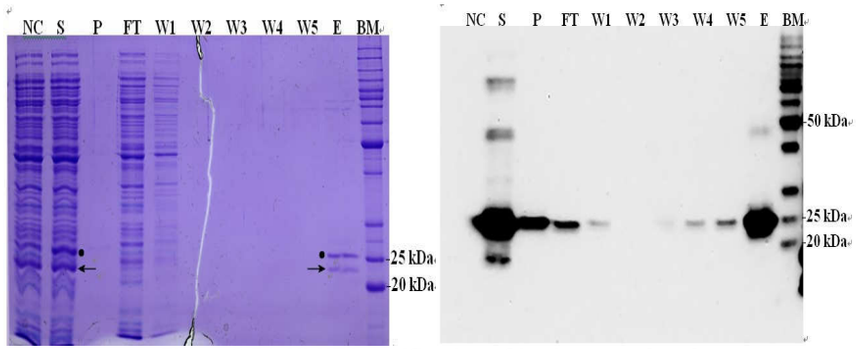

Figure 3.74: Ni-NTA purification of *in vitro* translated His-PS2-CTF-Strep with nanodiscs.

Coomassie staining (left) and western blot (right) showing the *in vitro* translated His-PS2-CTF-Strep with nanodiscs. Each lane corresponds to the same part of total reaction volume. NC: negative control; S: supernatant after 20 000×g; P: pellet after 20 000×g; FT: flow through of Ni-NTA; W1: first 4 CV wash with binding buffer; W2: second 4 CV wash with binding buffer; W3:15 mM imidazole wash; W4: 20 mM imidazole wash; W5: 25 mM imidazole wash; E: elution with 100 mM imidazole; BM: bench marker; Black dots indicate His-PS2-CTF-Strep; black arrow indicates the MSP (membrane scaffold protein). Note the 4:1 intensity difference of His-PS2-CTF-Strep and MSP on coomassie stainning.

As shown by **Figure 3.76** and **Figure 3.77**, empty nanodisc was eluted at 15.68 ml and was predicted at a hydrodynamic radius of 4.41 nm and a molecular weight of 123.01 kDa; His-PS2-CTF-Strep nanodisc complex was eluted at 14.5 ml and was predicted to have a hydrodynamic radius of 5.98 nm and a molecular weight of 275.48 kDa. When subtracting the nanodisc MW from that of the "filled" nanodisc, a molecular weight for His-PS2-CTF-Strep corresponding to an octamer in nanodisc is obtained ((275.48-123.01) / 18.7= 8.15).

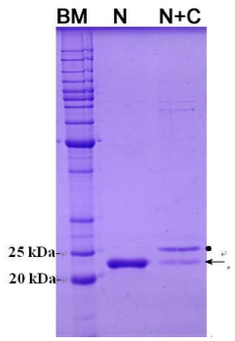

Figure 3.75: Coomassie staining showing empty nanodisc and PS2-CTF filled nanodisc.
N: nanodisc; N+C: His-PS2-CTF-Strep filled nanodisc.

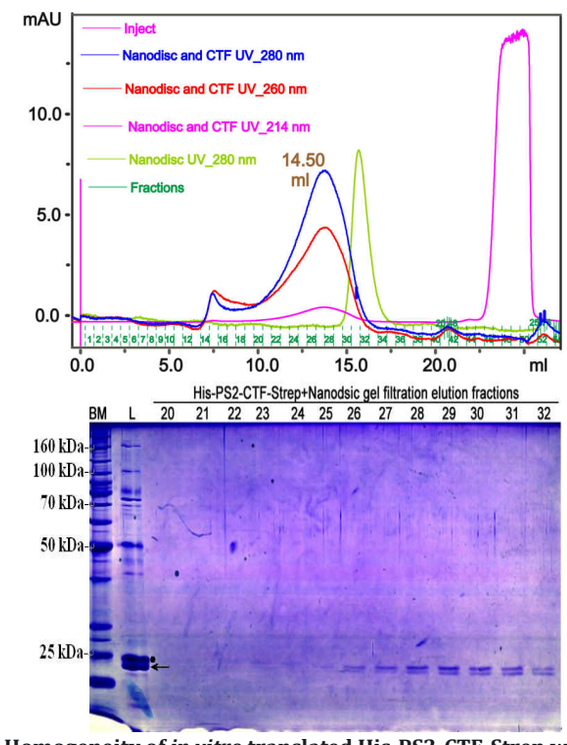

Figure 3.76: Homogeneity of *in vitro* translated His-PS2-CTF-Strep with nanodiscs.
SEC profile of His-PS2-CTF-Strep filled nanodisc (upper) on superose 6 analytical column and distribution of protein detected by coomassie staining (lower). BM: bench marker; L: load. Black dot indicates His-PS2-CTF-Strep; black arrow indicates the MSP.

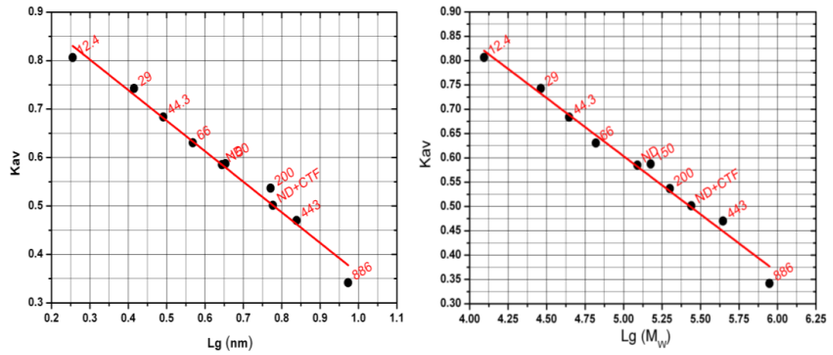

Figure 3.77: M_W and R_h determination of His-PS2-CTF-Strep-nanodisc complex by SEC.

3.3.10 Effect of increased nanodiscs concentration on the oligomerisation of *in vitro* translated His-PS2-CTF-Strep

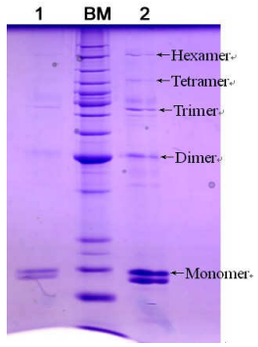

Figure 3.78: *In vitro* translation of His-PS2-CTF-Strep with increased nanodiscs concentration.

Coomassie staining showing the increase of nanodisc concentration in *in vitro* reaction did not change the oligomerisation state of His-PS2-CTF-Strep given the intensity ratio of His-PS2-CTF-Strep to MSP remained constant. 1: nanodisc concentration 1.35 µg/µl; BM: bench marker; 2: nanodisc concentration 2.70 µg/µl. Oligomer state of His-PS2-CTF-Strep was indicated with black arrows.

Due to the existence in the pellet after centrifugation and the oligomerisation state of His-PS2-CTF-Strep in nanodisc mode, I then investigate the effect of increasing concentration of nanodisc on the oligomerisation state of His-PS2-CTF-Strep. As shown by **Figure 3.78**, on lane 1 and lane 2 the same oligomerisation states of His-PS2-CTF-Strep were observed and the intensity difference between His-PS2-CTF-Strep and MSP remained constant.

4 Discussion

4.1 Expression purification and refolding of His-PS2-FL

4.1.1 Expression

Membrane protein over expression often influences the cell membrane integrity due to its insertion into the membrane and thus cell viability. In addition, it will cause the saturation of the host protein sorting and translocation system, which is responsible for protein translocation and insertion. Saturation of the translocation machinery will leads to protein mis-placing and protein aggregation in the cytoplasm fraction. It will also cause reduced levels of respiratory chain complexes in cytoplasmic membrane as well as activation of the Arc response, which leads to inefficient ATP production and the formation of acetate. Acetate will bring down the pH of medium which is detrimental for cell growth. All the above stresses are well agreed bottlenecks for membrane protein overexpression (113, 114).

For these reasons, different strains and media were screened seeking for the condition for best yield and quality of target membrane proteins. Of the four strains investigated, His-PS2-FL exhibits toxicity to STAR and RP cells resulting in the cell death after 16 h induction. However C41 and C43 strains survived after 16 h induction (**Figure 3.1** and **Table 3.1**). This is due to the well-studied mutations in lacUV5 promoter governing expression of T7 RNA polymerase. These characterized mutations significantly down regulates the polymerase levels thus decrease the speed of protein translation hence release the burden on host translation and translocation system living enough time for the cells to transport the newly translated protein to cytoplasmic membrane. Consequently, the final cell biomass which can be obtained is increased significantly as compared with strains which contain no mutations in lacUV5 promoter when expressing toxic membrane proteins (115, 116). In this way overexpression of membrane protein is achieved. Meanwhile, a lower temperature after induction was used to slow down protein expression rate allowing the translation system to accommodate to the stress upon induction (117).

What's more, to minimize protein mis-folding problems often encountered by heterologously overexpression, codon-usage optimized DNA was used for expression. The target protein could be expressed in *E.coli* with amounts of 1 to 2 mg/l culture. It therefore can be concluded that by employing proper optimisation procedures human PS2 and its two functional domains can be expressed in *E.coli* in sufficient amount for further structural studies.

4.1.2 Purification

His-PS2-FL was purified to reasonable purity under denaturing condition (**Figure 3.5**) by Ni-NTA and gel filtration chromatography. However, efforts in obtaining pure His-PS2-FL natively failed although many purification conditions and techniques were applied. The reason for this could be the instability of its tertiary structure. Presenilins natively interact with the other three subunits of γ-secretase. A stable tertiary structure may require the presence of other binding partners. When heterologously expressed in *E.coli*, presenilin exposes its surface to *E.coli* host proteins and interacts with them. Therefore after natively purification, presenilin is eluted with impurities. However, this kind of interaction is weak that can be impaired by addition of urea. This explains why presenilin could be purified under denaturing condition. Purified presenilin after refolding aggregated as detected by SEC (**Figure 3.19**) although a typical secondary structure in detergent (**Figure 3.15**) and in lipids (**Figure 3.18**) were recorded. These results suggested the instability of presenilin tertiary structure. Indeed, Harnasch, Grau et al reported that heterologously expressed presenilin in *E.coli* binds to a number of heat shock proteins such as DnaK and GroEL, which could not be removed by further chromatographic steps during purification. They argued that other members of the γ-secretase complex could be required to obtain pure presenilin (118). The observation that the N-terminal and the C-terminal products of PS2 could be purified also presents further evidence that the purification problems for His-PS2-FL are caused by aggregation due to its tertiary structure instability.

4.1.3 Refolding

Purified His-PS2-FL under denaturing condition was firstly bound to Ni-NTA matrix and refolded by quick dilution. The refolded protein was then solublised and eluted from the column. Refolded His-PS2-FL displayed the characteristics of a predominantly α–helical protein. Deconvolution showed a helical content of 50 % in FC12 and 39 % in Cy6 indicating that FC12 favourites the formation of α–helical structure. The structure of FC12 is chemically similar to phosphatidylcholine lipids. Therefore, the FC12 micelles probably closely mimic the biological membrane environment (119). This may explains why refolded His-PS2-FL exhibits more helix content in FC12 than in Cy6. However, after being concentrated and subjected to SEC analysis, the His-PS2-FL aggregated and was eluted very close to the column dead-volume (**Figure 3.19)**. This result indicates again that the tertiary structure of presenilins is not stable.

Therefore, the attempt to produce good quality material of PS2-FL for structural investigation failed. For this reason, a C-terminal strep tag was introduced to the presenilin 2 and its N-terminal as well as the C-terminal fragment to improve purification.

4.2 Solubilisation, purification and characterization of His-PS2-NTF-strep

4.2.1 Solubilisation

Heterogeneously overexpressed membrane protein requires to be solubilized before its purification. Membrane protein solubilisation is defined as the process to extract the protein of interest from the lipidic membrane using detergents. The aim of solubilisation is to screen detergents to fully extract the target protein in a native and homogeneous state (120).

In this work, 13 detergents including nonionic, ionic and zwitterionic detergents commonly used in membrane protein purification and crystallization were screened. For all the three protein, similar results were obtained. For the five nonionic detergents (OG, NG, DM, DDM and Cy6), as the hydrophobic tail length

increased an increasing extracting ability was observed (**Figure 3.22)**. However, double extraction with the same mild detergents failed to increase the amount of target protein in supernatant (**Figure 3.23** and **Figure 3.24**). Among the 6 zwitterionic detergents investigated, foscholine detergents can achieve full solubilization whose signals in supernatant were as strong as in positive control (NLS, a denaturing ionic detergent).

It is proposed that membrane protein solubilisation is a process for detergents to compete against lipids for membrane protein in the lipid bilayer. Detergent which exhibits high affinity with the overexpressed membrane protein will preferentially bind to protein rather than lipids. This binding is a vital premise for a successful solubilisation. Over certain critical concentration, solubilisation by detergent with affinity to the target membrane protein will occur. For the detergents which have poor affinity to the target membrane protein, solubilisation will fail even at very high detergent concentration (121, 122). This is in agreement with the observation that of the 13 detergents investigated only foscholine detergents and NLS but not the mild detergents achieved complete solubilisation thereby indicating their affinity to the respective membrane protein.

Foscholine is a lipid-like zwitterionic detergent which has the same head group as phospholipids but a single hydrophobic tail. Foscholine-12 (FC12) with 12 methylene hydrophobic groups is one of the most commonly used detergents in membrane protein solubilisation and purification. What' more, FC12 was found to be useful in membrane protein crystallisation (123) and NMR studies (124). These features make foscholine detergents very efficient in membrane protein extraction from *E. coli* membrane due to its similarity with phospholipids. For PS2 it was found that a detergent with 12 methylene groups and a zwitterionic head group is optimal for solubilisation. Therefore FC12 was chosen for further investigations of the respective proteins.

4.2.2 Purification

Different detergent micelle may shields affinity tags therefore reduce the binding affinity (108, 125). To find the optimal detergent for purification, Ni-NTA and Strep-Tactin purification of the respective protein were performed with 5 detergents respectively. FC-12, among the 5 detergents investigated, yields the most protein in elution fractions by Ni-NTA (**Figure 3.27**) and Strep-Tactin (**Figure 3.28**) purification. However, none of the protein binds strongly to Strep-Tactin in the presence of the detergents although for PS2-NTF some protein was found in elution fractions. After reducing the FC-12 concentration to 0.1 % the protein did bind to the matrix strongly but the overall yield was still not satisfactory (**Figure 3.29**). These results can be explained by the moderate affinity of the Strep-tag II peptide for Strep-Tactin (dissociation constant about 1 µM) (126) and the strong affinity between his-tag against Ni-NTA (dissociation constant around 14 nM) (127). Hence, FC-12 and Ni-NTA were chosen for protein solubilisation and purification.

After determination of the imidazole concentration for binding and elution, mid-scale native purifications were performed. However, none of the efforts, such as second Ni-NTA purification **(Figure 3.32)** or a combination of Ni-NTA and Strep-Tactin purification **(Figure 3.33)**, yield reasonable purity.

Osmotic shock was then performed before cell lysis. By doing so, periplasmic fraction which is considered to cause metal ions leakage and consequently reduce the purification efficiency is removed before applying the target protein to the column (48). Indeed as observed, the purities for all the three proteins were significantly improved (**Figure 3.35**) as compared with **Figure 3.32.**

The purified proteins were identified by mass spectrometry **(Table 3.5** and **Figure 3.36)**. The SEC profiles **(Figure 3.40)** revealed that PS2-FL exists as a hexamer and trimer, PS2-NTF exists as a dimer and PS2-CTF as a tetramer in FC-12 micelle. The hexamer and trimer forms of PS2-FL could not be separated from each other by superpose 6 column **(Figure 3.37)**. PS2-CTF exhibited the

poor expression level from *in vivo* **(Figure 3.39)**, however it could be obtained with reasonable yield and homogeneity from *in vitro* production **(Figure 3.64)**. PS2-NTF was purified with a yield of about 2 mg/l culture as a homogeneous dimer **(Figure 3.43)**. All these results strengthened again the hypothesis of the instability of PS2-FL tertiary structure which explained why the protein could be obtained with reasonable quality only after the cleavage of full length protein into its functional N-terminal and C-terminal fragment as illustrated in **Figure 4.1.**

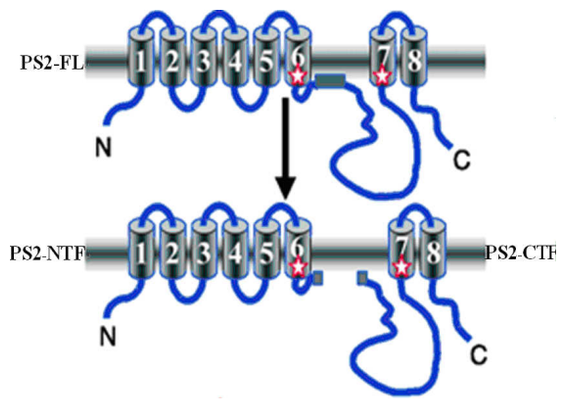

Figure 4.1 Illustration of PS2-FL, PS2-NTF and PS2-CTF.
Shown are the presenilin full length (FL), N-terminal fragment (NTF) and C-terminal fragment (CTF). Red stars **represent the** aspartate amino acids (128).

4.2.3 Biophysical characterization

4.2.3.1 Oligomerisation in different detergents

FC12 purified PS2-NTF was determined by SEC as a dimer. Consequently, the effect of detergent type, detergent concentration, buffer pH and TCEP concentration (oxidation state) on its dimerization was studied. The results revealed that only FC-12 detergent was able to maintain PS2-NTF in a dimer form. However, in the presence of other four detergents investigated, His-PS2-NTF-Strep exhibited different extent of oligomerisation. Furthermore, in LDAO no peak was detected in the elution profile indicating the protein precipitated after filtration and centrifugation (**Figure 3.44** and **Figure 3.45**). Increasing FC12 concentration to 10 CMC (**Figure 3.46**) and TCEP concentration

to 5 mM (**Figure 3.48**) did not change the oligomerisation status indicating strong dimer interaction.

4.2.3.2 Far UV and near UV CD

FC12 purified PS2-NTF dimer exhibits a typical helical structure and a decent tertiary structure as investigated by far UV **(Figure 3.50)** and near UV CD **(Figure 3.57)**. Due to the fact that membrane protein may adopt different conformations in the presence of different detergents (129, 130), the detergents effects on the PS2-NTF secondary structure were investigated by far UV CD. As shown in **Table 3.6**, among the five detergents investigated, FC12 yields the most helix signal (48.7 %). The other three detergents yield values which are very close to the predicted value (**Figure 3.49**). However, with LDAO α-helix decreases to 16 % and β-strand increased to 31.2 % indicating the denaturing effect of LDAO which was also demonstrated by the gel filtration elution profile (**Figure 3.45**) and SDS-PAGE analysis (**Figure 3.44**). Interestingly, it was observed that there was a more denaturing effect of LDAO than of urea. This indicates that the integrity of the tertiary structure depends strongly on the hydrophobic interaction of α-helices.

In summary, the PS2-NTF dimer exhibits different conformations in the presence of different detergents. PS2-NTF in FC12 yields the most helical signal and in LDAO exhibits the most β-strand content indicating its denaturing, respectively secondary structure altering effect. Therefore, it must be concluded that the detergent can affects the PS2-NTF secondary structure and thereby its oligomerisation state.

It is reported that γ-secretase activity has an optimal pH at around 7 (131, 132) . The effect of pH on secondary structure of PS2-NTF was investigated by far UV CD. As expected, in pH 7, PS2-NTF exhibited the most helix content (53 %) as compared with pH 6 (49.8 %) and pH 8 (50.6 %) (**Table 3.7**). However, the gel filtration results showed that in pH 6 and pH 7 peaks near the dead volume were detected indicating the aggregation of PS2-NTF in these conditions (**Figure 3.47**).

Therefore pH 8 was chosen for the further investigation of PS2-NTF. Conclusively, pH can affect the PS2-NTF secondary structure and its aggregation state.

The presence of near UV CD spectra is usually interpreted as an good indication for the presence of tertiary structure in proteins because only when the aromatic residues is placed in an asymmetric environment will the protein exhibit signal in near UV range (81). The near UV CD spectrum of His-PS2-NTF-Strep dimer solubilised in 2 CMC FC12, as shown in **Figure 3.57**, displays the characteristics of a distinct tertiary structure peak with strong, well defined, negative bands between 255 and 300 nm indicating a stable folding of His-PS2-NTF-Strep in FC12.

4.2.3.3 Detergents and pH dependence of protein fluorescence

Tryptophan has a wavelength of maximum absorption of 280 nm and an emission peak ranging from around 300 to 350 nm depending on the polarity of the local environment. Burstein and his colleagues classified protein tryptophan fluorescence into 5 classes depending on the polarity and dynamics of the micro-environments surrounding the side chain (71). Tryptophan fluorescence spectra of His-PS2-NTF-Strep in different detergents all showed an emission maximum between 329 to 332 nm (**Figure 3.58**). According to Burstein's classification, the dominant fluorescence at around 330 nm corresponds closely to a class of tryptophan side chains that are in a relatively non-polar environment. There are no significant changes of the emission maximum position between the 5 detergents or even as compared with urea. This can be explained by the presence of the detergent micelle which mimics the lipidic hydrophobic environment and the protein aggregation induced by denaturing effect of urea which buries tryptophan side chains in a non-polar environment.

As far as the quantum yield is concerned, among the 5 detergents investigated, FC12 yields the highest intensity. DM, DDM and Cy6 had the similar intensity as compared with each other. While there was a 22 % decrease of the maximum intensity for LDAO comparing with FC12. The decrease of fluorescence maximum intensity may indicate different extent of unfolding of the tertiary structure

induced by different detergent. All these results suggest that different detergents likely induced the quenching of the intrinsic fluorescence but the overall microenvironment of the intrinsic tryptophan remained largely unchanged.

When varying pH in FC12 **(Figure 3.59)**, the fluorescence maximum intensities are comparable between pH 7 and pH 8. However, there was a 15 % decrease of fluorescence maximum intensity with pH 6 as compared with pH 8 and the fluorescence maximum position also blue shifted from 333 nm in pH 8 to 330 nm in pH 6. When combined with the gel filtration results, this blue shift can be explained by the fact that in pH 6 and pH 7 peaks near the dead volume were detected indicating the aggregation of PS2-NTF in these conditions (**Figure 3.47**). These results suggest that reducing pH continuously quench tryptophan (Trp) emission and that the change of the Trp side chain microenvironment is not due to a different extent of protonation but to the aggregation of PS2-NTF.

Collectively, in FC12 at pH 8 PS2-NTF yields a single peak in gel filtration elution profile and shows the most helical signal and a decent near UV signal as well as the highest fluorescence intensity. Therefore, FC12 among the 5 detergents investigated, was chosen for the structural analysis of PS2-NTF.

4.2.3.4 Functional implication of dimerization

Despite the great efforts in obtaining information for γ-secretase, there are many open questions remaining to be answered. A single specific enzymatic activity by γ-secretase couldn't explain the scattered cleavage sites on the substrates given that the substrate and the catalytic site are constrained within the lipid bilayer. It is still unclear that how the mutations alter the cleavage specificity. The alteration of catalytic activity in the presence of different inhibitors has been also under debate.

However, the existence of di-aspartyl group **(Figure 4.2)** in the catalytic interface can explain all these questions. Raphael Kopan's group found that there exists a PS dimer in the catalytic core of γ-secretase and that substrate is processed at the interface of two PS molecules. The experimental evidence came from the results that differentially tagged PS molecules could be

co-immunoprecipitated and that PS N-terminal fragment dimers were labelled by a photo-affinity probe based on a transition state analog γ-secretase inhibitor (133). What's more, Gemma Marfany's groups succeed in reconstituting gamma-secretase activity from two catalytically inactive presenilin aspartic mutants. Interestingly, from their results, it was shown that NTF-NTF and NTF-CTF dimer were cross-linked but not the CTF-CTF dimer (134). These results provide strong evidences for an active di-aspartyl group assembled at the interface between two presenilin monomers. Similarly, the signal peptide peptidase (SPP) which belongs to the same family as γ-secretase was also reported to function as a homo-dimer and can be labelled by the same active site-directed photo-affinity inhibitor. *In vivo* studies of presenilin (135) and SPP (136) by fluorescent lifetime imaging microscopy also revealed the existence of dimer of these two molecules *in situ* indicating dimerization was a biological meaningful event.

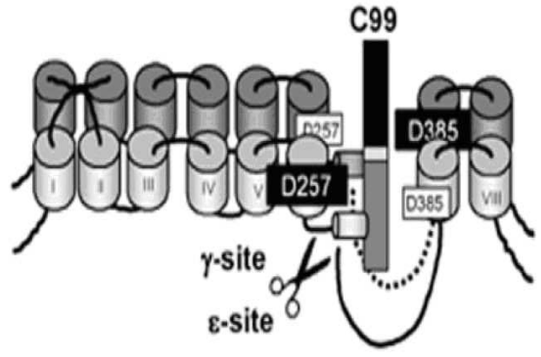

Figure 4.2 Model of C99 cleavage by presenilin dimer within gamma-secretase.
Two PS1 monomers (in black and in grey) are shown to form a di-aspartyl group to process C99 at γ and ε sites (134).

These findings suggest that dimerization may be a general requirement for the function or regulation for this proteases family (137). In this work, PS2-NTF is expressed in *E.coli* and purified as a dimer which is resistant to up to 10 CMC FC12 and 5 mM TCEP indicating strong intermolecular interaction. Gemma Marfany's group also demonstrated that presenilin trans-membrane domains contribute to the formation of the dimer which explains the strong resistance of the PS2-NTF dimer to the FC12 detergent and TCEP. However, on SDS-PAGE

PS2-NTF exist mainly as a monomer form although dimer and tetramer as well as octamer were observed indicating that the strong interaction can be displaced by SDS (**Figure 3.53**).

4.2.3.5 Thermal stability of the dimer in FC12

For a diluted protein solution (single molecule), the folded state is considered to be the state of the lowest Gibbs energy. However, this is not true for a protein solution containing many molecules since many experimental data suggested that the aggregated state is the state with the lowest Gibbs energy. The folded state is only considered to be the metastable state. An energy barrier needed to be overcome when transforming from folded state to aggregated state a process called unfolding. This process could be accelerated by heating. Heating often cause protein partial unfolding which facilities molecule aggregation due to exposure of the hydrophobic surface. Experimental data suggested that such aggregation during thermal unfolding is often accompanied with a structural transition from the correctly folded structure into a collapsed β-sheet rich structure. The protein aggregation normally undergoes two steps. The first step is the reversible nucleation during which the protein molecule is sequentially added to the nucleus in a thermal dynamically reversible manner. Very often, different states of oligomers could be observed during this step. As the mass of nucleus increase to a critical point, irreversible addition of the protein molecule to the nucleus occurs leading to eventually the formation of the very stable large aggregates which is the second step called irreversible aggregation (138).

In this work, upon thermal unfolding, SDS-PAGE analysis revealed that as the temperature increased from 20 to 60 ℃, there is a tendency for the decreasing of the monomer intensity and increase of the tetramer as well as octamer intensity. However, the dimer intensity remained quite constant. This result indicates that the dimer represents the actual sample state and the existence of the monomer is due to the dissociation effect of SDS-PAGE. After 60 ℃, the aggregates intensity gradually increased as observed on top of the gel, while the

oligomer intensity decreased. This is due to the formation of the very stable aggregates which couldn't be dissociated by SDS-PAGE. Finally, all the oligomers disappeared on SDS-PAGE for the sample preheated at 99 ℃ (**Figure 3.53**).

The thermal unfolding of PS2-NTF secondary structure was investigated by far UV CD spectroscopy (**Figure 3.52**). During thermal unfolding, proteins often undergo irreversible aggregation (**Figure 3.53**). However, the transition midpoints during thermal unfolding could be used to evaluate the protein thermal stability (139). Plot of MRE at 221 nm as a function of temperature fitted into a two-state unfolding transition was shown in **Figure 3.54**. From these experiments, a T_m value of 56.8±1.9 ℃ was obtained**.** Another membrane protein Glycerol facilitator (GF) in DDM under the same unfolding rate had a T_m value of 69.7±0.7 ℃ (140). Monomeric bacteriorhodopsin in detergent is thermally denatured with a T_m value of around 80 ℃ (141). The lower T_m value indicates less thermal stability of PS2-NTF than GF and BR. Deconvolution of the raw CD spectra at different temperatures into pure component spectra revealed exactly a decreasing tendency of α-helix content and an increasing tendency of β-strand content (**Table 3.8**). The correlation of these two was shown in **Figure 3.56**. The helix content decreased as the temperature increased. However, there were still 20 % helix content even at 99℃ indicating the residual highly stable helical structure which was resistant to thermal unfolding (142).

The thermal unfolding of PS2-NTF tertiary structure was also investigated by Trp fluorescence spectroscopy **(Figure 3.60)**. As the temperature increased with a heating rate of 1 ℃/min, the fluorescence intensity was progressively quenched. A 2 nm red shift from 332 to 334 nm was detected with the emission maximum position at the temperatures above 60 ℃ indicating the minor changes of Trp microenvironment. Fluorescence intensity at 333 nm as a function of temperature was fitted into a two state transition with a T_m value of 31.8±0.7 ℃ (**Figure 3.61**) indicating the instability of tertiary structure.

In all, the electrophoresis data, the CD and the fluorescence analysis all together suggest that the thermal unfolding of PS2-NTF in FC12 involves a concomitant loss of secondary and tertiary structure with a transition midpoint about 56.8 and 31.8 ℃ respectively.

4.2.4 Crystallization in MO cubic phase

It is reported that at 22 ℃ pure water with solid MO self-organizes into cubic phase without mixing within a time duration of 20-40 min. However it took as long as 24 h for His-PS2-NTF-Strep to fully reconstitute into MO cubic phase (**Figure 3.63**). This time difference can be explained by the fact that the presence of protein, detergent, buffer and salt may promote a competition with MO against absorbing water. MO preferably absorbs water to form cubic phase within short time duration. The solutes in the solution however prefer to retain water in the aqueous phase. What's more, incorporation of protein into membrane like MO bilayer also takes longer time due to its size and complexity (93).

4.3 *In vitro* translation

In vivo expression of PS2-CTF produced very poor yield (**Figure 3.20**). *In vitro* translation however produced PS2-CTF to reasonable quality and quantity (**Figure 3.64**). Due to the fact that PS2-FL and PS2-NTF can be obtained with a yield of milligrams amount per liter culture via *in vivo* expression, *in vitro* translation of PS2-CTF were performed.

Different *in vitro* translation modes have been developed for membrane protein expression. In order to produce a reasonable quantity and homogeneity of PS2-CTF for structural analysis, different *in vitro* translation modes were tried. Along with translation, Ni-NTA purification and SEC analysis were performed to investigate the quality of the protein.

When translated as a precipitate, due to the high hydrophobicity of membrane proteins, normally centrifugation and washing is enough to separate the background proteins from *E.coli* extract (41). Indeed a dominant band

corresponding to PS2-CTF with few impurities was detected by comassive staining on SDS-PAGE (**Figure 3.64**). However, SEC analysis (**Figure 3.70**) revealed that FC12 solubilised PS2-CTF did not exhibits a Gaussian-shaped peak and the loss of protein during solubilisation and concentrating.

Different detergents effects on translation were investigated with PS2-FL. Reports (143, 144) that Brij 35, Brij 58 and Brij 98 are compatible with *in vitro* translation system and can maintain most of the protein in supernatant after centrifugation could be confirmed for the case of PS2. For the detergents OG, LDAO, FC12 and CHAPS, where no signal corresponding to the target protein in either supernatant or pellet fraction was detected by western blot (**Figure 3.65**), an inhibitory effect was observed. This result indicates that different detergents may interfere with the translation system like disrupting ribosome therefore no protein was produced. When produced in the presence of Brij 35, Ni-NTA purification was performed in order to purify PS2-CTF and exchange detergent to FC12 (**Figure 3.71**). The purified PS2-CTF in FC12 was then concentrated and subjected to SEC analysis. SEC elution file showed shoulders before and after the main peak which contained the protein of interest. According to the SEC calibration, PS2-CTF exists as an octamer under these conditions (**Figure 3.73**).

Because of the detrimental effect of detergent and the insufficient yield as well as homogeneity problems of *in vitro* translated PS2-CTF in presence of detergent, the effect of the addition of nanodiscs was investigated. Nanodiscs are soluble nano-scale phospholipid bilayers wrapped by two helical membrane scaffold protein (MSP) (145). The addition of nanodiscs into *in vitro* translation as compared with other membrane mimicking components (detergent micelles, lipid/detergent bicelles and liposomes) can result in a functionally active, water-soluble, and mono-dispersed form of integral membrane proteins for biophysical, enzymatic or structural investigations (103, 145, 146). Surprisingly, i*n vitro* translation of PS2-CTF in presence of nanodiscs, not only increased protein yield (**Figure 3.74**) but also improved the homogeneity as shown in **Figure 3.76** where a mono-dispersed PS2-CTF-nanodiscs complex was detected by SEC. Interestingly, M_W determination using the calibration curve reveal that

PS2-CTF in the presence of DMPC exists also as an octamer (**Figure 3.77**), the same oligomerization state as in the presence of detergent (**Figure 3.73**). DMPC (1,2-Dimyristoyl-*sn*-glycero-3-phosphocholine) is a synthetic derivate of phospholipid PC (Phosphatidylcholine). Lipids are reported to play an essential role for (147, 148) or to enhance γ-secretase activity (149, 150) . Therefore the existing PS2-CTF octamer may be a biological relevant structure. Increased nano-discs concentrations failed to change the oligomerization state (**Figure 3.78**), which indicates that the octamer is stable with respect to smaller or bigger oligomers. However, *E coli in vivo* expressed PS2-CTF after partial purification exists as a tetramer in the presence of FC12 (**Figure 3.41**). Therefore the biological effect of PS2-CTF oligomerisation requires further investigation.

5 Summary

Presenilin proteins are part of the γ-secretase complex which consists of four different membrane proteins. This complex plays an important role in the development of Alzheimer's disease. The cleavage of APP-C99 by γ-secretase generates the amyloid beta peptide which is the major component of amyloid plaques. Presenilins are considered to be the catalytic subunit of γ-secretase. They are activated by auto-cleavage into its N-terminal and C-terminal domain to act as a protease within the membrane. Structural information of presenilins and the γ-secretase are of great importance to understand the activity of the complex and its mechanism of action.

In the presented work, human PS2 full length (PS2-FL) and its N-terminal domain (PS2-NTF) as well as its C-terminal domain (PS2-CTF) were heterologously expressed in *E.coli* via *in vivo* or by *in vitro* expression in order to characterize the proteins and to obtain material of sufficient quantity and quality for structural investigation via X-ray crystallography or NMR spectroscopy.

By optimization of the expression conditions and using codon-usage optimized DNA, PS2-FL and PS2-NTF can be expressed with a level of about 1 to 2 mg per liter culture via *in vivo* expression. Purification of PS2-FL was performed under native and denaturing condition by a combination of affinity chromatography and SEC. SEC analysis revealed that PS2-FL exists in equilibrium of hexamer and trimer. The observed tendency of the protein to aggregate, especially material obtained by refolding, appears to be caused at least partially by instability of the tertiary structure. A structural instability of a tertiary structure of a protein whose domains will be part of the quaternary structure of a protein complex after cleavage may be simply caused by flexibility of the domain assembly in the absence of other proteins of the complex. Indeed, the functional domains of PS2 show different oligomerisation than the full-length protein.

CD and fluorescence spectroscopy measurements of the refolded His-PS2-FL reconstituted into MO cubic phase revealed that the protein still exhibits the characteristics of a predominantly α–helical protein and the localisation of the tryptophan side chains in a relatively non-polar environment. Therefore first

crystallization experiments were performed in monoolein based cubic meso-phase.

The biophysical characterization of PS2-NTF showed the highest fraction of helical structure as well as the highest fluorescence in FC12, which indicated this detergent to be most compatible with the protein. The near UV CD spectrum of PS2-NTF in FC12 displayed the characteristics of a distinct tertiary structure peaks with strong, well-defined, negative bands between 255 and 300 nm. The PS2-NTF dimer probably represents the native state of the protein as supported by the near UV CD data. Thermal stability of the PS2-NTF dimer in FC12 was investigated by far UV CD and fluorescence spectroscopy. The MRE at 221 nm as a function of temperature could be fitted with a two-state unfolding transition. The obtained T_m value of 56.8±1.9 ℃ indicated that the protein secondary structure is relatively stable, which provided further evidences for the hypothesis that the observed aggregation of the full-length protein is due to instability of domain positioning. Deconvolution of the raw CD spectra at different temperatures into pure component spectra revealed a strongly correlated decrease of α-helical and an increase of β-strand structure, indicating a structural transformation of about 62 amino acids from α-helix to β-strand structure when the temperature increases from 20° to 90°C.

PS2-CTF expressed poorly *in vivo* and could be obtained via *in vitro* translation. *In vitro* translation was carried out using different forms of solubilisation to improve the yield and the homogeneity of PS2-CTF. The direct reconstitution into lipid-containing nanodiscs (MSP protein) gave a yield of ca. 1 mg per ml *in vitro* reaction. SEC elution profile revealed a monodispersed peak of PS2-CTF-nanodiscs complex suitable for structural analysis via solution NMR. Interestingly the oligomerisation of PS2-CTF is lipid dependent: While it forms a tetramer in FC12, in the presence of DMPC it exists as an octamer. However, for the separately expressed domains the oligomerisation was found to be a mono-dispersed dimer for PS2-NTF.

The SEC analysis revealed that for presenilin various different modes of oligomerisation exist which depend on the state of processing (activation by cleavage) and the environment, specifically the lipids. This explains why previously γ-secretase complexes of different stoichiometry were reported.

Zusammenfassung

Presenilin sind Teil des γ-Sekretase Komplexes, welcher aus vier verschiedenen Proteinen besteht. Der Komplex spielt eine wichtige Roll in der Entwicklung von *Morbus Alzheimer*. Die Spaltung von APP-C99 durch γ-Sekretase erzeugt das amyloid beta-peptid, welches die Hauptkomponente der amyloiden Plaques ist. Die Presenilin sind die katalytische Untereinheit der γ-Sekretase, welche nach Aktivierung durch Spaltung in eine N- und eine C-terminale Domäne innerhalb der Membran proteolytisch aktiv sind. Strukturelle Informationen über die Presenilin Moleküle und den γ-Sekretase sind notwendig, um die Aktivität der γ-Sekretase und ihren Wirkmechanismus zu verstehen.

In dieser Arbeit wurden das humane PS2 (PS2-FL) und das N-terminale (PS2-NTF) und das C-terminale Fragment (PS2-CTF) heterolog in in *E.coli* sowie *in vitro* exprimiert, um einer erste Charakterisierung des Proteins zu erreichen, und hinreichend Material hinreichender Qualität für weiterführende strukturelle Untersuchungen durch Röntgenkristallographie bzw. NMR-Spektroskopie zu erhalten.

Durch Optimierung der Expressionsbedingungen und die Verwendung Codon-optimierter DNA-Konstrukte ließen sich PS2-FL und PS2-NTF zu 1-2 mg/l Kultur in *E. coli* exprimieren. Die Reinigung von PS2-FL erfolgte unter nativen und denaturierenden Bedingungen durch eine Kombination von Affinitätschromatographie und Gelfitration. Hierbei zeigte sich das PS2-FL im Gleichgewicht von Hexamer und als Trimer vorliegt. Die beobachtete Neigung von PS2-FL, besonders nach Rückfaltung, zu aggregieren, scheint in Zusammenhang mit einer instabilen Tertiärstruktur zu stehen. Eine strukturelle Instabilität der Tertiärstruktur eines Proteins, dessen Domänen nach Spaltung Teil der Quartästruktur eines Proteinkomplexes werden, könnte allein durch die mangelnde Stabilisierung der Domänenanordnung in Abwesenheit der anderen Proteine des Komplexes verursacht sein. Tatsächlich zeigen die funktionalen Domänen andere Formen von Oligomerisierung als das Gesamtprotein.

CD und Fluoreszenzmessungen an rückgefaltetem His-PS2-FL, welches in kubische Phase von Monoolein rekonstituiert wurde, zeigte dass das es alle

Charakteristika eines α–helicalen Proteins besitzt, und die Tryptophane sich in einer relativ unpolaren Umgebung befinden. Daher konnten erste Kristallisationsexperimente durchgeführt werden.

Die biophysikalische Charakterisierung von PS2-NTF zeigte den höchsten Anteil an helicaler Struktur und maximale Fluoreszenz in Foscholin-12, wodurch sich dieses Detergenz als am besten geeignet erwies. Das CD-Spektrum von PS2-NTF im nahen UV zeigt die distinkten Signale für Tertiärstruktur mit einer gut definierten negativen Bande zwischen 255 und 300 nm. Dies unterstützt die Interpretation, dass es sich bei dem PS2-NTF Dimer um den nativen Zustand des Proteins handelt. Weitere Evidenz für die Hypothese, dass die beobachtete Aggregation von Presenilin auf eine instabile Domänenanordnung zurückzuführen ist, wurde durch die Untersuchung der Thermostabilität des PS2-NTF Dimers durch CD- und Fluoreszenzspektroskopie gefunden, die erwies, dass diese Domäne mit einem Schmelzpunkt T_m von 56.8±1.9 ℃, als relativ stabil anzusehen ist. Die Dekonvolution der CD-Spectren ergab, dass mit zunehmender Temperatur eine Strukturumwandlung von α-helikal nach β-Strang von 62 Aminosäuren stattfand, wenn die Temperatur von 20° nach 90°C erhöht wurde.

Die C-terminale Domäne PS2-CTF war in *E. coli* nur gering exprimierbar, sie konnte besser durch *in vitro* Expression erhalten werden. Zur Optimierung der *in vitro* Expression wurde neben einer Untersuchung des Einflusses der verwendeten Detergenzien auch eine direkte Rekonstitution in lipidhaltige *nanodiscs* (MSP Protein) untersucht. Die Ausbeute an PS2-CTF von ca. 1mg/ml in *in vitro* Reaktion in Form von monodispersem rekonstituierten PS2-CTF erlaubt weitergehende NMR Untersuchungen der Struktur. Bemerkenswerterweise war die Oligomerisierung von PS2-CTF vom Lipid abhängig: Während in Foscholin-12 ein Tetramer vorlag, fand sich in DMPC ein Oktamer. Dagegen bildete die einzeln exprimierte N-terminale Domäne ein stabiles Dimer.

Die Analyse des Oligomerisierung von Presenilin zeigte, dass sie vom Prozessierungszustand (der Aktivierung durch Spaltung) und der der Umgebung abhängt, speziell von den Lipiden. Dies erklärt warum bisher γ-Sekretase-komplexe unterschiedlicher Stöchiometrie gefunden wurden.

Abbreviations

AD	Alzheimer's disease
AICD	APP intracellular domain
APH1	Anterior pharynx defective 1
APOE	Apolipoprotein E
APP	Amyloid precursor protein
ASP	Ammonium sulphate precipitation
ATP	Adenosinetriphosphate
Aβ	beta-amyloid
BACE	β-site of amyloid precursor protein cleaving enzyme
BSA	Bovine serum albumin
℃	Degree centigrade
CBBG	Coomassie brilliant blue G-250 dye
CD	Circular Dichroism
cm	Centimeter
C_V	Column volume
ddNTP	Didesoxy-nucleotide triphosphate
DLS	Dynamic light scattering
DNA	Desoxyribonucleic acid
DTT	Dithiothreitol
EDTA	Ethylendiethyltetraacetic acid
ER	Endoplasmic reticulum
EtBr	Ethidium bromide
FAD	Familial AD
GndHCl	Guanidine hydrochloride
h	Hour
HABA	2-(4'-hydroxy-benzeneazo) benzoic acid
IEX	Ion Exchange Chromatography
IMAC	Immobilized metal affinity chromatography
IPTG	Isopropyl β-D-1-thiogalactopyranoside
kDa	Kilo Dalton
l	Liter

M	Molar
MALDI-TOF	Matrix Associated Laser Desorption Ionization-Time of Flight
min	Minute
ml	Milliliter
mm	Milimeter
mM	Millimolar
µl	Microliters
µm	Micrometer
µM	Micromolar
MO	Monoolein
M_w	Molecular weight
MRE	Mean Residue Ellipticity
MRW	Molar residual weight
MS	Mass spectrometry
MS/MS	Tandem MS
NCT	Nicastrin
NFD	Non-fat dry milk
NLS	N-Lauroylsarcosine sodium salt
nm	Nanometer
NTP	Nucleotidediphosphate
OD	Optical density
PAGE	Polyacrylamide gel electrophoresis
PCR	Polymerase chain reaction
PEN2	Presenilin enhancer 2
pH	Potentia hydrogenii
PMSF	Phenylmethanesulfonyl fluoride
PSEN1	Presenilin 1genes
PSEN2	Presenilin 2 genes
PS1	Presenilin1 protein
PS2	Presenilin2 protein
rpm	Rotations per minute
R_h	Hydrodynamic radius
S	Seconds

sAPPα	Soluble fragment of APP after α-secretases cleavage
sAPPβ	Soluble fragment of APP after β-secretase cleavage
SDS	Sodium dodecyl sulfate
SDS-PAGE	Sodium dodecyl sulphate polyacrylamide gel electrophoresis
SEC	Size exclusion chromatography
TCA	Trichloroacetic acid
TCEP	Tris (2-chlorethyl) phosphine
TEMED	Tetramethylethylenediamine
TM	Transmembrane
Tris	Tris (hydroxymethyl) aminomethane
UV	Ultra violet
V_e	Elution volume,
V_0	Void volume
V_t	Total column volume
β-ME	β-mercaptoethanol

Bibliography

1. Brookmeyer R, Johnson E, Ziegler-Graham K, & Arrighi HM (2007) Forecasting the global burden of Alzheimer's disease. *Alzheimers Dement* 3(3):186-191.
2. Glenner GG & Wong CW (1984) Alzheimer's disease: initial report of the purification and characterization of a novel cerebrovascular amyloid protein. *Biochem Biophys Res Commun* 120(3):885-890.
3. Grundke-Iqbal I*, et al.* (1986) Abnormal phosphorylation of the microtubule-associated protein tau (tau) in Alzheimer cytoskeletal pathology. *Proc Natl Acad Sci U S A* 83(13):4913-4917.
4. Kopke E*, et al.* (1993) Microtubule-associated protein tau. Abnormal phosphorylation of a non-paired helical filament pool in Alzheimer disease. *J Biol Chem* 268(32):24374-24384.
5. http://www.ahaf.org/alzheimers.
6. Alzheimer A, Stelzmann RA, Schnitzlein HN, & Murtagh FR (1995) An English translation of Alzheimer's 1907 paper, "Uber eine eigenartige Erkankung der Hirnrinde". *Clin Anat* 8(6):429-431.
7. Harvey RJ, Skelton-Robinson M, & Rossor MN (2003) The prevalence and causes of dementia in people under the age of 65 years. *Journal of neurology, neurosurgery, and psychiatry* 74(9):1206-1209.
8. Goate A*, et al.* (1991) Segregation of a missense mutation in the amyloid precursor protein gene with familial Alzheimer's disease. *Nature* 349(6311):704-706.
9. Sherrington R*, et al.* (1995) Cloning of a gene bearing missense mutations in early-onset familial Alzheimer's disease. *Nature* 375(6534):754-760.
10. Levy-Lahad E*, et al.* (1995) Candidate gene for the chromosome 1 familial Alzheimer's disease locus. *Science* 269(5226):973-977.
11. http://www.molgen.ua.ac.be/ADMutations.
12. http://www.molgen.ua.ac.be/Admutations/default.cfm?.
13. Strittmatter WJ*, et al.* (1993) Apolipoprotein E: high-avidity binding to beta-amyloid and increased frequency of type 4 allele in late-onset familial Alzheimer disease. *Proc Natl Acad Sci U S A* 90(5):1977-1981.
14. Farrer LA*, et al.* (1997) Effects of age, sex, and ethnicity on the association between apolipoprotein E genotype and Alzheimer disease. A meta-analysis. APOE and Alzheimer Disease Meta Analysis Consortium. *Jama* 278(16):1349-1356.
15. Jiang Q*, et al.* (2008) ApoE promotes the proteolytic degradation of Abeta. *Neuron* 58(5):681-693.
16. Lammich S*, et al.* (1999) Constitutive and regulated alpha-secretase cleavage of Alzheimer's amyloid precursor protein by a disintegrin metalloprotease. *Proc Natl Acad Sci U S A* 96(7):3922-3927.
17. Hong L*, et al.* (2000) Structure of the protease domain of memapsin 2 (beta-secretase) complexed with inhibitor. *Science* 290(5489):150-153.
18. Steiner H, Fluhrer R, & Haass C (2008) Intramembrane proteolysis by gamma-secretase. *J Biol Chem* 283(44):29627-29631.

19. Stempfle D, Kanwar R, Loewer A, Fortini ME, & Merdes G (2010) In vivo reconstitution of gamma-secretase in Drosophila results in substrate specificity. *Mol Cell Biol* 30(13):3165-3175.
20. Kimberly WT, *et al.* (2003) Gamma-secretase is a membrane protein complex comprised of presenilin, nicastrin, Aph-1, and Pen-2. *Proc Natl Acad Sci U S A* 100(11):6382-6387.
21. Yagishita S, Futai E, & Ishiura S (2008) In vitro reconstitution of gamma-secretase activity using yeast microsomes. *Biochem Biophys Res Commun* 377(1):141-145.
22. Edbauer D, *et al.* (2003) Reconstitution of gamma-secretase activity. *Nat Cell Biol* 5(5):486-488.
23. Sato T, *et al.* (2007) Active gamma-secretase complexes contain only one of each component. *J Biol Chem* 282(47):33985-33993.
24. Wolfe MS, *et al.* (1999) Two transmembrane aspartates in presenilin-1 required for presenilin endoproteolysis and gamma-secretase activity. *Nature* 398(6727):513-517.
25. Li YM, *et al.* (2000) Photoactivated gamma-secretase inhibitors directed to the active site covalently label presenilin 1. *Nature* 405(6787):689-694.
26. Kaether C, *et al.* (2002) Presenilin-1 affects trafficking and processing of betaAPP and is targeted in a complex with nicastrin to the plasma membrane. *J Cell Biol* 158(3):551-561.
27. Herreman A, *et al.* (2003) gamma-Secretase activity requires the presenilin-dependent trafficking of nicastrin through the Golgi apparatus but not its complex glycosylation. *J Cell Sci* 116(Pt 6):1127-1136.
28. Yu G, *et al.* (2000) Nicastrin modulates presenilin-mediated notch/glp-1 signal transduction and betaAPP processing. *Nature* 407(6800):48-54.
29. Gu Y, *et al.* (2003) APH-1 interacts with mature and immature forms of presenilins and nicastrin and may play a role in maturation of presenilin.nicastrin complexes. *J Biol Chem* 278(9):7374-7380.
30. Lee SF, *et al.* (2002) Mammalian APH-1 interacts with presenilin and nicastrin and is required for intramembrane proteolysis of amyloid-beta precursor protein and Notch. *J Biol Chem* 277(47):45013-45019.
31. Crystal AS, *et al.* (2003) Membrane topology of gamma-secretase component PEN-2. *J Biol Chem* 278(22):20117-20123.
32. Takasugi N, *et al.* (2003) The role of presenilin cofactors in the gamma-secretase complex. *Nature* 422(6930):438-441.
33. Prokop S, Shirotani K, Edbauer D, Haass C, & Steiner H (2004) Requirement of PEN-2 for stabilization of the presenilin N-/C-terminal fragment heterodimer within the gamma-secretase complex. *J Biol Chem* 279(22):23255-23261.
34. Ahn K, *et al.* (2010) Activation and intrinsic gamma-secretase activity of presenilin 1. *Proc Natl Acad Sci U S A* 107(50):21435-21440.
35. Lessard CB, Wagner SL, & Koo EH (2010) And four equals one: presenilin takes the gamma-secretase role by itself. *Proc Natl Acad Sci U S A* 107(50):21236-21237.
36. Lehmann S, Chiesa R, & Harris DA (1997) Evidence for a six-transmembrane domain structure of presenilin 1. *J Biol Chem* 272(18):12047-12051.
37. Dewji NN & Singer SJ (1997) The seven-transmembrane spanning topography of the Alzheimer disease-related presenilin proteins in the plasma membranes of cultured cells. *Proc Natl Acad Sci U S A* 94(25):14025-14030.

38. Nakai T, *et al.* (1999) Membrane topology of Alzheimer's disease-related presenilin 1. Evidence for the existence of a molecular species with a seven membrane-spanning and one membrane-embedded structure. *J Biol Chem* 274(33):23647-23658.
39. Li X & Greenwald I (1998) Additional evidence for an eight-transmembrane-domain topology for Caenorhabditis elegans and human presenilins. *Proc Natl Acad Sci U S A* 95(12):7109-7114.
40. Spasic D, *et al.* (2006) Presenilin-1 maintains a nine-transmembrane topology throughout the secretory pathway. *J Biol Chem* 281(36):26569-26577.
41. Sobhanifar S, *et al.* (2010) Structural investigation of the C-terminal catalytic fragment of presenilin 1. *Proc Natl Acad Sci U S A* 107(21):9644-9649.
42. Miles JS & Wolf CR (1989) Principles of DNA cloning. *Bmj* 299(6706):1019-1022.
43. Vosberg HP (1989) The polymerase chain reaction: an improved method for the analysis of nucleic acids. *Human genetics* 83(1):1-15.
44. Bernard P, Gabant P, Bahassi EM, & Couturier M (1994) Positive-selection vectors using the F plasmid ccdB killer gene. *Gene* 148(1):71-74.
45. Newby ZE, *et al.* (2009) A general protocol for the crystallization of membrane proteins for X-ray structural investigation. *Nature protocols* 4(5):619-637.
46. Georgiou G & Valax P (1999) Isolating inclusion bodies from bacteria. *Methods in enzymology* 309:48-58.
47. Block H, *et al.* (2009) Immobilized-metal affinity chromatography (IMAC): a review. *Methods in enzymology* 463:439-473.
48. Magnusdottir A, Johansson I, Dahlgren LG, Nordlund P, & Berglund H (2009) Enabling IMAC purification of low abundance recombinant proteins from E. coli lysates. *Nature methods* 6(7):477-478.
49. Surrey T & Jahnig F (1992) Refolding and oriented insertion of a membrane protein into a lipid bilayer. *Proc Natl Acad Sci U S A* 89(16):7457-7461.
50. Schmidt TG & Skerra A (2007) The Strep-tag system for one-step purification and high-affinity detection or capturing of proteins. *Nature protocols* 2(6):1528-1535.
51. Haddad PR & Jackson PE (1990) *Ion chromatography: principles and applications* (Elsevier Science).
52. Stanton P (2004) Ion-exchange chromatography. *Methods in molecular biology* 251:23-44.
53. Doonan S (1996) Bulk purification by fractional precipitation. *Methods in molecular biology* 59:135-144.
54. Mori S & Barth HG (1999) *Size exclusion chromatography* (Springer).
55. Cutler P (2004) Size-exclusion chromatography. *Methods in molecular biology* 244:239-252.
56. Smith RD, Loo JA, Loo RRO, Busman M, & Udesth H (1992) Principles and Practice of Electrospray Ionization-Mass Spectrometry for Large Polypeptides and Proteins. *ChemInform* 23(33):no-no.
57. http://www.astbury.leeds.ac.uk/facil/MStut/mstutorial.htm.
58. Cotter RJ (1994) Time-of-flight mass spectrometry.
59. McLafferty FW (1980) Tandem mass spectrometry (MS/MS): a promising new analytical technique for specific component determination in complex mixtures. *Accounts of chemical research* 13(2):33-39.

60. Finehout EJ & Lee KH (2004) An introduction to mass spectrometry applications in biological research. *Biochemistry and molecular biology education : a bimonthly publication of the International Union of Biochemistry and Molecular Biology* 32(2):93-100.
61. Li M, Su ZG, & Janson JC (2004) In vitro protein refolding by chromatographic procedures. *Protein expression and purification* 33(1):1-10.
62. Poliakov A & Danielson UH (2005) Refolding of the full-length non-structural protein 3 of hepatitis C virus. *Protein expression and purification* 41(2):298-305.
63. Oganesyan N, Kim SH, & Kim R (2005) On-column protein refolding for crystallization. *Journal of structural and functional genomics* 6(2-3):177-182.
64. http://web.expasy.org/protparam.
65. Georgiou CD, Grintzalis K, Zervoudakis G, & Papapostolou I (2008) Mechanism of Coomassie brilliant blue G-250 binding to proteins: a hydrophobic assay for nanogram quantities of proteins. *Analytical and bioanalytical chemistry* 391(1):391-403.
66. Bradford MM (1976) A rapid and sensitive method for the quantitation of microgram quantities of protein utilizing the principle of protein-dye binding. *Analytical biochemistry* 72:248-254.
67. Voytas D (2001) Agarose gel electrophoresis. *Current protocols in immunology / edited by John E. Coligan ... [et al.]* Chapter 10:Unit 10 14.
68. Chrambach A & Rodbard D (1971) Polyacrylamide gel electrophoresis. *Science* 172(3982):440-451.
69. Burnette WN (1981) "Western blotting": electrophoretic transfer of proteins from sodium dodecyl sulfate--polyacrylamide gels to unmodified nitrocellulose and radiographic detection with antibody and radioiodinated protein A. *Analytical biochemistry* 112(2):195-203.
70.http://www.invitrogen.com/site/us/en/home/References/Molecular-Probes-The-Handbook/Introduction-to-Fluorescence-Techniques.html.
71. Reshetnyak YK & Burstein EA (2001) Decomposition of protein tryptophan fluorescence spectra into log-normal components. II. The statistical proof of discreteness of tryptophan classes in proteins. *Biophysical journal* 81(3):1710-1734.
72. Lakowicz JR (2006) *Principles of fluorescence spectroscopy* (Springer).
73. Berova N, Nakanishi K, & Woody RW (2000) *Circular dichroism: principles and applications* (Wiley-VCH New York).
74. http://www.ruppweb.org/cd/cdtutorial.htm.
75. Lobley A, Whitmore L, & Wallace BA (2002) DICHROWEB: an interactive website for the analysis of protein secondary structure from circular dichroism spectra. *Bioinformatics* 18(1):211-212.
76. Whitmore L & Wallace BA (2004) DICHROWEB, an online server for protein secondary structure analyses from circular dichroism spectroscopic data. *Nucleic acids research* 32(Web Server issue):W668-673.
77. Abdul-Gader A, Miles AJ, & Wallace BA (2011) A reference dataset for the analyses of membrane protein secondary structures and transmembrane residues using circular dichroism spectroscopy. *Bioinformatics* 27(12):1630-1636.
78. Sreerama N & Woody RW (2004) On the analysis of membrane protein circular dichroism spectra. *Protein science : a publication of the Protein Society* 13(1):100-112.

79. http://www.ap-lab.com/circular_dichroism.htm.
80. Kelly SM, Jess TJ, & Price NC (2005) How to study proteins by circular dichroism. *Biochimica et Biophysica Acta (BBA)-Proteins & Proteomics* 1751(2):119-139.
81. Kelly SM & Price NC (2000) The use of circular dichroism in the investigation of protein structure and function. *Curr Protein Pept Sci* 1(4):349-384.
82. http://dichroweb.cryst.bbk.ac.uk/html/home.shtml.
83. Sreerama N & Woody RW (2000) Estimation of protein secondary structure from circular dichroism spectra: comparison of CONTIN, SELCON, and CDSSTR methods with an expanded reference set. *Analytical biochemistry* 287(2):252-260.
84. http://bioinf.cs.ucl.ac.uk/psipred.
85. Consalvi V*, et al.* (2000) Thermal unfolding and conformational stability of the recombinant domain II of glutamate dehydrogenase from the hyperthermophile Thermotoga maritima. *Protein Eng* 13(7):501-507.
86. Sehgal P & Otzen DE (2006) Thermodynamics of unfolding of an integral membrane protein in mixed micelles. *Protein science : a publication of the Protein Society* 15(4):890-899.
87. Santoro MM & Bolen DW (1988) Unfolding free energy changes determined by the linear extrapolation method. 1. Unfolding of phenylmethanesulfonyl alpha-chymotrypsin using different denaturants. *Biochemistry* 27(21):8063-8068.
88. Berne BJ & Pecora R (2000) *Dynamic light scattering: with applications to chemistry, biology, and physics* (Dover Publications).
89. Landau EM & Rosenbusch JP (1996) Lipidic cubic phases: a novel concept for the crystallization of membrane proteins. *Proc Natl Acad Sci U S A* 93(25):14532-14535.
90. Cherezov V, Clogston J, Misquitta Y, Abdel-Gawad W, & Caffrey M (2002) Membrane protein crystallization in meso: lipid type-tailoring of the cubic phase. *Biophysical journal* 83(6):3393-3407.
91. Nollert P, Qiu H, Caffrey M, Rosenbusch JP, & Landau EM (2001) Molecular mechanism for the crystallization of bacteriorhodopsin in lipidic cubic phases. *FEBS letters* 504(3):179-186.
92. Qutub Y*, et al.* (2004) Crystallization of transmembrane proteins in cubo: mechanisms of crystal growth and defect formation. *Journal of molecular biology* 343(5):1243-1254.
93. Kubicek J*, et al.* (2012) Controlled in meso phase crystallization--a method for the structural investigation of membrane proteins. *PloS one* 7(4):e35458.
94. Caffrey M & Cherezov V (2009) Crystallizing membrane proteins using lipidic mesophases. *Nature protocols* 4(5):706-731.
95. Katzen F, Chang G, & Kudlicki W (2005) The past, present and future of cell-free protein synthesis. *Trends in biotechnology* 23(3):150-156.
96. Savage DF, Anderson CL, Robles-Colmenares Y, Newby ZE, & Stroud RM (2007) Cell-free complements in vivo expression of the E. coli membrane proteome. *Protein science : a publication of the Protein Society* 16(5):966-976.
97. Schwarz D*, et al.* (2007) Preparative scale expression of membrane proteins in Escherichia coli-based continuous exchange cell-free systems. *Nature protocols* 2(11):2945-2957.

98. Berrier C, *et al.* (2004) Cell-free synthesis of a functional ion channel in the absence of a membrane and in the presence of detergent. *Biochemistry* 43(39):12585-12591.
99. Corin K, *et al.* (2011) A robust and rapid method of producing soluble, stable, and functional G-protein coupled receptors. *PloS one* 6(10):e23036.
100. Elbaz Y, Steiner-Mordoch S, Danieli T, & Schuldiner S (2004) In vitro synthesis of fully functional EmrE, a multidrug transporter, and study of its oligomeric state. *Proc Natl Acad Sci U S A* 101(6):1519-1524.
101. Wang X, *et al.* (2011) Peptide surfactants for cell-free production of functional G protein-coupled receptors. *Proc Natl Acad Sci U S A* 108(22):9049-9054.
102. Corin K, *et al.* (2011) Designer lipid-like peptides: a class of detergents for studying functional olfactory receptors using commercial cell-free systems. *PloS one* 6(11):e25067.
103. Lyukmanova EN, *et al.* (2012) Lipid-protein nanodiscs for cell-free production of integral membrane proteins in a soluble and folded state: comparison with detergent micelles, bicelles and liposomes. *Biochimica et biophysica acta* 1818(3):349-358.
104. Katzen F, Peterson TC, & Kudlicki W (2009) Membrane protein expression: no cells required. *Trends in biotechnology* 27(8):455-460.
105. Katzen F, *et al.* (2008) Insertion of membrane proteins into discoidal membranes using a cell-free protein expression approach. *Journal of proteome research* 7(8):3535-3542.
106. Gluck JM, *et al.* (2009) Integral Membrane Proteins in Nanodiscs Can Be Studied by Solution NMR Spectroscopy. *Journal of the American Chemical Society* 131(34):12060.
107. http://www.matrixscience.com/ search_form_select.html.
108. Arnold T & Linke D (2008) The use of detergents to purify membrane proteins. *Curr Protoc Protein Sci* Chapter 4:Unit 4 8 1-4 8 30.
109. Cherezov V, Clogston J, Papiz MZ, & Caffrey M (2006) Room to move: crystallizing membrane proteins in swollen lipidic mesophases. *Journal of molecular biology* 357(5):1605-1618.
110. http://bioinf.cs.ucl.ac.uk/psipred/.
111. Dries DR & Yu G (2008) Assembly, maturation, and trafficking of the gamma-secretase complex in Alzheimer's disease. *Curr Alzheimer Res* 5(2):132-146.
112. Casey JR, Grinstein S, & Orlowski J (2010) Sensors and regulators of intracellular pH. *Nature reviews. Molecular cell biology* 11(1):50-61.
113. Wagner S, *et al.* (2007) Consequences of membrane protein overexpression in Escherichia coli. *Mol Cell Proteomics* 6(9):1527-1550.
114. Klepsch MM, Persson JO, & de Gier JW (2011) Consequences of the overexpression of a eukaryotic membrane protein, the human KDEL receptor, in Escherichia coli. *Journal of molecular biology* 407(4):532-542.
115. Miroux B & Walker JE (1996) Over-production of proteins in Escherichia coli: mutant hosts that allow synthesis of some membrane proteins and globular proteins at high levels. *Journal of molecular biology* 260(3):289-298.
116. Wagner S, *et al.* (2008) Tuning Escherichia coli for membrane protein overexpression. *Proc Natl Acad Sci U S A* 105(38):14371-14376.

117. Siller E, DeZwaan DC, Anderson JF, Freeman BC, & Barral JM (2010) Slowing bacterial translation speed enhances eukaryotic protein folding efficiency. *Journal of molecular biology* 396(5):1310-1318.
118. Harnasch M, *et al.* (2004) Characterization of presenilin-amyloid precursor interaction using bacterial expression and two-hybrid systems for human membrane proteins. *Mol Membr Biol* 21(6):373-383.
119. Gorzelle BM, *et al.* (1999) Reconstitutive refolding of diacylglycerol kinase, an integral membrane protein. *Biochemistry* 38(49):16373-16382.
120. Duquesne K & Sturgis JN (2010) Membrane protein solubilization. *Methods in molecular biology* 601:205-217.
121. Maslennikov I, *et al.* (2007) NMR spectroscopic and analytical ultracentrifuge analysis of membrane protein detergent complexes. *BMC Struct Biol* 7:74.
122. Maslennikov I, *et al.* (2009) Characterization of protein detergent complexes by NMR, light scattering, and analytical ultracentrifugation. *Journal of structural and functional genomics* 10(1):25-35.
123. Kefala G, *et al.* (2010) Structures of the OmpF porin crystallized in the presence of foscholine-12. *Protein science : a publication of the Protein Society* 19(5):1117-1125.
124. Columbus L, *et al.* (2009) Mixing and matching detergents for membrane protein NMR structure determination. *Journal of the American Chemical Society* 131(21):7320-7326.
125. Tsai CJ & Ziegler C (2005) Structure determination of secondary transport proteins by electron crystallography: Two-dimensional crystallization of the betaine uptake system BetP. *J Mol Microb Biotech* 10(2-4):197-207.
126. Voss S & Skerra A (1997) Mutagenesis of a flexible loop in streptavidin leads to higher affinity for the Strep-tag II peptide and improved performance in recombinant protein purification. *Protein Eng* 10(8):975-982.
127. Knecht S, Ricklin D, Eberle AN, & Ernst B (2009) Oligohis-tags: mechanisms of binding to Ni2+-NTA surfaces. *J Mol Recognit* 22(4):270-279.
128. Haass C & De Strooper B (1999) The presenilins in Alzheimer's disease--proteolysis holds the key. *Science* 286(5441):916-919.
129. Yun CH, Song M, & Kim H (1997) Conformational change of cytochrome P450 1A2 induced by phospholipids and detergents. *J Biol Chem* 272(32):19725-19730.
130. Kuroda Y, *et al.* (2003) Effects of detergents on the secondary structures of prion protein peptides as studied by CD spectroscopy. *Journal of peptide science : an official publication of the European Peptide Society* 9(4):212-220.
131. McLendon C, *et al.* (2000) Cell-free assays for gamma-secretase activity. *FASEB J* 14(15):2383-2386.
132. Franberg J, *et al.* (2007) Rat brain gamma-secretase activity is highly influenced by detergents. *Biochemistry* 46(25):7647-7654.
133. Schroeter EH, *et al.* (2003) A presenilin dimer at the core of the gamma-secretase enzyme: Insights from parallel analysis of Notch 1 and APP proteolysis. *Proc Natl Acad Sci U S A* 100(22):13075-13080.
134. Cervantes S, Saura CA, Pomares E, Gonzalez-Duarte R, & Marfany G (2004) Functional implications of the presenilin dimerization: reconstitution of gamma-secretase activity by assembly of a catalytic site at the dimer interface of two catalytically inactive presenilins. *J Biol Chem* 279(35):36519-36529.

135. Herl L, *et al.* (2006) Detection of presenilin-1 homodimer formation in intact cells using fluorescent lifetime imaging microscopy. *Biochem Biophys Res Commun* 340(2):668-674.
136. Nyborg AC, *et al.* (2006) Signal peptide peptidase (SPP) dimer formation as assessed by fluorescence lifetime imaging microscopy (FLIM) in intact cells. *Molecular neurodegeneration* 1:16.
137. Nyborg AC, *et al.* (2004) Signal peptide peptidase forms a homodimer that is labeled by an active site-directed gamma-secretase inhibitor. *J Biol Chem* 279(15):15153-15160.
138. Gazit E (2002) The "Correctly Folded" state of proteins: is it a metastable state? *Angew Chem Int Ed Engl* 41(2):257-259.
139. Minetti CA & Remeta DP (2006) Energetics of membrane protein folding and stability. *Arch Biochem Biophys* 453(1):32-53.
140. Galka JJ, Baturin SJ, Manley DM, Kehler AJ, & O'Neil JD (2008) Stability of the glycerol facilitator in detergent solutions. *Biochemistry* 47(11):3513-3524.
141. Brouillette CG, McMichens RB, Stern LJ, & Khorana HG (1989) Structure and thermal stability of monomeric bacteriorhodopsin in mixed phospholipid/detergent micelles. *Proteins* 5(1):38-46.
142. Haltia T & Freire E (1995) Forces and factors that contribute to the structural stability of membrane proteins. *Biochimica et biophysica acta* 1228(1):1-27.
143. Schneider B, *et al.* (2010) Membrane protein expression in cell-free systems. *Methods in molecular biology* 601:165-186.
144. Klammt C, *et al.* (2005) Evaluation of detergents for the soluble expression of alpha-helical and beta-barrel-type integral membrane proteins by a preparative scale individual cell-free expression system. *The FEBS journal* 272(23):6024-6038.
145. Borch J & Hamann T (2009) The nanodisc: a novel tool for membrane protein studies. *Biological chemistry* 390(8):805-814.
146. Bayburt TH & Sligar SG (2010) Membrane protein assembly into Nanodiscs. *FEBS letters* 584(9):1721-1727.
147. Wrigley JD, *et al.* (2005) Functional overexpression of gamma-secretase reveals protease-independent trafficking functions and a critical role of lipids for protease activity. *J Biol Chem* 280(13):12523-12535.
148. Zhou H, Zhou S, Walian PJ, & Jap BK (2010) Dependency of gamma-secretase complex activity on the structural integrity of the bilayer. *Biochem Biophys Res Commun* 402(2):291-296.
149. Holmes O, Paturi S, Ye W, Wolfe MS, & Selkoe DJ (2012) Effects of membrane lipids on the activity and processivity of purified gamma-secretase. *Biochemistry* 51(17):3565-3575.
150. Osawa S, *et al.* (2008) Phosphoinositides suppress gamma-secretase in both the detergent-soluble and -insoluble states. *J Biol Chem* 283(28):19283-19292.

Appendix I: DNA and protein sequences

All sequences shown below are N-his and C-strep tagged.

Human presenilin 2 full length (PS2-FL) DNA sequence:

```
   1 ATGAAGCACC ATCATCACCA TCACCATATG CTGACCTTTA TGGCGAGCGA TAGCGAGGAA
  61 GAAGTGTGCG ACGAACGTAC CAGCCTGATG AGCGCGGAAA GCCCGACCCC GCGTAGCTGT
 121 CAGGAAGGCC GTCAGGGCCC GGAAGATGGC GAAAACACCG CCCAGTGGCG TAGCCAAGAA
 181 AACGAAGAGG ATGGCGAAGA AGATCCGGAT CGTTACGTGT GTAGCGGCGT GCCGGGTCGT
 241 CCGCCGGGTC TGGAAGAAGA ACTGACCCTG AAATATGGCG CGAAACATGT GATTATGCTG
 301 TTTGTGCCGG TGACCCTGTG CATGATTGTG GTGGTGGCGA CCATTAAAAG CGTGCGCTTC
 361 TACACCGAAA AAAACGGCCA GCTGATCTAT ACCACCTTTA CCGAAGATAC CCCGAGCGTG
 421 GGCCAGCGTC TGCTGAACAG CGTGCTGAAC ACCCTGATTA TGATTAGCGT GATTGTGGTG
 481 ATGACCATTT TTCTGGTGGT GCTGTATAAA TATCGCTGTT ATAAATTTAT TCACGGCTGG
 541 CTGATTATGA GCAGCCTGAT GCTGCTGTTT CTGTTCACCT ATATCTATCT GGGCGAAGTG
 601 CTGAAAACCT ATAACGTGGC AATGGATTAT CCGACCCTGC TGCTGACCGT GTGGAACTTT
 661 GGCGCGGTGG GCATGGTGTG CATTCATTGG AAAGGCCCGC TGGTGCTGCA GCAGGCGTAT
 721 CTGATCATGA TCTCTGCCCT GATGGCGCTG GTGTTTATTA AATATCTGCC GGAATGGTCT
 781 GCGTGGGTGA TTCTGGGCGC GATTAGCGTG TATGATCTGG TGGCGGTGCT GTGCCCGAAA
 841 GGTCCGCTGC GTATGCTGGT TGAAACCGCG CAGGAACGTA ACGAACCGAT TTTTCCGGCG
 901 CTGATTTATT CTAGCGCAAT GGTGTGGACC GTGGGCATGG CGAAACTGGA CCCGAGCAGC
 961 CAGGGTGCGC TGCAGCTGCC GTATGATCCG GAAATGGAAG AAGATAGCTA CGATAGCTTT
1021 GGCGAACCGA GCTATCCGGA AGTGTTTGAA CCGCCGCTGA CCGGCTATCC GGGCGAAGAA
1081 CTGGAAGAAG AAGAAGAACG CGGCGTTAAA CTGGGCCTGG GCGATTTTAT TTTTTATAGC
1141 GTGCTGGTTG GCAAAGCGGC GGCGACCGGT AGCGGCGATT GGAACACCAC CCTGGCCTGC
1201 TTTGTGGCGA TTCTGATTGG CCTGTGCCTG ACCCTGCTGC TGCTGGCCGT GTTTAAAAAA
1261 GCGCTGCCGG CCCTGCCGAT TAGCATTACC TTTGGCCTGA TCTTTTATTT CAGCACCGAT
1321 AACCTGGTGC GTCCGTTTAT GGATACCCTG GCCAGCCATC AGCTGTATAT TAGCGCTTGG
1381 AGCCACCCGC AGTTCGAAAA ATAA
```

Human presenilin 2 full length (PS2-FL) protein sequence：

```
  1 MKHHHHHHHM LTFMASDSEE EVCDERTSLM SAESPTPRSC QEGRQGPEDG ENTAQWRSQE
 61 NEEDGEEDPD RYVCSGVPGR PPGLEEELTL KYGAKHVIML FVPVTLCMIV VVATIKSVRF
121 YTEKNGQLIY TTFTEDTPSV GQRLLNSVLN TLIMISVIVV MTIFLVVLYK YRCYKFIHGW
181 LIMSSLMLLF LFTYIYLGEV LKTYNVAMDY PTLLLTVWNF GAVGMVCIHW KGPLVLQQAY
241 LIMISALMAL VFIKYLPEWS AWVILGAISV YDLVAVLCPK GPLRMLVETA QERNEPIFPA
301 LIYSSAMVWT VGMAKLDPSS QGALQLPYDP EMEEDSYDSF GEPSYPEVFE PPLTGYPGEE
361 LEEEEERGVK LGLGDFIFYS VLVGKAAATG SGDWNTTLAC FVAILIGLCL TLLLLAVFKK
421 ALPALPISIT FGLIFYFSTD NLVRPFMDTL ASHQLYISAW SHPQFEK
```

Human presenilin 2 N-terminal fragment (PS2-NTF) DNA sequence：

```
  1 ATGAAGCACC ATCATCACCA TCACCATATG CTGACCTTTA TGGCGAGCGA TAGCGAGGAA
 61 GAAGTGTGCG ACGAACGTAC CAGCCTGATG AGCGCGGAAA GCCCGACCCC GCGTAGCTGT
121 CAGGAAGGCC GTCAGGGCCC GGAAGATGGC GAAAACACCG CCCAGTGGCG TAGCCAAGAA
181 AACGAAGAGG ATGGCGAAGA AGATCCGGAT CGTTACGTGT GTAGCGGCGT GCCGGGTCGT
241 CCGCCGGGTC TGGAAGAAGA ACTGACCCTG AAATATGGCG CGAAACATGT GATTATGCTG
301 TTTGTGCCGG TGACCCTGTG CATGATTGTG GTGGTGGCGA CCATTAAAAG CGTGCGCTTC
361 TACACCGAAA AAAACGGCCA GCTGATCTAT ACCACCTTTA CCGAAGATAC CCCGAGCGTG
421 GGCCAGCGTC TGCTGAACAG CGTGCTGAAC ACCCTGATTA TGATTAGCGT GATTGTGGTG
481 ATGACCATTT TTCTGGTGGT GCTGTATAAA TATCGCTGTT ATAAATTTAT TCACGGCTGG
541 CTGATTATGA GCAGCCTGAT GCTGCTGTTT CTGTTCACCT ATATCTATCT GGGCGAAGTG
601 CTGAAAACCT ATAACGTGGC AATGGATTAT CCGACCCTGC TGCTGACCGT GTGGAACTTT
661 GGCGCGGTGG GCATGGTGTG CATTCATTGG AAAGGCCCGC TGGTGCTGCA GCAGGCGTAT
721 CTGATCATGA TCTCTGCCCT GATGGCGCTG GTGTTTATTA AATATCTGCC GGAATGGTCT
781 GCGTGGGTGA TTCTGGGCGC GATTAGCGTG TATGATCTGG TGGCGGTGCT GTGCCCGAAA
841 GGTCCGCTGC GTATGCTGGT TGAAACCGCG CAGGAACGTA ACGAACCGAT TTTTCCGGCG
901 CTGATTTATT CTAGCGCATG GAGCCACCCG CAGTTCGAAA AATAA
```

Human presenilin 2 N-terminal fragment (PS2-NTF) protein sequence：

```
  1 MKHHHHHHHM LTFMASDSEE EVCDERTSLM SAESPTPRSC QEGRQGPEDG ENTAQWRSQE
 61 NEEDGEEDPD RYVCSGVPGR PPGLEEELTL KYGAKHVIML FVPVTLCMIV VVATIKSVRF
121 YTEKNGQLIY TTFTEDTPSV GQRLLNSVLN TLIMISVIVV MTIFLVVLYK YRCYKFIHGW
181 LIMSSLMLLF LFTYIYLGEV LKTYNVAMDY PTLLLTVWNF GAVGMVCIHW KGPLVLQQAY
241 LIMISALMAL VFIKYLPEWS AWVILGAISV YDLVAVLCPK GPLRMLVETA QERNEPIFPA
301 LIYSSAWSHP QFEK
```

Human presenilin 2 C-terminal fragment (PS2-CTF) DNA sequence：

```
  1 ATGAAGCACC ATCATCACCA TCACCATATG GTGTGGACCG TGGGCATGGC GAAACTGGAC
 61 CCGAGCAGCC AGGGTGCGCT GCAGCTGCCG TATGATCCGG AAATGGAAGA AGATAGCTAC
121 GATAGCTTTG GCGAACCGAG CTATCCGGAA GTGTTTGAAC CGCCGCTGAC CGGCTATCCG
181 GGCGAAGAAC TGGAAGAAGA AGAAGAACGC GGCGTTAAAC TGGGCCTGGG CGATTTTATT
241 TTTTATAGCG TGCTGGTTGG CAAAGCGGCG GCGACCGGTA GCGGCGATTG GAACACCACC
301 CTGGCCTGCT TTGTGGCGAT TCTGATTGGC CTGTGCCTGA CCCTGCTGCT GCTGGCCGTG
361 TTTAAAAAAG CGCTGCCGGC CCTGCCGATT AGCATTACCT TTGGCCTGAT CTTTTATTTC
421 AGCACCGATA ACCTGGTGCG TCCGTTTATG GATACCCTGG CCAGCCATCA GCTGTATATT
481 AGCGCTTGGA GCCACCCGCA GTTCGAAAAA TAA
```

Human presenilin 2 C-terminal fragment (PS2-CTF) protein sequence：

```
  1 MKHHHHHHHM VWTVGMAKLD PSSQGALQLP YDPEMEEDSY DSFGEPSYPE VFEPPLTGYP
 61 GEELEEEEER GVKLGLGDFI FYSVLVGKAA ATGSGDWNTT LACFVAILIG LCLTLLLLAV
121 FKKALPALPI SITFGLIFYF STDNLVRPFM DTLASHQLYI SAWSHPQFEK
```

Acknowledgements

After a long journey of four years' stay in Jülich, now it is the time for me to look back all the impressive sceneries I have experienced. Words are so pale under the shadow of the colourful life I had. I now want to express my sincere acknowledgement for all the people I met without whom this journey would not have been so great.

First of all, I would like to thank the Helmholtz-CSC program for its financial support during my stay in Forschungszentrum Jülich.

I am then indebted to my doctor father Prof. Dr. Jörg Labahn for allowing me to work under his guidance. It was him who brought me into the world of membrane proteins. It was also his belief in me strengthened and stabilized my mind from the very beginning of my project when I knew nothing about protein work and was kept thinking giving up. With his continuous patience and knowledge, I was able to find a way out the fog surrounding me.

I wish to express my deep sense of gratitude to Prof. Dr. Georg Büldt from whom I learned to always think positively. He could always make tough thing easy to go with his great sense of humor. Every time after chatting with him I felt so happy and peaceful. I also want to thank him for companying me in the lab till late evening and for asking me to join him with his car during winter times.

I sincerely thank Taras for his help academically and personally. I always went to him directly whenever I had problems which I could not solve by myself. His knowledge and experience in biology was so impressive. He was always so kind and generous to me and I felt from the bottom of my heart grateful for having a friend like him.

I am thankful to Prof. Dr. Jörg Fitter, Dr. Joachim Granzin and Dr. Oliver H. Weiergräber for their discussion and suggestion for my project whenever necessary. It is my pleasure to thank Dr. Alex for showing me how to do cloning,

Dr. Tobi for his help with CD measurement and Dr. Jaydeep for his discussion with fluorescence experiment as well as Dr. Peixiang Ma for giving me valuable suggestions with cloning. I thank Dr. Tino Polen for his help in mass spectroscopy.

I also want to thank Yufu, Marina and Sameer for their help with nanodiscs with which I can produce PS2-CTF via *in vitro* translation.

I wish to thank Dr. Uday, Dr. Yanbin Ma, Dr. Dia, Dr. Sylvia, Matteo, Axel, Andrii and Christian for being such nice lab mates. I will always remember the fun we had in our lab.

I sincerely acknowledge Sascha for fixing all the equipments I damaged. I would like to thank Ilona from whom I could always get whatever lab materials I want. I take this opportunity to thank Ramona for her helps with ÄKTA. I would like also to thank Nicole for helping me with my lab work and taking care of me when I damaged my foot. I am also thankful for Birgit for her official help during my stay.

I also want to acknowledge all my friends together with whom I played cards and football during weekends. Those were such nice experiences one could wish for when staying abroad. We used to play every weekends football no matter it rained or snowed. I really thank your guys for being good companies.

I am thankful to Kun Yu who is a new pH D student in our Hamburg lab for her supports in formatting my thesis and I wish her a great success in her scientific career.

I sincerely acknowledge my friend Jingyi Wang to whom I owed so much. Without her understanding and support I could not have been able to go through all these years. I am terribly sorry for all the wrongs I did to her and I wish her a happy life.

Finally I would like to thank my neighbour and relatives for taking care of my parents specially my younger sisters and brother in law. They spent a lot of time in companying my parents which is my responsibility when I was in Germany.

I am forever thankful to my parents from whom I become what I am now. From my Mom, I learned to become a strong person and to always think positively. From my Dad, I learned to be courageous to take my responsibility. The character they inherited to me is such a wonderful life-long fortune which makes me always a happy person. I cannot forget the pain that my parents have taken all these years. Without their constant support and encouragement, I could not overcome all the twists and turns in my life.

Erklärung

Ich erkläre, dass ich die vorliegende Arbeit selbständig und ohne unerlaubte Hilfe verfasst habe. Die vorliegende Arbeit wurde weder in der jetzigen oder in ähnlicher Form bei einer anderen Institution eingereicht. Es wurden zuvor keine Promotionsversuche unternommen

Jülich,

Ge Yang

Band / Volume 54
Eine kritische Evaluierung FRET-basierter Biosensoren als Werkzeuge für die quantitative Metabolitanalytik
R. Moussa (2012), 113 pp
ISBN: 978-3-89336-792-4

Band / Volume 55
Development of Surface-FIDA towards a diagnostic tool for Alzheimer's disease
L. Wang-Dietrich (2012), VI, 103 pp
ISBN: 978-3-89336-801-3

Band / Volume 56
Untersuchungen zur sekretorischen Proteingewinnung industriell relevanter Enzyme mit *Corynebacterium glutamicum*
S. Scheele (2012), vii, 127 pp
ISBN: 978-3-89336-815-0

Band / Volume 57
Novel insights into the energy metabolism of *Corynebacterium glutamicum* by comprehensive analysis of mutants defective in respiration or oxidative phosphorylation
A. Koch-Körfges (2012), III, 137 pp
ISBN: 978-3-89336-826-6

Band / Volume 58
Prozessnahe Hochdurchsatzoptimierung der heterologen Proteinproduktion in alternativen Wirtsorganismen
P. Rohe (2012), 165 pp
ISBN: 978-3-89336-834-1

Band / Volume 59
Validation and characterisation of novel cellular ligands of membrane-associated HIV-1 Nef
E.C.Kammula (2012), 151 pp
ISBN: 978-3-89336-839-6

Band / Volume 60
Untersuchungen zur Membranintegrität während der Tat-abhängigen Proteintranslokation in *Escherichia coli*
S. Fleckenstein (2013), VI, 160 pp
ISBN: 978-3-89336-841-9

Schriften des Forschungszentrums Jülich
Reihe Gesundheit / Health

Band / Volume 61
Characterization of Novel Amyloid-β Peptide (Aβ) Binding Ligands
S. Dornieden (2013), vii, 129 pp
ISBN: 978-3-89336-844-0

Band / Volume 62
Regulatorische Aspekte der Expression und Sekretion heterologer Proteine in *Corynebacterium glutamicum*
A. R. Chattopadhyay (2013), VIII, 195 pp
ISBN: 978-3-89336-845-7

Band / Volume 63
***Gluconobacter oxydans* strain development: Studies on central carbon metabolism and respiration**
J. Richhardt (2013), III, 181 pp
ISBN: 978-3-89336-851-8

Band / Volume 64
Metabolic Engineering von *Corynebacterium glutamicum* für die Produktion einer Dicarbonsäure
A. Otten (2013), 98 pp
ISBN: 978-3-89336-860-0

Band / Volume 65
Rapid Development of Small-Molecule producing Microorganisms based on Metabolite Sensors
S. Binder (2013), 138 pp
ISBN: 978-3-89336-872-3

Band / Volume 66
Increasing the NADPH supply for whole-cell biotransformation and development of a novel biosensor
S. Solvej (2013), 130 pp
ISBN: 978-3-89336-900-3

Band / Volume 67
Expression, purification and biophysical characterization of human Presenilin 2
G. Yang (2013), 158 pp
ISBN: 978-3-89336-928-7

Weitere ***Schriften des Verlags im Forschungszentrum Jülich*** unter
http://wwwzb1.fz-juelich.de/verlagextern1/index.asp

Gesundheit / Health
Band / Volume 67
ISBN 978-3-89336-928-7

JÜLICH
FORSCHUNGSZENTRUM

67

Member of the Helmholtz Association

Expression and purification of human Presenilin 2

Ge Yang

Gesundheit
Health

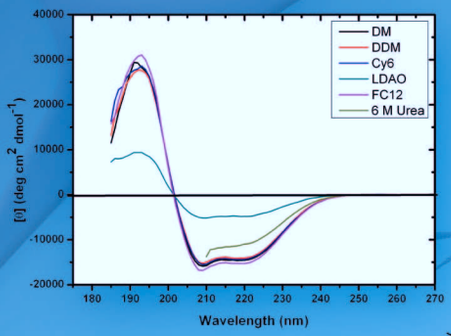

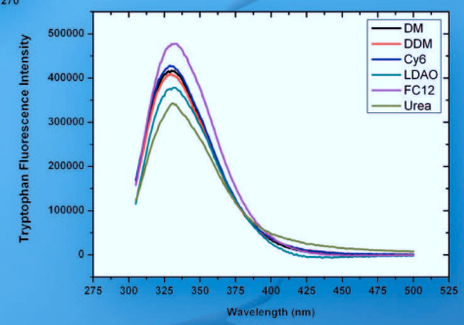

Expression, purification and biophysical characterization of human Presenilin 2

Ge Yang

JÜLICH
FORSCHUNGSZENTRUM